Understanding the effect of objective function weightings on posture prediction: application to predicting lifting postures in un-fatigued and fatigued states.

by

Justin Davidson

A thesis

presented to the University of Waterloo

in fulfillment of the

thesis requirement for the degree of

Master of Science

in

Kinesiology

Waterloo, Ontario, Canada, 2021

Authors Declaration

I hereby declare that I am the sole author of this thesis. This is a true copy of the thesis, including any required final revisions, as accepted by my examiners. I understand that my thesis may be made electronically available to the public.

Abstract

Physical prototyping is often required when developing new equipment and workspaces so that human-systems integration can be considered. Digital human modelling facilitates more efficient, upstream assessment of human interactions with new equipment within a virtual environment. However, predicting how humans will behave (i.e., move and position) to perform industry relevant tasks, requires the ability to consider state-based influences, like fatigue, on predicted behaviours (Davidson, Graham, Beck, Marler, & Fischer, 2021). The overarching objective of this thesis was to understand how objective function weightings should be configured within a multi-objective task-focused human behaviour prediction model to simulate postures within a floor-to-shoulder height lifting task under different fatigue states. To achieve this aim, simulated lifting postures were generated by systematically altering objective function weightings where each simulation was compared with experimentally captured lifting posture data to determine the closest match and subsequent ideal optimal weighting configuration. Fifteen participants were recruited and completed a lifting protocol at 30% of their EPIC predicted maximum box lifting capacity. Participant fatigue level was evaluated based on their RPE and task completion time. Changes in participants lifting strategy over the course of the fatigue lifting protocol was also verified. Participants who were deemed fatigued and exhibited movement strategy changes were included in the simulation portion of the thesis where participant's first and last lift kinematic data were used as inputs to a multi-objective optimization digital human model. Avatar's were generated to match participant anthropometry and were constrained to maintain the same hand and foot position as the participants. Simulations were run while altering three objective functions including the minimization of: Discomfort, Total Joint Torque and, Maximum Joint Torque. The different objective functions

represent performance measures to be minimized in order to predict the design variables, in this case joint angles, within the avatar's available degrees of freedom. Simulations were run for objective function weighting coefficients between 0-100% at 10% intervals for each subject, each posture and each fatigue state. Each simulation was compared to the simulation that was generated using the participant-specific motion capture data and the error between the motion capture and optimization predicted data were calculated. A total root mean squared error (RMSE) value was calculated including the ankle, knee, hip, trunk, shoulder, and elbow errors. Error was modeled as a function of objective function weightings using participant specific multivariate regression equations. Multivariate regression equations were then used to determine the objective function weighting configuration that would results in the lowest error for each participant, at lift origin and destination and for un-fatigued and fatigued lifting states. A two-way repeated measures Friedman's test was used to detect for difference in optimal objective functions weightings between locations (origin vs. destination) and fatigue state (un-fatigued vs. fatigued lift). Results showed a median objective function weighting of sixty, zero, and zero for the discomfort, maximum joint torque and total joint torque objective functions, respectively. Friedman's test did not detect significant differences between fatigue states or location for any of the three objective function weightings. The discomfort objective function alone tended to predict box lifting postures best. Discomfort may include aspects of the torque based objective functions leading to its increased priority for predicting postures over the minimization of maximum and total joint torque. Future studies should build on the current suite of objective functions to improve predictive capabilities of digital human models for novel tasks. More accurate digital human models will allow for earlier consideration of humans-in-the-loop and significantly reduce industry costs of physical prototypes.

Acknowledgements

I would like to thank the support team that I have had throughout the process of completing this thesis. To Dr. Steven Fischer, my supervisor, thank you for welcoming me to the Occupational Biomechanics and Ergonomics Lab family during my undergraduate degree and pushing me to grow as an individual and researcher throughout the completion of my graduate degree. To my committee, Dr. Jack Callaghan, and Dr. Clark Dickerson, thank you for your helping steer this thesis in the right direction and challenging me think deeply about the problems that I am attempting to address in this work.

Having such an intelligent cohort of classmates to learn the fundamentals of biomechanics alongside throughout this degree was incredibly helpful in this journey so thank you to those individuals. Thank you to the OBEL team with a special thank you to Sarah Remedios and Sheldon Hawley for all the feedback and discussions that not only improved this thesis but helped in building my knowledge within this field. Another special thank you to Nathalie Oomen, for generously sharing your thesis data for the completion of this work.

Finally, I would like to thank my family and friends, whom I consider family. From being a sound board for problems, to just bringing me back to reality after a long week of work, your support has been invaluable. To mom and dad, you have pushed me early on to do my best and persevere regardless of what I do in life. You have also taught me what it means to commit to something despite how difficult it may be and without these lessons I would not made it as far as I have. Jessa, you have been my rock, picking me up when I am down and giving me the tough love exactly when I need it. You are the most incredible, intelligent women, and I am so lucky that I have your love and care in my life.

Table of Contents

List of Figures

List of Tables

List of Equations

1.0 Introduction

New workspace designs and equipment, which require human interaction, commonly necessitate physical prototypes to be developed for human performance testing and evaluation. Physical prototype testing can be time-consuming, costly, and often requires subjective feedback to inform decision making on the prototype rather than biomechanically relevant outputs (Ahmed, Irshad, Demirel, & Tumer, 2019; Duffy, 2012; Jun, Lee, Kim, & Noh, 2019). Modelling and evaluating prototypes in a virtual or computer aided design (CAD) environment can substantially reduce costs. By leveraging CAD-based modeling packages (e.g. FEA, multi-body dynamics), emerging ideas can be rapidly developed to evaluate structural and geometric parameters virtually, allowing iterative testing and improvement prior to physical prototyping and manufacturing (Bordegoni & Rizzi, 2011). However, consideration of human-in-the-loop interactions with new workspace designs and equipment is often poorly considered until the physical prototype is already developed (Chaffin, 2009). Digital human models (DHM) provide a virtual representations of a human within a digital environment, where the virtual human can then be used to predict safety or performance outcomes based on modeled interactions with products, equipment and workspaces (Demirel & Duffy, 2007). Leveraging DHMs throughout the CAD development phase allows for the early identification of human-systems integration concerns, where such issues would otherwise be discovered in the more expensive physical prototyping stage of development (Figure 1). DHMs can also allow for rapid trade-off analyses, where design components are altered and evaluated, to create better products for end-users. Though the use of DHMs have the potential to address human-system-integration considerations earlier in design, differences in underlying prediction and simulation approaches are important to consider.
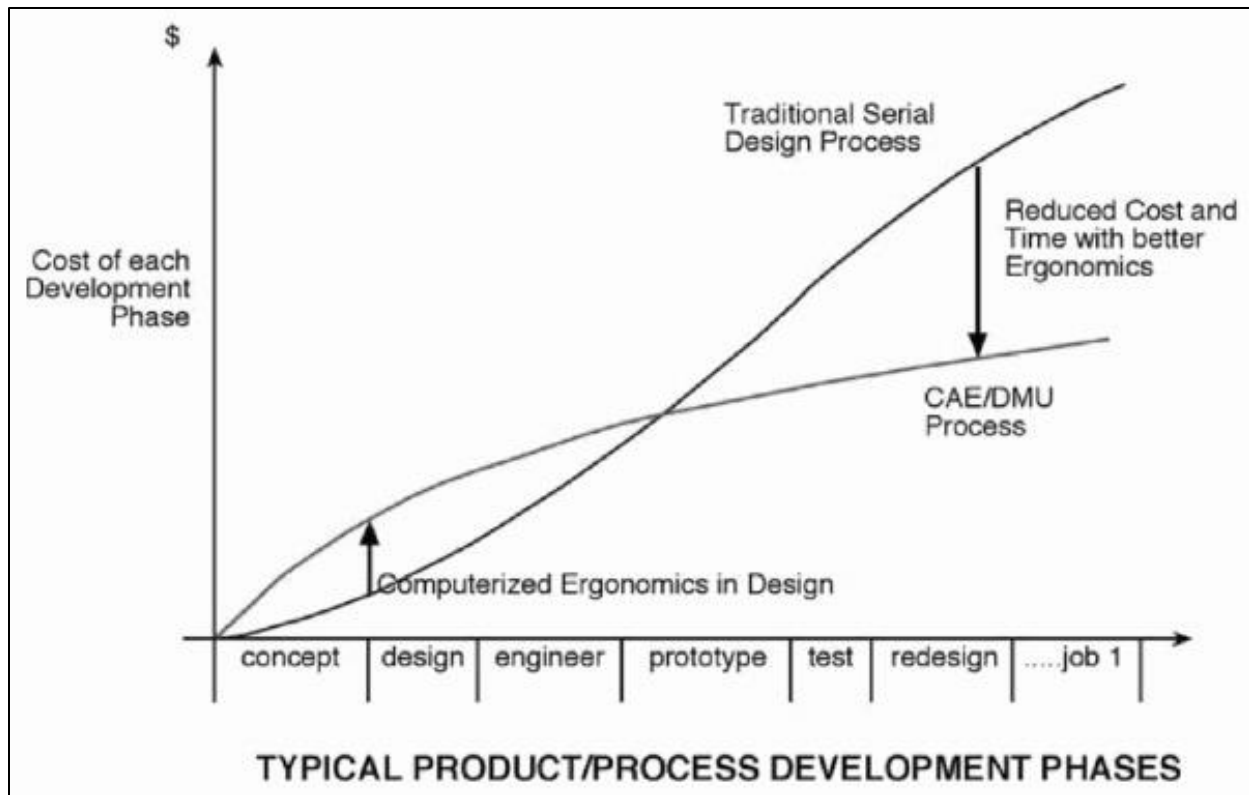
Figure 1. Cost effects of two design approaches where the "Computerized Ergonomics in Design" curve represents DHM use early in the design process (Chaffin, 2005).

There are three main types of DHMs designed to predict and simulate human motion including: manually manipulated models, experimental data driven models, and optimization-based models. Chapter 2 of this thesis discusses the three primary DHM types in more detail. This thesis focuses on an optimization-based DHM, as the theoretical basis for the optimization approach is more aligned with contemporary motor control theories (Abdel-Malek & Arora, 2013; Scott, 2004; Yang, 2009). Optimization-based DHMs assume that humans inherently choose postures that minimizes or maximizes physiologically relevant performance criteria where design variables such as joint angles can be predicted given a set of internal (i.e. joint torque and range of motion limits) and external (i.e. body endpoint must contact a target location) constraints. The mathematical formulations of the physiologically relevant performance

2

criteria being minimized or maximized are considered as objective functions. In emerging DHM's, multiple objective functions are available for users to include in their predictions; however, little evidence is available to guide end users in deciding which objective functions to use and when to predict biofidelic task-focused behaviour, and particularly when considering individual state factors such as fatigue.

Physiologically relevant objective functions used to represent motor control laws governing human movement are dynamic. Multiple physiologically relevant performance criteria may compete and/or cooperate in controlling human behaviour when performing a given task and can change with a change in task, an individual's state, and the environment (Berret, Delis, Gaveau, & Jean, 2019; Cashaback & Cluff, 2015; Jin, Kulic, Lin, Mou, & Hirche, 2019; Sparrow & Newell, 1998; Yang, 2009). Human gait is well studied in this regard, where associated objective functions are well defined such as minimizing muscle activations and maximizing gait stability and smoothness (Miller, Umberger, Hamill, & Caldwell, 2012; Nguyen, Johnson, Sup, & Umberger, 2019); however, other objective functions that best predict other movements, like lifting still require further investigation. Moreover, how individual states (i.e. fatigue) and environmental conditions (i.e. thermal) alter the relative weightings of objective functions remain as under studied areas (Ma, Zhang, Chablat, Bennis, & Guillaume, 2009). Understanding prospective differences in underlying objective functions and weightings will improve the ability to deploy DHMs to support virtual prototyping for a wider range of design characteristics.

The purpose of this thesis was to explore existing objective functions within an optimization-based DHM to determine how those objective function weightings can be optimally tuned to predict floor to shoulder height box lifting under different fatigue states. Additionally, this study investigated if there was a systematic shift in the weights assigned to objective

functions when attempting to predict lifting postures in un-fatigued and fatigue states. Two postures (lift origin and lift destination) were assessed along with two fatigue states (un-fatigued and fatigued). Simulated postures were compared to participant specific lifting posture data that were obtained experimentally to generate an error response surface relative to unique objective function weightings. Response surfaces were modeled using multivariate polynomial regression where emergent regression equations were optimized to find the optimal objective function weighting configuration that predicted postures that best matched the experimentally captured origin and destination postures.

2.0 Literature Review

2.1 Digital Human Modelling

Digital human modelling (DHM) allows for the representation of humans within a virtual environment. Human representation within DHMs can include biomechanical, physiological, and psychological principles. Psychological models are typically not included with commercial DHMs aimed to model the full body biomechanics and physiology and will therefore be excluded for the purposes of this thesis. When modelling the human body in the commercial DHM there are generally three approaches used:

1. Manually manipulated models,

2. Experimental data driven models and,

3. Optimization-based models.

2.1.1 Manually Manipulated Models

Manual manipulation allows the users to position an avatar or virtual mannequin into a desired posture by altering joint profiles (position and angles), constrained by the degrees of freedom allowed within the DHM. Some examples include NexGen Ergonomics' HumanCAD and the University of Michigan's 3DSSPP software (Center for Ergnomics, n.d.; NexGen Ergonomics Inc., 1997). The manual manipulation approach is conceptually simple, where a user can manipulate joint angles as required to mimic observed task behaviours to understand and evaluate corresponding biomechanics. Manually manipulated models cannot predict postures or movement and cannot assess dynamic scenarios within the software (Abdel-Malek & Arora, 2013). Additionally, manual posturing has limited repeatability and the accuracy of the model is highly dependent on the DHM user's experience (Li, et al., 2018; Zhu et al., 2019). The manual

posturing approach is often used when modelling a pre-existing task or required posture, if a novel task is created the modeler would need to estimate the required human behaviour to complete the new task (Abdel-Malek & Arora, 2013). Though manually manipulated DHM have limited posture prediction functionality, they allow for quick visual representations of occupationally relevant task-focused behaviours, and they can provide useful outputs for ergonomic analyses of postures.

2.1.2 Experimental Data Driven Models

Experimental data driven models are a predictive DHM type relying on pre-recorded motion capture data to drive an avatars postures and movements. Data-driven posture prediction models have been widely adopted within the automotive manufacturing industry due to the ease of representing common manual materials handling movements (Blanchonette, 2010). Experimental data driven predictive models take the large databases of pre-recorded kinematic data and use them to generate statistical regressions from which new motions can be predicted (Abdel-Malek & Arora, 2013; Blanchonette, 2010; Chaffin, 2005). Not every task that may need to be evaluated within a DHM can be captured with motion capture data considering the diversity of possible movements and therefore some limitations of this prediction approach exist. Limitations include inaccuracies when predicting kinematics for tasks where obstacle avoidance is required, as well as inaccuracies when representing unique tasks or tasks that are highly dynamic in nature (Abdel-Malek & Arora, 2013; Marler et al., 2009; Marler, et al., 2005; Yang et al., 2004). Limitations in predicting movement behaviours for unique or novel tasks poses a specific problem when attempting to deploy DHM in upstream design for the evaluation of human-system integrations by considering unique or novel designs.

2.1.3 Optimization-Based Models

The third type of DHM utilizes optimization to predict and simulate postures and

motions. In this approach, joint angles serve as design variables to be solved for by using an

optimization approach. Constraints on the optimization problem include joint range of motion

and torque limits based on experimentally captured physiological data (Abdel-Malek & Arora,

2013). Optimization-based DHMs are also modifiable by including end-effectors on the avatar

model which can be constrained to reach a point, or zone defined by the user within the virtual

environment (Abdel-Malek & Arora, 2013; Xiang, Arora, & Abdel-Malek, 2012; Xiang et al.,

2010). Objective functions serve to minimize or maximize specific criteria at the joint or whole-

body level such as energy efficiency or discomfort (Marler, Rahmatalla, et al., 2005).

Optimization-based DHMs allow for the prediction of movements and postures without the need

to drive avatar motions with pre-recorded motion capture data. Instead, motion capture can serve

as a validation for a given scenario being modelled. Optimization-based DHM accuracy and

validity is dependent on the objective function or functions that are chosen to be minimized or

maximized (Marler, Yang, Arora, & Abdel-Malek, 2005). Understanding what objective

functions to use and why will be discussed within the optimal control section of this thesis.

Since DHM avatars are generally made up of rigid links with scaled anthropometry,

inverse kinematics (IK) is generally used as a posture prediction method. Optimization or

regression equation fitting allow for the IK problem to be solved with the available link segments

and joint degrees of freedom (Abdel-Malek & Arora, 2013; Beck & Chaffin, 1992; Blanchonette,

2010). Commonly, an end-effector is chosen somewhere on the avatar's body to be constrained

to a marker target, if the marker target cannot be reached within the constraints of the avatar, the

posture cannot be predicted. If the marker target is within capable range of the avatar's limits, a

posture will be predicted as represented by joint angles, that best minimize / maximize the underlying objective function or functions. Since segment lengths and weights are estimated by the input anthropometry, and since joint loads can be added to the avatar in 3D space, inverse dynamics calculations can be conducted within the DHM software to understand net joint moments and forces experienced by the avatar for a given posture (Chaffin, 2009).

2.2 Optimal Control, Optimization and Objective Function Weightings

Human motion prediction is a difficult undertaking as there are many degrees of freedom within the human body allowing for numerous solutions to achieve the same movement objective (Scott, 2004). Simply reaching for an object in front of you can be accomplished in an infinite number of ways due to the abundancy of degrees of freedom available within the anatomy of the human body. This creates an indeterminacy problem when modelling and predicting how human postures and movements are generated. Optimal control theory may provide a basis for navigating the indeterminacy involved when attempting to predict human kinematics. Optimal control theory assumes movement behaviours are minimizing or maximizing relevant criteria such as minimizing discomfort (Marler, Rahmatalla, et al., 2005) or maximizing jump height (Pandy & Zajac, 1991). The criterion that is being optimized for, according to the optimal control theory, can be operationalized by objective functions which are functions that can mathematically represent what the nervous system is trying to achieve (Todorov, 2004).

In posture prediction, different objective functions can be used to estimate what an individual is optimizing for within a given task. Complex movements may consider multiple objective functions to be optimized throughout, thereby requiring different objective functions to represent the smaller units of the movement also known as movement primitives (Todorov &

Jordan, 2002). Single objective functions have been used to represent whole movements or movement primitives for a given task, this is called single objective optimization. Gait, for example, has been previously modelled using single objective optimization and the objective function of minimizing total muscular effort (Ghista, Toridis, & Srinivasan, 1976). Minimizing total effort falls under the overarching optimization assumption that human kinematic behaviour tends to minimize metabolic costs or maximize efficiency. This coincides with the observations that potential energy change of the human center of mass is low during walking, metabolic costs at self selected paces are low, and the center of mass motion generally maintains a smooth trajectory (Nguyen et al., 2019; Winter, 1976). Though the minimization of metabolic cost has been useful in gait modelling, it may not be appropriate in all movement behaviour scenarios as it alone does not predict average behaviour for other movements (Todorov, 2004). In fact, many different optimization strategies have been adopted to model movement including maximizing joint stability (Cashaback & Cluff, 2015), minimizing muscle stress (Crowninshield & Brand, 1981), minimizing joint discomfort (Marler, Rahmatalla, et al., 2005), and minimizing joint loads (Yettram & Jackman, 1982). Movements or movement primitives may be better represented; however, by combining multiple optimization assumptions at a given time rather than only considering a single objective.

Multi-objective optimization (MOO), allows for the consideration that many different control laws, operationalized by objective functions, may influence movement behaviour simultaneously. In MOO, a scenario where all objectives have a minimum simultaneously (utopia point) is rare (Marler, Yang, et al., 2005). Without a utopia point solution, there are multiple local optimums (pareto optimal solutions) that can be possible within a set of feasible solutions, therefore requiring a method to choose between the different pareto optimal solutions.

Many methods exist to navigate the pareto optimal space; however, the weighted sum method allows for the allocation of preferential weightings a priori (Yang, Marler, & Rahmatalla, 2011), that may give insight into the importance of a given objective function for a movement or movement primitive. One study, exploring three different methods for navigating through the number of possible solutions from a MOO using a digital human model and simple reach to point tasks, found that the weighted-sum method tended to provide the most natural postures when compared to a min-max and global criterion method for MOO (Marler & Arora, 2010). Furthermore, MOO solutions out-performed single objective optimization solutions for posture prediction outcomes (Xiang et al., 2010). Therefore, following the optimal control assumption that human movement behaviours are minimizing or maximizing relevant criteria, MOO and the weighted sum method may allow for the accurate prediction of human kinematic behaviours while simultaneously allowing for the understanding of how different movements are controlled.

The optimal control laws that control movement behaviour, operationalized as objective functions and their assigned weightings, are modulated by different factors. Figure 2 shows Sparrow and Newell's constraint model displaying how the task, environment, and organism can alter the coordination and control of movement (Sparrow & Newell, 1998). Theoretically, this constraint model can be applied to the optimal control space. When the individual's state, the task being completed, or the environment, is altered, that individual's movement behaviour may change, which can be represented by a change in the objective functions and their assigned weighting within a MOO framework. Previous studies within the DHM realm have investigated the different combinations of objective functions and their respective weightings in modelling postures for a given task (Marler & Arora, 2010; Marler, Yang, et al., 2005; Yang et al., 2011). Few studies, however, have investigated the changing of objective functions and their assigned

weightings when attempting to model the task-focused behaviour that might emerge from changes in an individual's state or environment. This thesis will focus on fatigue as an individual state factors that can alter movement behaviours, with a focus on lifting.
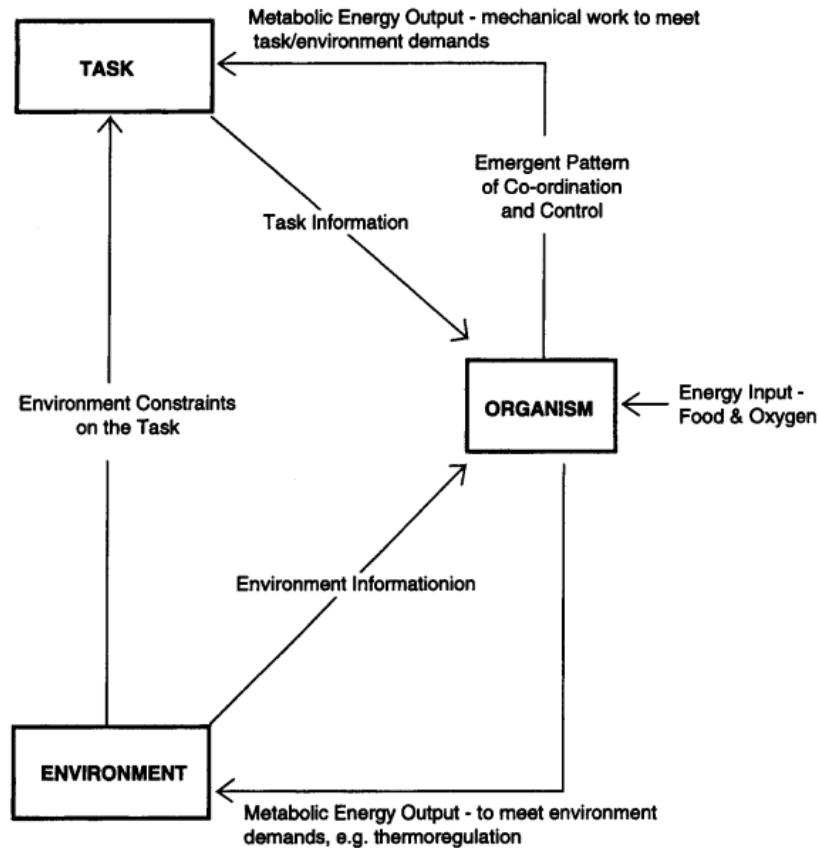
Figure 2. Shows the Sparrow and Newell (1998) constraint model as it pertains to metabolic energy expenditure and its potential influence the control and coordination of movement.

2.3 Fatigue and Movement Behaviour Changes

Fatigue is an individual state factor that can alter movement behaviour, theoretically by altering overarching objective functions and their assigned weightings within the context of a MOO problem. Fatigue is a multifaceted phenomenon that can emerge at the central and peripheral levels to reduce the maximum force capacity of the muscle (Gandevia, 2001; Noakes

& Gibson, 2004; Xia & Frey Law, 2008). Central fatigue is defined as the progressive decrease in voluntary activation of muscle fibers; while peripheral fatigue is produced by alterations at the neuromuscular junction or beyond it (Gandevia, 2001). In other words, central fatigue is the failure to drive motor neurons, while peripheral fatigue is the failure at the site of skeletal muscle contraction. Though fatigue can have central and peripheral causes, it can sometimes be difficult to distinguish between the two and separating them is not always required (Vøllestad, 1997). Fatigue can manifest from cognitively demanding tasks, a lack of sleep (sleep exhaustion), physically demanding tasks, boredom and more (Matthews & Hancock, 2017; Nibbeling, Oudejans, Ubink, & Daanen, 2014). For the purposes of this thesis, cognitive fatigue, exhaustion, and fatigue related diseases will not be addressed; however, these forms of fatigue are still common and influence an individual's force generating capability as well as their movement behaviour (Matthews & Hancock, 2017; Nibbeling et al., 2014).

Muscular fatigue has been well documented in biomechanics history and will be the personal state factor analyzed within this thesis. Muscular fatigue specifically, is defined as a decrease in force generating capability within a muscle that is only temporary and not caused by injuries (Bigland-Ritchie & Woods, 1984; Gandevia, 2001; Gates & Dingwell, 2008). Muscle fatigue can be observed using several different approaches. When compared to an un-fatigued muscle state, a fatigued muscle has measurable metabolite concentration changes (Allen, Lamb, & Westerblad, 2008; H. Westerblad, Bruton, Allen, & Lannergren, 2000; Håkan Westerblad, Allen, & Lännergren, 2002). Also, when comparing fatigued muscle to un-fatigued muscle, at a given force, EMG amplitude increases and mean power frequency decreases (Bigland-Ritchie & Woods, 1984; Petrofsky, 1979). Synchronous firing of motor unit action potentials as well as decreased conduction velocities of electrical signals are also common indicators of fatigue or

fatigue development within muscle (Arendt-Nielsen & Mills, 1988; Broman, Bilotto, & De Luca, 1985; De Luca, Roy, & Erim, 1993). Being that a decrease in the muscles ability to generate a desired force defines a fatigued muscle, changes in force via maximum voluntary efforts is another way to measure fatigue development (Bigland-Ritchie & Woods, 1984). More indirect measurements of muscle fatigue can also be surveyed such as ratings of perceived exertion and fatigue assessment scales although these are generally better used as complimentary measures to the aforementioned methods.

Fatigue is not exclusive to changes at the muscular level and force production level. Fatigue has been known to change human movement and its control as well (Chen, 2000). This is important as differing kinematics will directly result in altered joint loading and performance. Researchers have observed movement related changes associated with the progression of fatigue including an increase in net joint moment variability and increased co-contraction (Cashaback & Cluff, 2015; O'Brien & Potvin, 1997; Psek & Cafarelli, 1993; Reeves, Cholewicki, Milner, & Lee, 2008; Singh, Arampatzis, Duda, Heller, & Taylor, 2010). From an optimal control standpoint, fatigue likely alters the objective(s) being optimized. Cashaback and Cluff (2015) found that with fatigue, less weight was given to optimizing energy efficiency and more weight was given to prioritize joint stability, likely to preserve end-point control to meet the task's goals. This is counterintuitive as a logical conclusion for fatigue is to become more energy efficient to mitigate fatigue development. This means that overall, fatigue does not only reduce the force producing capabilities, but may also change the overarching control mechanisms which ties back to Newell and Sparrow's constraint model on movement behavior. This does not specifically imply a human will choose to now optimize for stability instead of efficiency, rather a shift in the amount of emphasis placed on each objective may change. This has been discussed

as a hierarchal shift with fatigue and other modifying factors on the control space (Li, Todorov, & Pan, 2004; Todorov, 2004).

In lifting, specific kinematic changes have been seen as fatigue progresses during prolonged lifting bouts. Bonato et al., (2003) found that individuals would move away from a stoop posture and towards a squat posture as fatigue progressed and similarly, Fischer et al., (2015) found that as fatigue progressed individuals altered their movement strategies to reduce trunk segment angles. In contrast, Fogleman and Smith (1995), Sparto et al., (1997), and Van Dieën et al., (1998), found increased lumbar flexion and less range of motion used at the knee joint during prolonged lifting bouts as fatigue progressed. Though different kinematic changes were found Fischer et al., (2015) and Van Dieën et al., (1998) agreed that the lifters adapt their lifting kinematics as they attempt to balance between the lifted mass and the diminishing force manifesting due to fatigue whether this force is due to a reduction at the knee joint (Sparto et al., 1997) or the trunk musculature (Van Dieën et al., 1998). Interpreting the kinematic differences of the aforementioned lifting fatigue studies from an optimal control standpoint, there was a potential shift in how individual's nervous system chose to optimize their lifting movement as fatigue progressed. While this was not specifically modelled using optimization methods, there is an opportunity to capture how the optimal control principles change due to a fatigue lifting protocol by leveraging MOO based DHMs.

Modelling fatigue within DHM tools is a desired capability for end users (Davidson et al., 2021); however, current modelling approaches alter joint strength capabilities exclusively which may not always account for the movement changes that occur due to fatigue development (Ma et al., 2009; NATO RTO Technical Task Group 019, 2009). To model fatigue related movement changes, within an experimental motion capture driven predictive model, more large-scale

14

motion capture collections post relevant fatiguing protocols would be necessary to develop the required regression models to draw upon when predicting kinematics. Within an optimization-based DHM however, a hierarchal shift in objective functions and their associated weighting may enable modeling of fatigue related movement changes. Ma and colleagues (2009) used the Anybody DHM (Damsgaard, Rasmussen, Christensen, Surma, & de Zee, 2006) to explore changing objective functions to represent a drilling task as fatigue progressed. This investigation showed the optimal distance for workers to be postured from the drilling location to minimize fatigue; however, the chosen task was a simple drilling task where specific joint kinematics where not evaluated or compared against experimentally gathered drilling data. More complex tasks such as box lifting, a whole-body task, may show different results.

2.4 Multi-Objective Optimization-based Digital Human Model

For this thesis, Santos Pro will be used as an optimization-based DHM that allows users to vary the weightings for up to nine different objective functions. Santos Pro was originally developed in the Virtual Soldier Research Program (Abdel-Malek & Arora, 2013). Santos Pro includes avatars representing males and females for visual shape accuracy. Anthropometry can be altered manually within the software to represent specific groups or individuals (SantosHuman Inc, n.d.). Santos Pro permits manual manipulation of avatars, motion prediction based on the provision of experimentally obtained motion capture data and posture prediction with the use of whole-body MOO while leveraging the weighted sum method.

Within an optimization-based model, three main components are necessary: design variables, constraints (internal and external) and objective functions. The design variables are the joint profiles of the model including joint angles of the available degrees of freedom (DOF) as

seen in Figure 3 (Abdel-Malek & Arora, 2013; Xiang et al., 2008). The shoulder complex that is modelled includes a glenohumeral joint with three degrees of freedom and a sterno-clavicular joint with two degrees of freedom. The Santos avatar's spine has 17 spinal units that have three DOF each and move in succession.
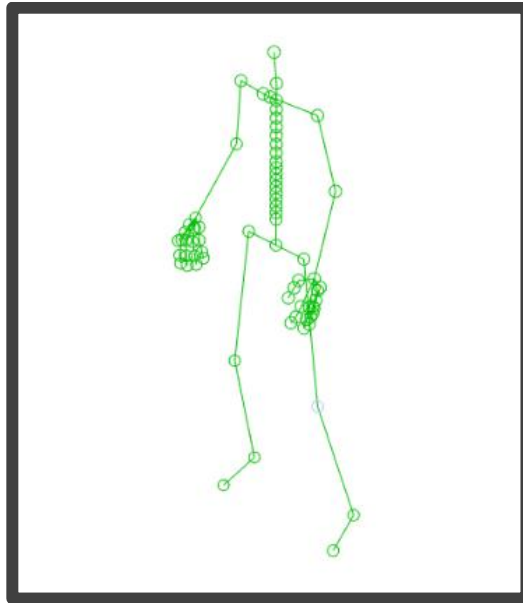
Figure 3. Shows the available degrees of freedom representing the Santos Pro human body.

The constraints create boundaries for the optimization problem and include joint torque limits and joint range of motion limits. Joint torque limits defined within the Santos Pro software were obtained from various studies (Cahalan, Johnson, Liu, & Chao, 1989; Gill, Murray, & Saunders, 2002; Kaminski, Perrin, & Gansneder, 1999; Kumar, 1996). Other internal design constraints are available within the Santos Pro model including obstacle-avoidance and self-avoidance which create constraining spheres for which the avatar cannot come in contact with. Finally, the model is constrained to follow basic laws of physics.

Objective functions within the Santos Pro model are labeled performance measures and the software uses MOO while leveraging a weighted sum method to allocate the various

objective functions available. This allows for differing coefficients to be allocated to multiple

objective functions which will alter the solution space as they attempt to reach pareto optimality

(Marler, Yang, et al., 2005). Within the Santos Pro DHM software, nine objective functions are

available to be altered within their weighted sum optimization. Two objective functions relate to

vision, and one related to balance and whole-body stability (Zero-Moment Point). For the

purposes of this thesis, the two vision objectives will not be included, and the one stability

objective function will be considered as constraints rather than an objective function. Figure 4

offers a visual representation of how altering objective function weightings can alter a given

posture within Santos Pro. This leaves six objective functions to be altered within the software

(Abdel-Malek & Arora, 2013; Marler, Rahmatalla, et al., 2005; SantosHuman Inc, n.d.; Yang et

al., 2011):

1. Minimization of Effort – models the inclination to avoid deviation from an initial position:

$$f_{effort}(\mathbf{q}) = \sum_{i=1}^{n} \gamma_i \left(q_i - q_i^{initial}\right)^2$$

Equation 1. Shows the objective function to minimize effort where γ_i is a weight used to stress
the relative stiffness of a joint. Variable n is the number of degrees of freedom, and $\mathbf{q}$ is the
posture. $(q_i - q_i^{initial})$ is the joint angle displacement from the initial posture (Mi, Yang, &
Abdel-Malek, 2009).

2. Minimization of Discomfort – models three factors in muscular discomfort:

- The tendency to maintain a neutral position (standing with arms at the side) (Equation 2).

- The tendency to move body segments sequentially (limbs, then spine, and then clavicle).

$$f_{Discomfort}\left(\mathbf{q}\right) = \sum_{i=1}^{DOF} \gamma_i \left(\Delta q_i^{norm}\right)^2$$

Equation 2. Shows the objective function optimizing for the tendency to gravitate towards a neutral position where $\mathbf{q}$ represents a posture, Δq_i^{norm} is the normalized change in joint angle for a degree of freedom from the neutral position. Variable γ_i is a weight used to stress the stiffness of a joint where it is assumed joints are moved sequentially (Marler et al., 2005).

- Finally, the tendency to avoid joint limits (Equation 3).

$$f_{Discomfort}\left(\mathbf{q}\right) = \frac{1}{G} \sum_{i=1}^{DOF} \left[\gamma_i \left(\Delta q_i^{norm}\right) + G \times QU_i + G \times QL_i\right]$$

Equation 3. Shows the second equation used to minimize discomfort where G x QU and G x QL are penalty terms associates with values approaching the joint upper and lower limits respectively.

3. Minimization of the Change in Potential Energy – minimizes the squared change in potential energy of each segments center of gravity heights at a neutral position (Equation 4).

$$f_{Delta-potential-energy}\left(\mathbf{q}\right) = \sum_{i=1}^{\kappa} (P_i - P_i')^2$$

Equation 4. Shows the delta potential energy objective function where $\mathbf{q}$ is the posture, k is the number of lumped masses. Variable $(P_i - P_i')$ is the change in potential energy from the neutral position (Mi et al., 2009).

4. Minimization of Total Joint Torque – minimize dynamic effort defined as the square of all joint torques (Equation 5).

$$f(\mathbf{q}) = \sum_{i=1}^{DoF} \tau_i^2$$

Equation 5. Shows the objective function for minimizing total joint torque (dynamic effort) adapted from Xiang et al., (2012) where variable τ_i represents the torque for a given degree of freedom, variable $(\mathbf{q})$ is the resultant posture.

5. Minimization of Maximum Joint Torque – minimize the squared torque with respect to the maximum torque limit of a joint (Marler, Knake, & Johnson, 2011). This objective function can be found in Equation 6.

$$f(\mathbf{q}) = \sum_{i=1}^{DoF} \left(\frac{\tau_i}{\tau_{max}}\right)^2$$

Equation 6. Shows the minimization of maximum joint torque objective function equation where τ_i represents the torque for a given degree of freedom, $(\mathbf{q})$ is the posture and τ_{max} represents the maximum torque limit of a degree of freedom.

6. Minimization of Joint Displacement – models minimization of joint displacement from the neutral position (standing with arms at the side) (Marler, Yang, et al., 2005). This objective function can be found in Equation 7.

$$f_{Joint\ displacement}(\mathbf{q}) = \sum_{i=1}^{n} \gamma_i \left(q_i - q_i^N\right)^2$$

Equation 7. Shows the joint displacement objective function where $\mathbf{q}$ represents a posture, q_i is the joint angle for a degree of freedom within a set of joint limits. Variable q^N represents the neutral angular position of a degree of freedom. Variable n is the number of degrees of freedom and γ_i is a weight introduced to stress the relative stiffness of a joint.
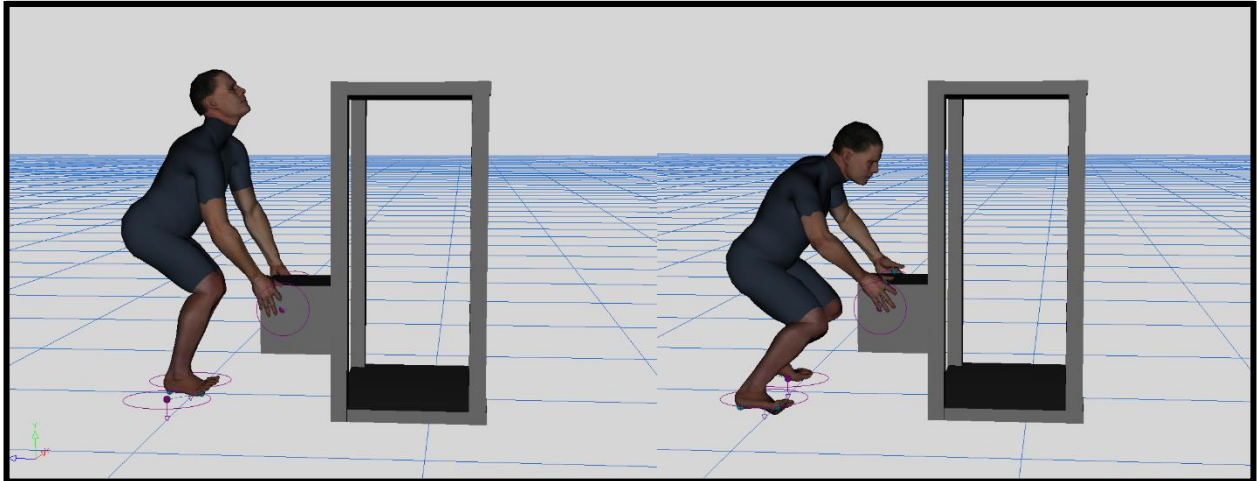
Figure 4. "A" Shows a lifting model with the minimization of maximum joint torque MOO weighting at 100% and B shows the same lifting model with the minimization of discomfort weighting at 100%.

3.0 Purpose, Objectives and Hypotheses

Increased use of DHM can help reduce the time and costs associated with human-systems integration evaluation via physical prototyping. However, to increase DHM use, end-users require a level of fidelity that is sufficient to not only model human kinematic behaviour, but also how that kinematic behaviour changes as a function of the physiological state of the human (i.e., fatigue-state) (Davidson et al., 2021; *Soldier Systems Technology Roadmap: Capstone Report and Action Plan*, 2011). DHM's that rely on multi-objective optimization, as a theoretically sound foundation for posture prediction, may provide the ability to model such state-based effects. However, understanding how to parameterize such models given a specific task, environment or state factor is currently unknown. To address this gap, this thesis explored if a multi-objective optimization-based DHM could be parameterized to predict box lifting behaviours under differing fatigued states. If so, understanding how objective functions and associated weightings change as a function of fatigue will also enhance our broader understand regarding overarching movement control under fatigue.

The purpose of this thesis was to identify the optimal objective function weighting configurations that most accurately simulate the origin and destination postures of floor-to-shoulder lifting relative to experimental data. Secondarily, this thesis aimed to determine if there were systematic changes in optimal weighting configurations when predicting lifting postures in un-fatigued and fatigue states.

Research Question 1: What is the best objective function weighting configuration, considering three objective functions (Minimization of Discomfort, Minimization of Maximum Joint Torque, and Minimization of Total Joint Torque), in order to simulate box lifting origin and destination postures with the least error when compared to experimentally captured postures in both fatigue and unfatigued states?

Research Outcome 1: The best objective function weighting configurations that minimize the normalized root mean squared error between simulated and experimentally captured data at the origin and destination under both fatigued states. It was predicted that the best objective function weighting coefficients would include a combination of non-zero weightings for the three tested objective functions.

Research Question 2: Are the best objective function weighting configurations different between fatigue conditions?

Hypothesis 2: It was hypothesized that the un-fatigued state will show higher weightings for the minimization of discomfort objective function. It is also hypothesized that the fatigued state would show higher weightings for the minimization of maximum joint torque and total joint torque objective functions.

6.0 Methodology

The methodology of this thesis is described in three distinct sections, the experimental methods, the simulation methods, and the statistical methods. The experimental methods describe the fatigue lifting protocol which participants completed (previously collected and used data), the kinematic data conditioning of the lifting protocol, and the fatigue likelihood criteria that were used to include/exclude participants in the simulation portion of this thesis. The simulation methods explain the process of driving the digital humans with motion capture for each participant specific lift posture and fatigue state. The simulation methods also describe the simulation design including the model internal and external constraints, the objective functions which were systematically altered for comparison with the motion capture data, and how the box lifting loads were applied to the simulation. The statistical methods describe the development of an error response surface using a normalized root mean square error (RMSE) between the participant's motion capture and their avatar simulations at the different objective function weightings. The statistical methods also describe the decision criteria used for choosing the multivariate regression models that fit the error response surface for each participant, lift posture and fatigue state. Lastly, a two-way repeated measure Friedman's test is described to address research question 2 which aimed to explore systematic changes in objective function weightings with fatigue state.

6.1 Experimental Methods

6.1.1 Participants

Data were collected from fifteen participants (8 Females, 7 Males) recruited from a university population. Prior to collection, an information letter and informed consent letter was

given to participants. For each participant, demographics information was collected (Table 1) and a Standard Nordic Questionnaire was completed (Kuorinka et al., 1987). The Standard Nordic Questionnaire can be found in Appendix A. This questionnaire ensured that participants did not report pain or injury at the time of collection or in 12 months leading to the collection (exclusion criteria).

Table 1. Participant demographics prior to fatigue-likeliness exclusion.

Demographic	Females (N=8)	Males (N=7)
Age (years)	22.9 ± 3.8	25.1 ± 4.1
Height (cm)	161.3 ± 5.1	178.7 ± 8.8
Weight (kg)	60.5 ± 9.1	68.5 ± 10.8

The study protocol was reviewed by the University of Waterloo Office of Research Ethics Committee and was approved (ORE# 41674).

6.1.2 Motion Capture Instrumentation

Participants were instrumented with whole-body passive reflective markers (Figure 5). Passive reflective markers (14mm) were placed on anatomical landmarks and ten rigid passive reflective marker clusters (four markers for each cluster with the exception of the thigh clusters which had five markers) were affixed to the shank, thigh, pelvis, trunk, upper arm, and lower arm body segments via Velcro straps. Static calibration trials (Vicon, Centennial, Co, USA) were collected with the full reflective marker set after which the rigid clusters remained on the participants for the duration of the lifting task collection and the anatomical landmarks were removed with the exception of the head, hand, radial styloid, ulnar styloid, trunk markers (C7, T7, Xyphoid, and suprasternal notch), and foot markers. The rigid cluster markers were used to track the motion of the anatomical landmark markers based on the static calibration. Box motion within the box lifting task were also tracked using passive reflective markers placed on the four

corners of the box. The passive reflective marker's motions were captured using a 12-camera

Vicon motion capture system (Vicon, Centennial, Co, USA) sampled at 100Hz.
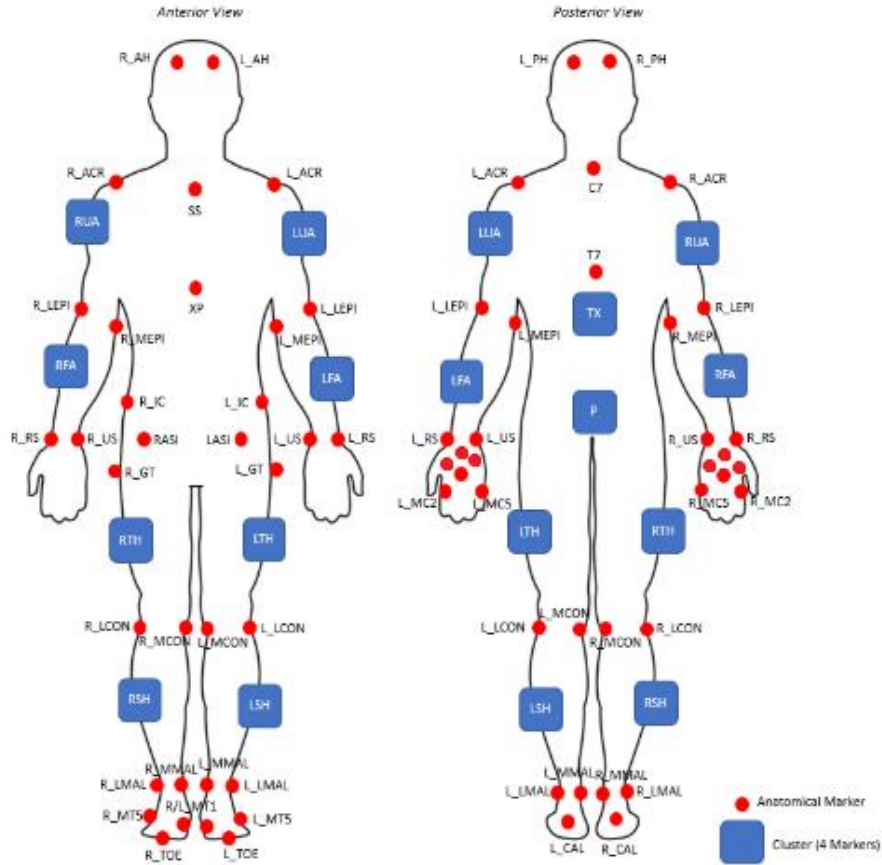
Figure 5. Passive reflective motion capture marker and cluster placement.

6.1.3 Fatigue Lifting Protocol

After completion of the demographics survey and the initial collection questionnaires,

participants were instrumented with anatomical landmark reflective markers and segment

reflective marker clusters. Once the participants were prepared, the collection space was

calibrated, and a static participant calibration trial was collected with participants standing in a

motor bike pose where upper arms are abducted and elbows are flexed to 90 degrees. Participants

completed two-handed floor-to-shoulder height box lifts at a self-selected pace for 60 minutes or until volitional fatigue. Three shelves were set up in succession (Figure 6) and one box was assigned for each of the three shelves, all containing the same load. Each participant's required lifting load corresponded to 30% of their maximum box lifting capacity as determined by the EPIC Lifting Capacity test (Matheson et al., 1995). Participants approached the first shelf, lifted the box from floor-to-shoulder height, and then progressed to the next shelf. After the third shelf lift was complete, the participant walked to a starting line and approached the first shelf again where the boxes were reset to the floor-height by a lab assistant.
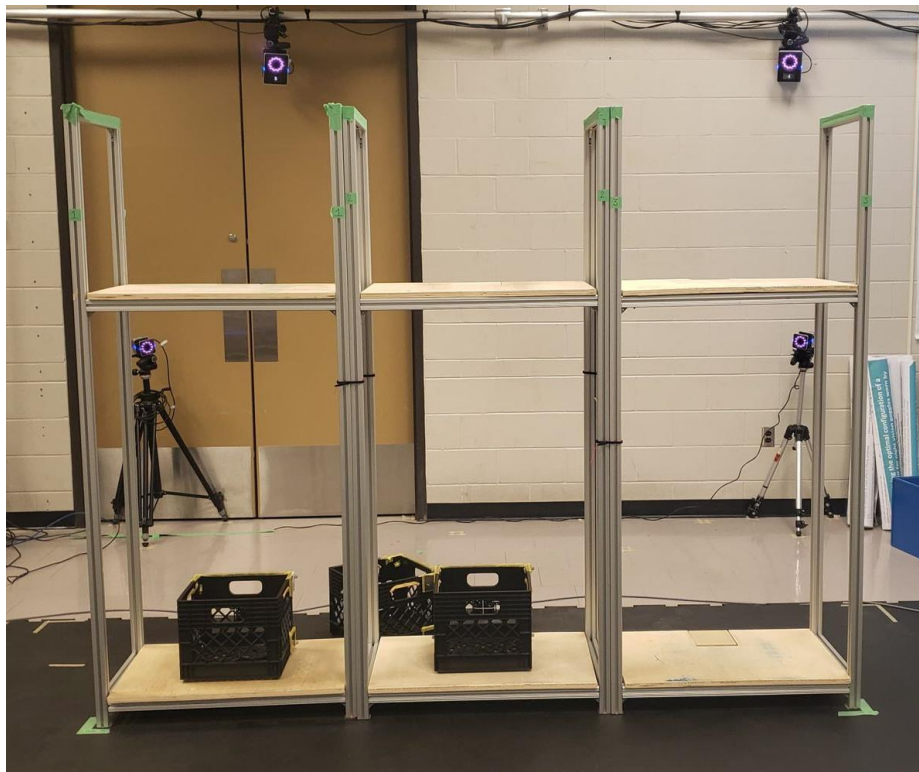
Figure 6. Shows the floor-to-shoulder height box lift set up where participants performed a fatigue lifting protocol.

Following every 15 lifts, participants were asked to provide their rating of perceived exertion (RPE) based on the Borg 6-20 scale (Borg, 1982). Participants were also asked if they

were able to continue the lifting protocol. If the participant was able, they continued the protocol for another 15 lifts. If the participant was not able to continue, the protocol was stopped, and this was identified as volitional fatigue.

6.1.4 Data Processing

Reflective marker data were processed within the Vicon Nexus software (Vicon, Centennial, CO, USA). Marker trajectory gaps were filled using the rigid body fill function which requires the position of three closely related markers (typically from the same cluster) to fill the missing data. When rigid body fill was not an option (less than three associated markers available), pattern fill was used to fill the gap based on one associated marker. If the gap was less than 200ms and rigid body fill and pattern fill were unavailable (no associated marker available), a cubic spline was used to fill the gap in the marker trajectory data. Data quality were visually assessed on two separate occasions, first within the Vicon Nexus software, and second using a custom Python code to plot the three-dimensional trajectory data of all markers (Py27, Spyder v.3.3.6).

After the marker trajectories were fully checked for high quality data, the motion capture data were imported into Visual3D (v.6.01.03, C-Motion, Germantown, MD, USA). Visual3D was first used to create a subject specific kinematic model using the anatomical landmark data from the static calibration trial. The kinematic model included bilateral foot, shank, thigh, upper arm, lower arm, and hand segments, as well as pelvis and trunk segments for each participant. ISB recommendations were followed to define all segment coordinate systems (Wu et al., 2002, 2005). A hip joint center was determined using methods detailed by Bell et al., (1989). The

glenohumeral joint center was projected as 50mm inferior to the acromion along the axial axis of the trunk (Nussbaum & Zhang, 2000).

Visual 3D was used to calculate joint center locations and joint angles. Firstly, all landmark marker data were filtered with a dual-pass 2nd order low pass Butterworth filter with an effective cut-off frequency of 6Hz (Winter, 2009). Using the filtered joint trajectory data, joint center locations and angles were calculated. Joint angles for the ankle knee hip and trunk were exported and used calculate a lifting index, where a Cohen's D measure of effect size was used to characterize kinematic changes from initial (un-fatigued) and final (fatigued) lifts (see section 6.1.5 below). To properly condition the data for avatar motion seeding within Santos (see section 6.2.1 below), projected landmark trajectory data were exported from Visual3D and imported into Vicon Nexus where the data were filtered with a zero-lag 2nd order low pass Butterworth filter with an effective cut-off frequency of 6Hz (Winter, 2009). The data were not dual pass filtered twice. The C3D file format exported from the Visual3D software did not allow filtered landmark data to be exported as a C3D file, where the landmark data were critical to drive the avatar motion. In addition, the data required importing into Vicon Nexus and exported as a C3D file format via the Nexus platform for proper compatibility with Santos Pro.

6.1.5 Defining Fatigue Likelihood Criteria

Although 15 participants completed the repetitive lifting protocol, only those who likely fatigued were included in the analysis. Three critical metrics were used to define fatigue likelihood. The first criteria required participants to complete more than 10 minutes of the lifting protocol. It was assumed that participants who completed less than 10 minutes of box lifting at 30% of their EPIC determined maximum box lift did not have sufficient exposure time to reach a fatigued state. Secondly, the RPE score was used as a decision criterion for inclusion into the

analysis. If participants did not articulate a RPE value greater than 14 by the end of their lifting protocol they were excluded from the simulation portion of the thesis. Jakobsen et al., (2014) found associations between high exertion (>4 on the Borg CR10 scale) and high muscle activity in the trapezius muscle when lifting. A Borg CR10 score of 4 matches a score of 14 on the Borg 6-20 scale used within this collection protocol. In addition, Sundelin and Hagberg, (1992) found that shoulder fatigue development, as defined by a mean power frequency decrease of greater than 8% in participants electromyographic signal (infraspinatus and trapezius), corresponded to Borg 6-20 score changes from 11-14. Combining these results, a RPE value greater than 14 was deemed an appropriate fatigue cut-off.

An additional requirement was required for participants' data to be included within the simulation section of this thesis. Since research question two aimed to identify objective function weighting changes that might occur due to a change in postures with fatigue state; not only did fatigue need to be likely, but also postural differences had to be observed when comparing the earlier lifts (un-fatigued) and the final lifts (likely-fatigued) in the protocol for the likely fatigued participants. To quantify postural differences that likely occurred due to fatigue the magnitude of the postural change from initial lifts to final lifts must be outside of what is considered normal trial-to-trial variability (Frost, Beach, McGill, & Callaghan, 2015). Initial and final lifting postures were characterized using a postural index (Equation 8).

$$Postural\ Index = \frac{Knee\ Joint\ Angle}{Ankle\ Joint + Hip\ Joint + Trunk\ Angle}$$

Equation 8. Shows the modified postural index equation where the inputs are the corresponding joints sagittal plane joint angle in degrees and the output is the postural index ratio.

A postural index value was calculated from sagittal plane joint angles of the ankle, knee, hip and trunk where a value closer to one implies a leg (squat) dominant lifting posture and a value closer to zero implies a back (stoop) dominant lifting posture (Burgess-Limerick & Abernethy, 1997). This calculation is based on the origin posture of a lift. Visual3D joint angle outputs for the frame number than corresponded to the origin of the first 10 lifts and last 10 lifts on shelf #1 were extracted and used to calculate a postural index. Ten lifts were chosen as Frost et al., (2015) found upper and lower limits of kinematic variability were defined successfully in 96% of all instances with 10 trails. To determine if there was a difference within subject's origin postural index values, a Cohen's D effect size calculation (Equation 9) was conducted within SPSS (Version 26, IBM Corp., Armonk, NY). Effect sizes were classified based on the standard effect size scale seen in Table 2 (Cohen, 1992). To be included within the simulation analysis, postural index changes from an un-fatigued state to a likely-fatigue state required a large effect size; therefore, any Cohen's d effect size less than 0.8 was excluded from the study. After combining these inclusion requirements, 5 subjects were removed and 10 were retained.

$$Cohen's\ d\ Effect\ Size = \frac{MeanDifference}{SDofDifference}$$

Equation 9. Shows the Cohen's d Effect Size equation used to quantify postural index differences with fatigue state within subjects.

Table 2. Shows the different Cohen's d effect size threshold values where anything equal to or greater than the defined threshold corresponds to the adjacent effect size definition.

Effect Size Classification	Threshold Value
Small Effect Size	≥ 0.2
Medium Effect Size	≥ 0.5
Large Effect Size	≥ 0.8

6.2 Simulation Methods

6.2.1 Avatar Motion Seeding Configuration

Prior to running simulations, the box lifting origin and destination postures were defined. The origin and destination of the lift was defined using the bottom left box marker position and velocity data, respectively. The box lift origin was defined when the bottom left box tracking marker was displaced by 5cm in the global Z position (using the standard engineering convention) from its resting position on the bottom shelf height. The box lift destination was defined as the frame number when the sum of marker velocities in X, Y and Z axes was equal to zero. This zero-velocity point was defined after peak marker velocity (peak box velocity during the lift). All origin and destination points were checked for accuracy prior to leveraging them to drive postures within Santos. When simulating postures, only the initial and final box lift were used corresponding to the un-fatigued and likely-fatigued states, respectively.

To establish baseline joint angles informed by motion capture, the anatomical landmark trajectory data from the Vicon Nexus software was imported into Santos Pro. Within Santos Pro, anatomical hardpoints (virtual landmark markers) were added to the Santos avatar in an identical manner to the anatomical marker positions on the participants within the experimental protocol. Marker placement was mimicked as closely as possible; however, due to the inability to palpate physical landmarks, some anatomical landmark misplacement errors may have persisted. Using the anthropometric data from the participants the avatars height and weight was scaled to match the anthropometry of each participant. Motion capture data from the relevant anatomical landmarks was paired with their respective virtual anatomical hardpoints to drive the avatars motion herein referred to as motion seeding. To ensure each segment was mapped appropriately onto the avatar, two landmark markers were mapped per segment as the anatomical landmark

mapping works to minimize the error between hardpoints and the input landmark data (mapping example seen in Figure 7 below). If all landmarks were included, priority would be given to segments that included multiple landmark markers such as the pelvis and trunk. Landmark mapping can be seen in Table 3 below. The approach of comparing all relevant joint angles within Santos Pro rather than comparing Santos Pro outputs with a more commonly used biomechanical human modelling software was chosen because it allowed consistency between the number of degrees of freedom that the underlying model contains providing a more direct comparison between simulation and motion capture recorded data. Joint angle data for the ankle, knee, hip, trunk, shoulder, and elbow were extracted for each of their respective degrees of freedom as defined within the model. Resulting data served as the benchmark data against which the optimization-based predicted behaviours were compared.
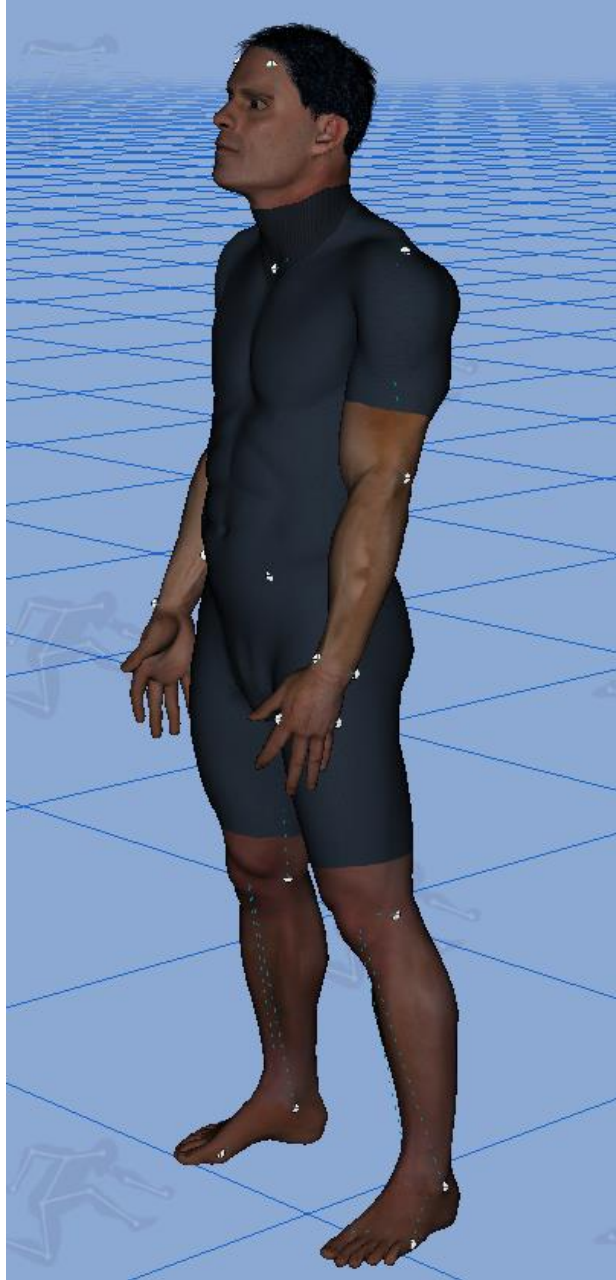
Figure 7. Shows the anatomical hardpoints (white markers) placed on the avatar in the same positions as the anatomical landmark markers of the experimental participants.

Table 3. Shows the which landmark markers were mapped to their associated anatomical hardpoints (virtual landmark markers) for each body segment.

Segment	Landmarks Mapped
Bilateral Foot	1st and 5th Metatarsals
Bilateral Shank	Medial and Lateral Malleoli
Bilateral Thigh	Medial and Lateral Femoral Condyles
Pelvis	Left and Right Anterior Superior Iliac Spines
Trunk	C7 and Center of Manubrium
Clavicle and Shoulder Blade	Left and Right Acromion
Bilateral Upper Arm	Medial and Lateral Epicondyles
Bilateral Lower Arm	Ulnar and Radial Styloid Processes
Bilateral Hand	2nd and 5th Metacarpals

6.2.2 Internal Avatar Constraints

Anthropometry within the Santos Pro software is scalable where link lengths are based on the ISO-3411 (International Organization for Standardization, 2007) anthropometric data and the segment mass proportions are based on the generator of body program data (GEBOD) (Cheng et al., 1994). Each avatar was scaled using the built-in anthropometric surveys previously mentioned. The scaling was based on participant height and weight as extracted from the demographics portion of the experimental data collection.

To ensure simulation differences were due to the objective functions, internal constraints outside of anthropometry remained consistent. Default joint range of motion limit data within Santos Pro were used. In addition, joint torque limits were standardized to the default limits defined within Santos Pro which were obtained from multiple strength studies (Cahalan et al., 1989; Gill et al., 2002; Kaminski et al., 1999; Kumar, 1996). The zero moment point (ZMP)

internal constraint was also included in the box lifting simulation (Matsunaga et al., 2004; Xiang et al., 2007). Zero moment point is a stability constraint assuming that balance is maintained by ensuring the ground reaction force at the feet must be within the individual's base of support. The zero moment point concept was developed mainly for bipedal robot locomotion modelling but has been seen to be effective in simulations of lifting tasks as well (Xiang et al., 2008).

6.2.3 External Avatar Constraints

To create a realistic simulation for comparison with experimentally collected kinematic lifting data, external design constraints are also required. Within Santos these are defined using end-effectors, marker targets, vision marker targets, and point loads. An end-effector is a point that can be linked to any point on the avatar and is designed to interact with a target point defined in space. An end-effector example within Santos Pro can be found in Figure 8 below.
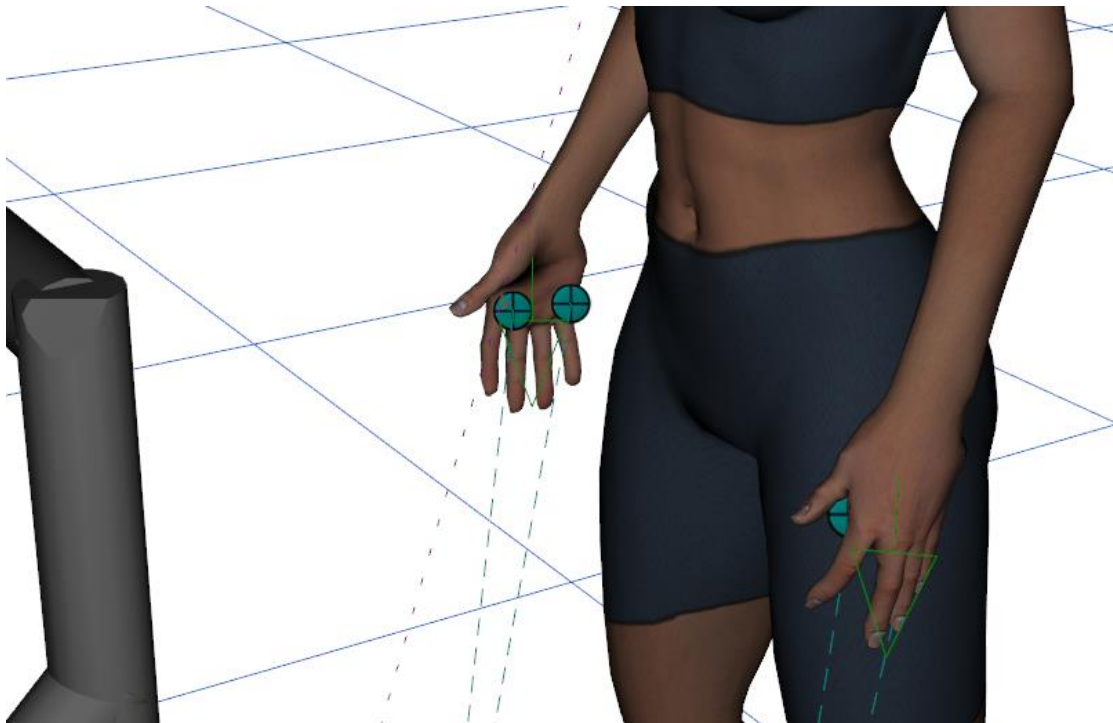

Figure 8. Shows end-effectors within the Santos Pro software (teal circular points).

35

The marker target is a point that the end-effector is constrained to contact and can be placed anywhere within the virtual space. Marker targets can be individual points that a single end-effector must contact, a bounded line where end-effectors are constrained to contact any point on the line, or a bounded plane where end-effectors are constrained to contact any point within the plane. Bounded lines and planes are adjustable in size and orientation to suit a desired goal. An example of a point, bounded line, and bounded plane marker target can be seen in Figure 9 below.
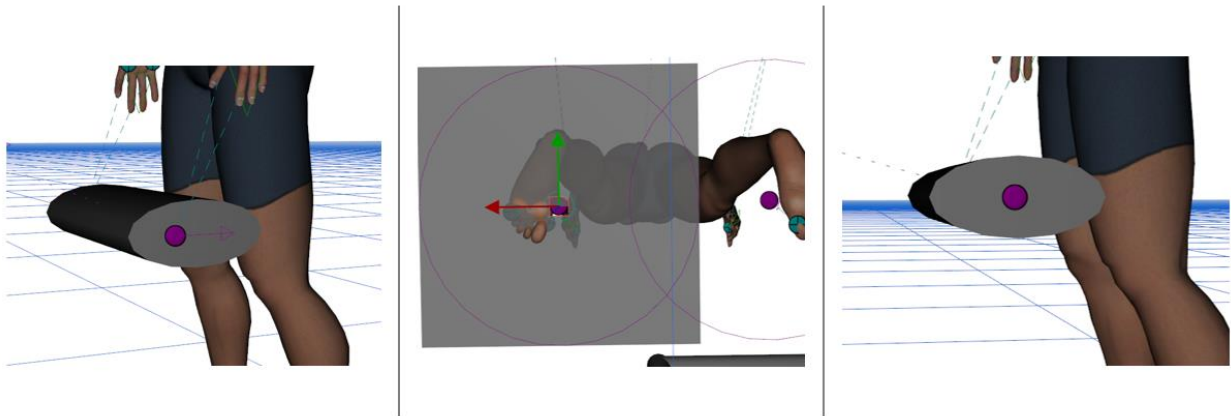
Figure 9. Shows three different marker target types (purple circular points) including the bounded line (left), the bounded plane (middle), and the bounded point (right) marker targets.

Point loads (reaction force vectors) can be applied to the avatar in any orientation. For example, a hand load during a lift can be represented by a point load acting in line with gravity. Point load magnitudes can be adjusted and can be applied bilaterally and unilaterally when applied to limbs. Figure 10 below shows a point load applied to the hand of a Santos Pro avatar.

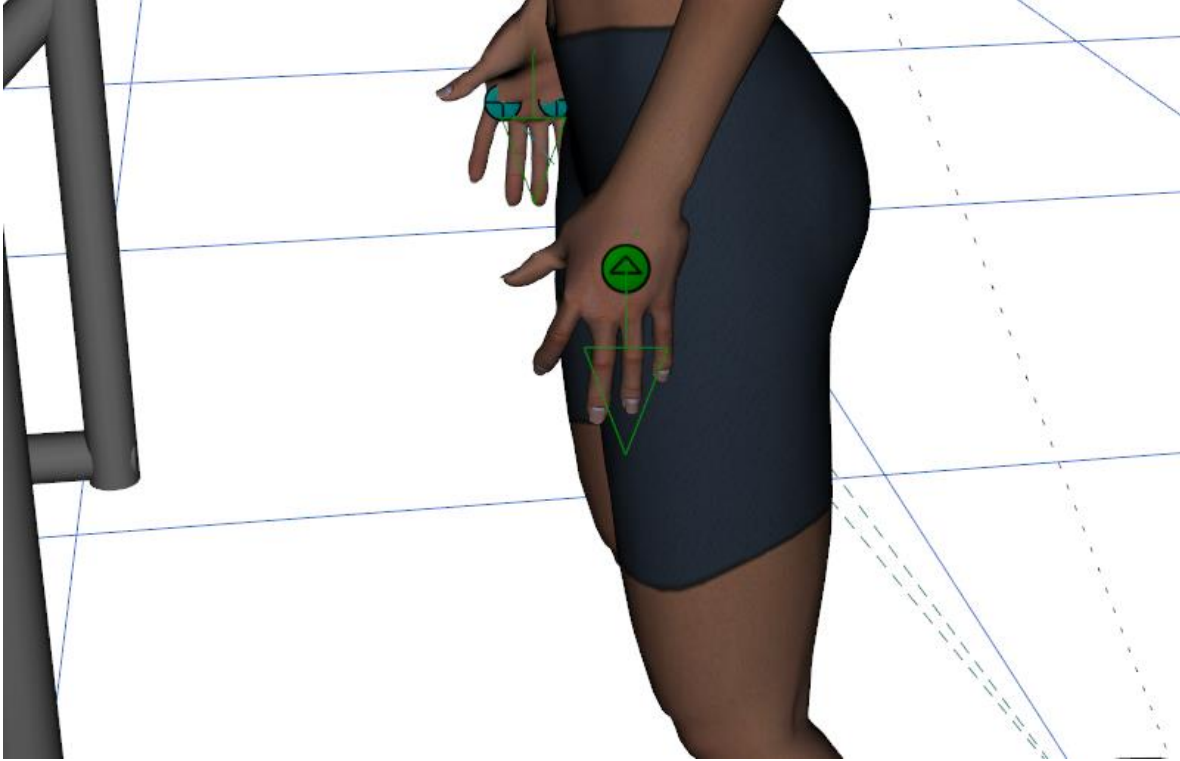Figure 10. Shows a point load vector within the Santos Pro software (green circular point with green vector arrow).

To simulate the box lifting for participants who completed the experimental data collection, end-effectors were placed bilaterally on the avatars 2nd and 5th metacarpal, and 1st and 5th metatarsal. All end-effectors were constrained to corresponding marker targets that were set to the same global position as the passive reflective markers from each participant's experimental data at the origin and destination of the box lift. This effectively constrained the avatar's feet and hands to the same location as the participants, while leaving the rest of the avatar degrees of freedom open to the influence of the objective functions and their assigned weightings.

Within the simulation software, the applied load can influence the posture prediction; therefore, hand forces, by means of point loads, were applied bilaterally to the 3rd metacarpal-

phalangeal joint with the forces acting in line with the global z-axis (in line with gravity). The load was assumed to be equally distributed between left and right hands, and inertial effects of the load were not considered.

The objective functions within Santos Pro have been previously discussed in Section 2.4. In this thesis, three of the available objective functions within the Santos Pro software were evaluated including the minimization of: Discomfort, Maximum Joint Torque, and Total Joint Torque. Joint displacement and effort were not evaluated as the discomfort objective function encompasses similar assumptions while adding objectives such avoiding end ranges of motion. The minimization of the change in potential energy objective function was not evaluated as it was previously found to not be a significant factor in governing human posture control (Marler et al., 2009).

For both origin and destination of the box lift, as well as the un-fatigued and fatigued states (first and last lifts, respectively), objective functions were systematically altered to generate a unique set of postures for each combination of objective functions for each participant. Considering three different objective functions and eleven weighting values (0-100% in 10% increments), 1331 simulations of different objective function weightings were evaluated for each participant within each lift posture and fatigue state. Ankle, knee, hip, trunk, glenohumeral, and elbow joint angle data were retained for comparison with the experimental data.

6.2.4 Statistical Methods

Research Question 1 was addressed using a normalized root mean squared error (RMSE) approach. Firstly, the simulated joint angles for the different degrees of freedom at each joint

38

were subtracted from the experimental seeded joint angles, divided by the total range of motion

for each specific degree of freedom, and squared to output a normalized joint degree of freedom

squared error (Equations 10, 11, 12). These differences were averaged across the different

degrees of freedom within a joint to produce an average squared joint error. For example, the

ankle joint includes two degrees of freedom; therefore, left and right ankle squared errors were

divided by four representing the total number of degrees of freedom bilaterally for the ankle. In

total, six joints were included to present a total joint error similar to methods from Xiang et al.,

(2010). To create the root mean squared error (RMSE), the average of the squared error

differences for each joint were calculated, squared and expressed as a percentage.

$$Normalized\ Joint\ DoF\ Squared\ Error = (\frac{Seeded\ DoF\ \theta\ -\ Simulated\ DoF\ \theta}{DoF\ RoM})^2$$

Equation 10. Shows the calculation for normalized difference between the simulated and motion
seeded joint angles (θ). This calculation was completed for all degrees of freedom (DoF) with
each of their respective ranges of motion (RoM). All normalized differences were squared.

$$Average\ Joint\ Squared\ Error\ (\epsilon)\ = \frac{\sum Normalized\ Joint\ DoF\ Difference}{nDoF}$$

Equation 11. Shows the calculation of the average normalized joint error (ϵ) across all degrees of
freedom within a joint.

$$RMSE\ = \sqrt{\frac{\sum(\epsilon_{Ankle} + \epsilon_{Knee} + \epsilon_{Hip} + \epsilon_{Trunk} + \epsilon_{Shoulder} + \epsilon_{Elbow})}{6}}\ *\ 100$$

Equation 12. Shows the root mean squared error (RMSE) for the combination of six joints of
interest. Where the mean of the six average joint squared errors are calculated and the square
root of that value is found and expressed as a percentage.

Resulting RMSE values were plotted as a function of objective function weightings as

seen in Appendix C. Since RMSE responses were only calculated at a 10% objective function

weighting resolution, the true objective function configuration than results in the lowest error may actually be found between the chosen resolution points. A response surface methodology approach was taken to bypass the computationally cumbersome method of simulating each possible objective function weighting configuration available within the software. The response surface methodology takes a set of measured variables, fits the surface with a multivariate function, and optimizes that function to find a maximum or minimum. The normalized RMSE response surfaces were fit with a function leveraging a multivariate regression (see Equation 11 below for a sample function) (Cecen, 2021). Data were organized into a structure as seen in Table 4 below, where objective function weightings and the associated error response values were used to determine functions which will predict the error response surface for each subject's lift posture and fatigue state. Being a multivariate regression R^2 values were output for linear, quadratic, cubic and quintic powers to determine the best fit. A predicted R^2 was calculated using a leave one out (LOO) cross-validation approach as a metric of model over-fitting, where an over-fit model may not predict new data points with high accuracy. Two criteria were used to determine which regression model's equation would be used to determine the best objective function weighting coefficients. Firstly, the highest R^2 was chosen assuming it was an improvement over the lower power by an R^2 of at least 0.05. Secondly, the highest R^2 was only chosen if the difference between the R^2 and the predicted R^2 was at most 0.05. Once the best regression model was chosen, the associated regression equation was optimized to find the objective function coefficients with the least error (Mathworks, R2020, Natrick, MA). The objective function configuration with the least error as determined by the optimized regression equations were retained for the investigation of Research Question 2 for each participant, lift posture and fatigue state.

$$f = A + BX_1 + \cdots CX_n + DX_1^2 + \cdots EX_n^2 + FX_1X_2 + \cdots GX_{n1}X_{n2}$$

Equation 13. Is a sample polynomial regression equation, adapted from Arora (2017), for modelling an error surface generated using Equation 10 for each objective function weighting where X_{1-3} are the three objective functions being used within the simulations. A, B, C, D, E, F, G are coefficient values within the model determined by the least squares difference between the model predicted error responses and the error responses obtained in Equation 10. Variable n represents a value between one and three corresponding to the different objective functions.

Table 4. Shows the organization of inputs for the regression model where X_{1-3} are the four objective functions being used within the simulations and the error response is the calculated error using Equation 10.

Response Point	X_1	X_2	X_3	Error Response
1	0	10	20	ϵ_{sum1}
2	10	20	30	ϵ_{sum2}
3	20	30	40	ϵ_{sum3}
…	…	…	…	…
1331	100	100	100	$\epsilon_{sum1331}$

A Shapiro-Wilk's test of normality was completed within SPSS to determine if the best objective function weighting coefficients were normally distributed within an objective function (Version 26, IBM Corp., Armonk, NY). Significance was evaluated with an alpha value of 0.05, where a resultant p-value less than 0.05 would mean that the data deviated significantly from the normal distribution. With results that deviate from the normal a Friedman's test is most appropriate. Three repeated measures Friedman's two-way analysis of variance tests were conducted within the SPSS software, one for each objective function weighting. The dependent variables are the best objective function weighting coefficients as determined by the multivariate regression equations and the independent variables are the postures and fatigue states. An alpha

value of less than 0.05 determined if significant differences were detected between an objective

function's weighting coefficients across location or fatigue state conditions.

7.0 Results

7.1 Fatigue Inclusion/Exclusion

Ten participants demonstrated sufficient evidence of fatigue and their data were retained for analysis. A total of five participants demonstrated volitional fatigue, an RPE greater than 14 and a large effect size difference in pre-post postural index values (Table 5). Five other participants completed the full 60-minute protocol; however, on completion time these participants reported an RPE greater than 14 and showed postural index changes which supported their inclusion into the analysis (Table 5). The five remaining participants were excluded. One participant was excluded as they did not meet the completion time of at least 10 minutes, three participants were excluded based on their final RPE score being 14 or less and one participant was excluded for their effect size being less than 0.8. A total of 10 participants (6 Female, 4 Male) were retained for the next phase of analysis (Table 6). Mean and standard deviation postural index scores for each participants' first 10 and last 10 lifts are presented in Appendix B.

Table 5. Shows participant inclusion/exclusion decision criteria where grey boxes indicate which stage in the decision criteria, participants data were excluded from the simulation phase.

Participant	Completion Time (min)	Total Lifts Completed	Final RPE	Postural Index Pre-Post Effect Size	Inclusion Decision (Yes/No)
1	38	333	19	2.38	Yes
2	35	285	20	2.68	Yes
3	60	510	16	1.36	Yes
4	59	615	19	1.26	Yes
5	60	540	17	4.78	Yes
6	60	495	17	1.76	Yes
7	27	255	20	1.4	Yes
8	60	510	18	1.91	Yes
9	60	495	18	1.66	Yes
10	57	345	20	2.23	Yes
11	60	450	17	0.59	No
12	7	60	17	N/A	No
13	60	489	9	0.02	No
14	60	420	14	0.57	No
15	60	450	13	0.81	No

Table 6. Demographics information for the final set of participants included within the simulations section of this thesis.

Demographic	Female (N=6)	Male (N=4)
Age (years)	22.2 ± 4.0	26.8 ± 3.9
Height (cm)	162.2 ± 4.0	176.3 ± 11.5
Weight (kg)	61.9 ± 10.2	64.5 ± 11.0

7.2 Simulation Root Mean Squared Error

RMSE error was plotted as a function of objective function weightings for each participant, specific to each location and fatigue state condition. Figure 11 demonstrates the RMSE error plot for Participant 8, as an example. Remaining plots for each participant in each condition are provided in Appendix C. Based on the exemplar plots least error objective function weighting configurations (dark blue data points) tended to prioritize the minimization of discomfort objective function with minimal contributions of the minimization of maximum and total joint torque objective functions.

Un-Fatigued Origin

Un-Fatigued Destination

Fatigued Origin

Fatigued Destination
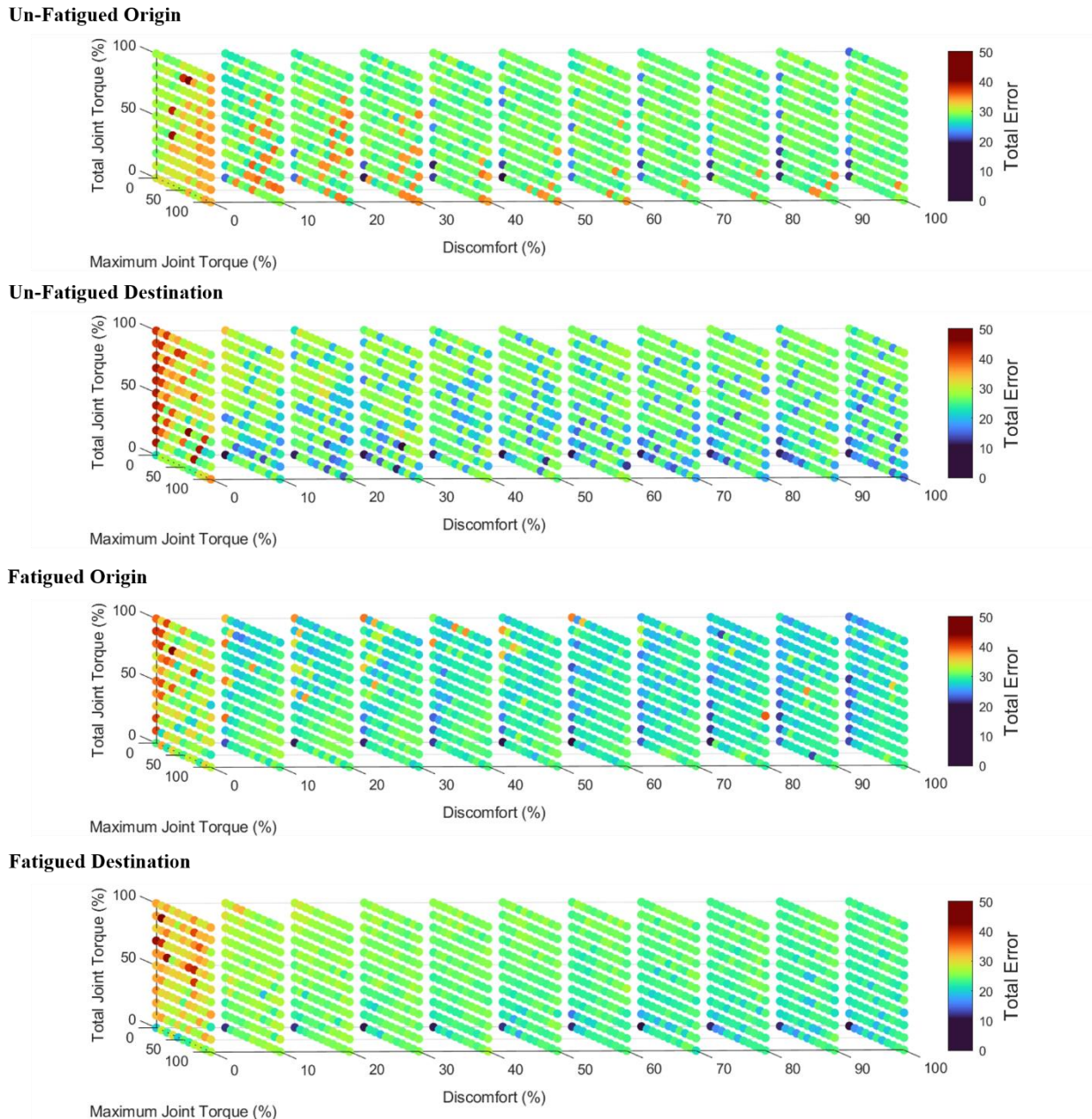
Figure 11. Shows the normalized RMSE error response for participant 8 where each axis represents a respective objective function weighting within the multi-objective optimization model (Santos). The colour bar corresponds to the normalized RMSE calculated at each objective function weighting where dark blue represents the lowest error and dark red represents the highest error.

7.3 Multivariate Polynomial Regressions

Each participant and condition specific RMSE surface was fit using a multivariate regression equation. Models were fit using linear, quadratic, cubic and quintic powers to determine the best model type. The type of model was specific to each RMSE surface where two RMSE surfaces were best fit using a linear model, three using a quadratic model, 13 using a cubic model, and 22 using quintic a model (Table 7). The mean R-squared model fit across all models was 0.50 ± 0.16 (Table 7). Mean predicted R-squared, using the LOO-CV approach across all models was 0.47 ± 0.16 (Table 7). Mean residual RMSE across all models was as $2.51\% \pm 1.06\%$ normalized RMSE (Table 7). Model fits varied between participant and condition. An exemplar scatter plot demonstrates predicted normalized RMSE vs actual normalized RMSE for participant (1) (Figure 12). Remaining model fit plots are provided in Appendix D.

Table 7. Multivariate model statistics for each participant under each condition. PR^2 is the predicted R^2 value calculated with a leave one out cross validation. RMSE is the root mean squared error of the residuals between the actual input values and the model predicted values.

Participant Number	Un-Fatigued Origin				Un-Fatigued Destination			
	Power	R^2	PR^2	RMSE	Power	R^2	PR^2	RMSE
1	4	0.54	0.51	1.57	3	0.53	0.51	2.54
2	4	0.66	0.64	1.74	3	0.62	0.61	2.37
3	2	0.24	0.23	1.63	3	0.73	0.72	1.75
4	2	0.73	0.72	2.50	1	0.27	0.26	5.01
5	4	0.65	0.62	1.57	4	0.50	0.47	2.81
6	3	0.52	0.50	3.14	4	0.67	0.65	1.83
7	1	0.32	0.32	1.99	3	0.24	0.21	3.38
8	4	0.41	0.37	1.83	3	0.36	0.34	4.01
9	4	0.60	0.57	1.23	3	0.40	0.38	3.10
10	4	0.71	0.69	1.58	4	0.68	0.65	2.31

Participant Number	Fatigued Origin				Fatigued Destination			
	Power	R^2	PR^2	RMSE	Power	R^2	PR^2	RMSE
1	4	0.52	0.48	1.69	4	0.45	0.42	3.73
2	4	0.36	0.32	1.94	3	0.61	0.60	3.66
3	3	0.35	0.33	2.91	4	0.67	0.64	1.98
4	4	0.53	0.49	1.48	2	0.26	0.25	5.27
5	3	0.41	0.38	2.26	3	0.35	0.33	5.18
6	4	0.45	0.43	3.82	3	0.47	0.45	2.66
7	4	0.31	0.26	2.26	4	0.62	0.59	1.75
8	4	0.49	0.46	1.95	4	0.73	0.70	1.60
9	4	0.28	0.23	2.27	3	0.35	0.33	2.95
10	4	0.63	0.60	1.20	4	0.73	0.70	1.83
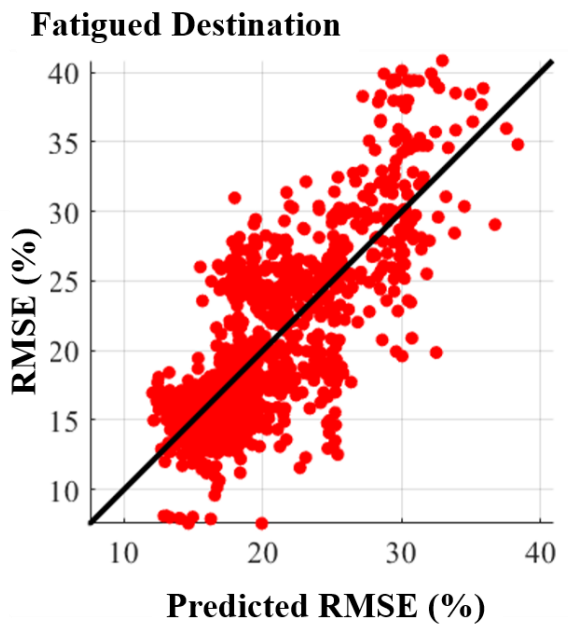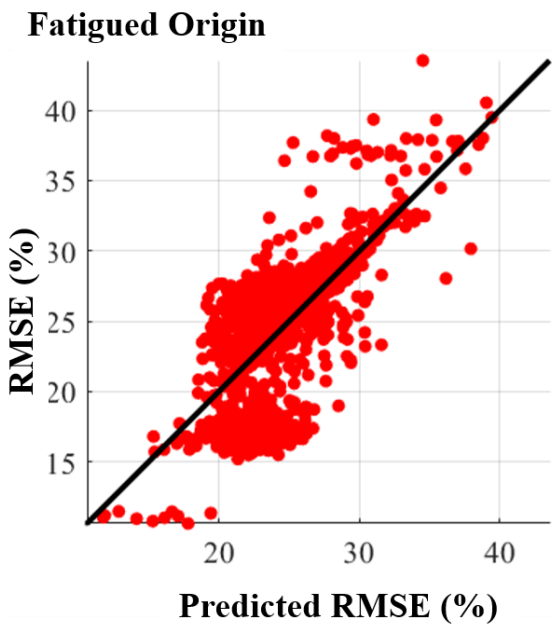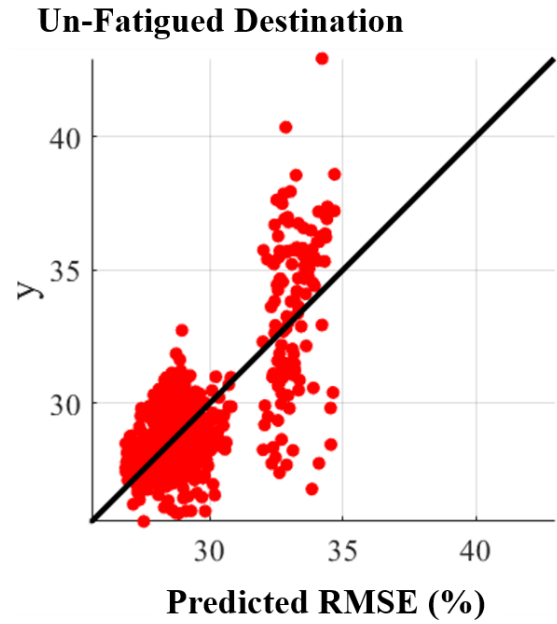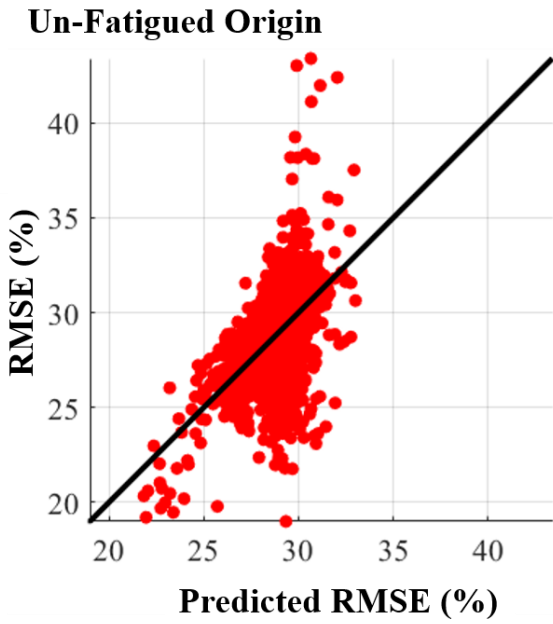
Figure 12. Shows the predicted (x) vs actual (y) plots displaying model fit for participant 8 under each condition. The solid line represents a r-value of 1.

7.4 Predicted Lowest Error

Regression models were optimized to determine the weighting coefficients for each of the three objective functions. Since resultant objective function weighting coefficients were not normally distributed, the median and interquartile range of the regression predicted lowest normalized RMSE for each posture and fatigue state is shown in Figure 13 below. Median optimal weighting for the minimization of discomfort objective function ranged between 50 and 90%, while the median of the minimization of maximum and total joint torque were all 0%. Interquartile range for the minimization of maximum joint torque was 31.2% and 6.1% for the un-fatigued destination and fatigued origin conditions, respectively. Least error objective function weighting coefficients for each participant under each lift posture and fatigue state are shown in Table 8.
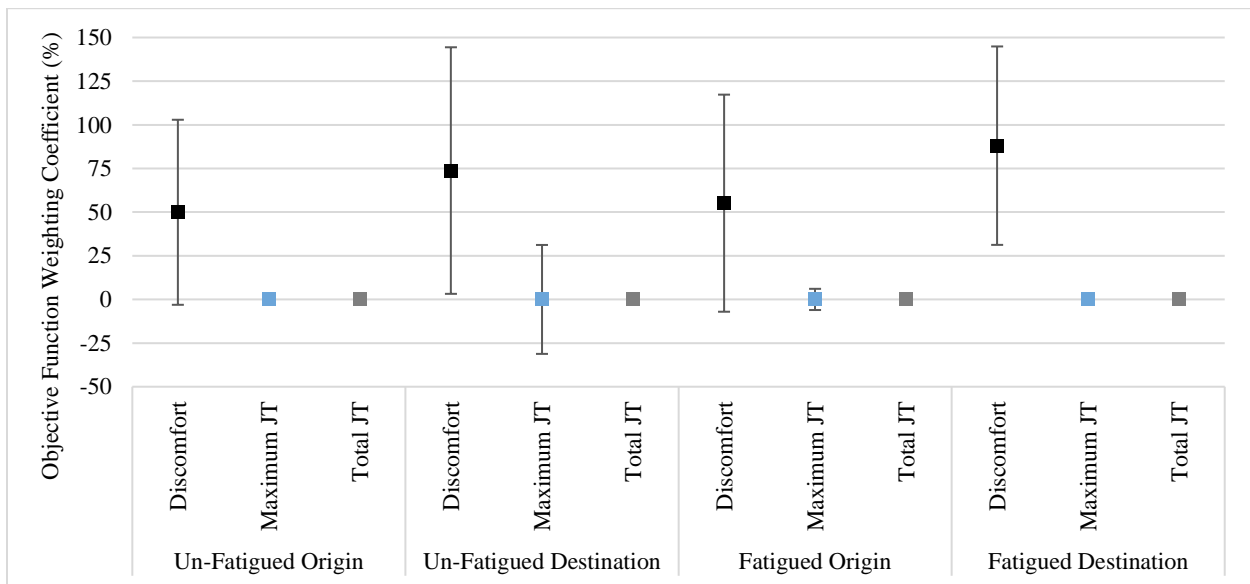
Figure 13. Shows the median and interquartile ranges of objective function weightings which had the lowest regression predicted RMSE between the simulation and experimental data for each posture and fatigue state. JT stands for Joint Torque.

Table 8. Shows the model predicted objective function weighting coefficients to minimize normalized RMSE where Disc is the minimization of discomfort objective function, Max JT in the minimization of maximum joint torque objective function, and Total JT is the minimization of total joint torque objective function.

Participant Number	Un-Fatigued Origin				Fatigued Origin		
	Disc	Max JT	Total JT		Disc	Max JT	Total JT
1	37	0	0		0	0	0
2	32	0	0		0	100	100
3	90	0	0		51	8	0
4	100	0	0		97	0	0
5	50	11	0		59	0	0
6	30	0	0		100	0	0
7	100	0	0		31	0	0
8	83	0	0		96	0	0
9	35	0	0		43	26	0
10	50	15	0		100	0	0

Participant Number	Un-Fatigued Destination				Fatigued Destination		
	Disc	Max JT	Total JT		Disc	Max JT	Total JT
1	26	1	0		38	0	0
2	100	0	0		92	0	0
3	25	0	0		100	0	0
4	100	100	0		88	0	0
5	100	0	0		100	0	0
6	87	0	0		32	0	0
7	16	0	0		88	0	0
8	26	41	0		50	13	0
9	62	49	0		100	0	0
10	86	0	0		38	0	0

7.5 Assessing Systematic Differences with Fatigue State

A Shapiro-Wilk score test of normality was conducted for each objective function under both fatigue states and lift postures. All but two conditions were significantly different from a normal distribution ($\alpha \leq 0.05$) (Table 9). Only discomfort in the un-fatigued origin and fatigue destination conditions were normally distributed where the rest of the data were skewed.

Table 9. Shapiro-Wilk significance score for the multivariate regression model predicted best objective function weightings. The Shapiro-Wilk score was calculated for each objective function, lift posture, and fatigue state. The minimization of discomfort, maximum joint torque, and total joint torque are denoted by "Disc", "Max JT" and "Total JT", respectively.

Posture	Fatigue State	Disc	Max JT	Total JT
Origin	Un-Fatigued	0.087	0.000	0.000
	Fatigued	0.020	0.000	0.000
Destination	Un-Fatigued	0.001	0.000	0.000
	Fatigued	0.062	0.001	0.000

Three pairwise Friedman's tests were conducted, one for each objective function. The Friedman's test summary statistics for each objective function are provided in Table 10. There were no statistically significant differences ($\alpha \leq 0.05$) found across all conditions and objective functions.

Table 10. Friedman's test statistic, degrees of freedom, and statistical significance (p-value) for each objective function which encompasses all conditions. The minimization of discomfort, maximum joint torque, and total joint torque are denoted by "Disc", "Max JT" and "Total JT", respectively.

Objective Function	Disc	Max JT	Total JT
Test Statistic	0.582	3.278	3
Degree of Freedom	3	3	3
Significance	0.901	0.351	0.392

8.0 Discussion

This study revealed that the minimization of discomfort, not maximum or total joint torque, was the objective function responsible for predicting lift origin and destination postures with the least error relative to empirically measured postures. Additionally, fatigue state did not influence the objective function weighting configuration that resulted in the least error. Having one objective function (discomfort) responsible for predicting the least error between simulated and motion capture kinematics is in contrast with our research outcome theory that least error objective function weightings would include a combination of non-zero weightings from all three objective functions. Objective function weighting configurations did not shift from higher weightings of discomfort to higher weightings of maximum and total joint torque when changing from an un-fatigued to a fatigue state posture; thus, hypothesis two was not supported.

8.1 Response Surface Approach to Find Best Objective Function Weightings

Leveraging surface response methodology is a novel approach to estimate the objective function weighting configurations that best predict experimental lifting postures. The goal was to generate a response surface, fit that surface with a function and optimize the function to identify the objective function weighting values of interest. Using a response surface methodology approach not only allowed for an estimate of error response values that lie between the weighting resolution points that were simulated, but also allowed for the visualization of the error response surfaces and quantification of model fit which can provide important insight into how the optimization is functioning. This study is the first to apply an RSM approach to identify optimal weighting function configurations, where past efforts have relied on alternate approaches.

Previous researchers have leveraged other techniques to identify the best objective function weightings to minimize error between simulated and experimental data. Xiang et al., (2010) and Song et al., (2016) both simulated lifting tasks and compared the posture prediction outputs to motion capture to calculate an error response with the goal of determining the objective function weightings with the least error. Xiang et al., (2010) evaluated the minimization of total joint torque and maximization of stability objective functions and Song et al., (2016) evaluated the minimization of maximum joint torque and minimization of motion jerk. Both Xiang et al., (2010) and Song et al., (2016) ran simulations at 10% weighting resolutions to make find the least error objective function weightings between simulated and experimentally captured joint angles. The actual best weightings, however, may lie between resolution points and the response surface method used within this thesis circumvents the limitation of only having a particular simulation resolution by fitting a multivariate function and predicting among all weighting possibilities. Bataineh (2012) used an artificial neural network (ANN) approach to estimate objective function weightings that predict the least error when compared to motion capture data. Similar to how multivariate functions were developed to fit the response surface within this thesis, the ANN approach allows for a function to be fit to the data within the hidden layers. This allowed for the best weighting configurations to be chosen without being limited to a chosen simulation resolution as seen in Xiang et al., (2010) and Song et al., (2016). The ANN approach, however required manual, subjective predictions of the best objective function weightings for different tasks to train the model and the subjectivity of the model training can influence the outputs of the ANN. With the response surface methodology approach no manual estimates of least error objective functions were required to train the model because the model fits the data directly using a regression approach.

8.2 Least Error Objective Function Weightings

Using a single objective function predicted postures with the least error when compared to motion seeded floor-to-shoulder lift origin and destination postures. This result held true regardless of the lift posture or fatigue state. In contrast, previous studies have shown that posture and motions are better predicted when combining various objective functions using the multi-objective optimization approach. Song and colleagues (2016) considered minimizing total joint torque and minimizing smoothness for two-dimensional lift prediction and found that combining these objectives produced more realistic results. Xiang et al., (2010) reported similar conclusions with the kinematics of lifting tasks, where it was observed that the use multiple objective functions simultaneously allow for the better prediction of experimentally captured joint angles. However, neither study considered a discomfort objective, where discomfort is already an inherently a multi-faceted function.

Even though the minimization of discomfort is not a true single objective function, it has previously predicted postures best when combined with other objective functions within a multi-objective optimization problem. Previous studies by Marler et al., (2005b; 2009) still suggest, however, that prediction accuracy of the discomfort objective function can be improved when combined with the minimization of the change in potential energy, a characteristic not considered with the discomfort function. This improved performance was evaluated qualitatively by visual comparison of one subject's reach to target posture; therefore, it is not known how greatly the addition of the second objective function reduced posture prediction error or if more participants would have showed the same result. A separate study did quantitatively investigate an error between motion capture and simulated joint angles while considering four different objective function weighting configurations for the minimization of discomfort, joint

displacement, maximum joint torque, and total joint torque (Bataineh, 2012). Bataineh still found that the best postures were predicted when combining discomfort with other objective functions including the minimization of joint displacement, maximum joint torque, and total joint torque. There are clear discrepancies between the results presented within this thesis and the results found within the relevant body of literature. The differences seen with the approaches in this thesis may be due to the normalized joint angle errors that were considered, the additional degrees of freedom considered within the error calculation used within this thesis, and the overlapping objectives between discomfort and the torque based objective functions.

8.2.1 Joint Error Normalization

The normalization method used when calculating RMSE responses may explain why results from this thesis differed from previous findings. Previous research comparing joint angle errors between experimentally captured data and simulation data used absolute values for their joint angle comparisons (Bataineh, 2012; Song et al., 2016; Xiang et al., 2010). Within this thesis, all joint angles were normalized to the range of motion defined for its respective degree of freedom. The normalization process could prove to be an improvement to previous methods as joint degrees of freedom with a greater range of motion will not dominate the error in the combined error responses. For example, the range of motion for ankle dorsi/plantarflexion is 83 degrees while range of motion for hip flexion/extension is 143 degrees as defined within the Santos model. This means that the hip flexion/extension error has the potential to be much larger than the ankle dorsi/plantarflexion error which can lead to the hip contributing more to a total error value than the ankle. If the objective is to evaluate the accuracy of whole-body error between optimization predicted and motion seeded data normalization should be used to ensure equal weighting of errors across all joint degrees of freedom.

8.2.2 Including All Joint Degrees of Freedom

Inclusion of all joint degrees of freedom when calculating an RMSE value may have led to the prioritization of a single objective function rather than a combination. In this thesis, transverse and frontal planes were of particular importance to consider as the experimental fatigued lifting protocol did not constrain participants to symmetrical lifting motions and participants were free to approach the box and shelf in their own desired manner. The asymmetrical lifting strategies that may have been used by participants implies that frontal and transverse degrees of freedom are likely important components of the lifting motion (Kingma et al., 1998). Unlike the current thesis which evaluated joint angles in up to three dimensions (as available), the majority of previous literature that evaluates objective functions focusses on sagittal plane joint angles (Ayoub, 1998; Song et al., 2016; Xiang et al., 2010). When considering sagittal plane lifting specifically, minimization of maximum joint torque (Ayoub 1998; Song et al., 2016), and minimization of total joint torque (Xiang et al., 2010), were effective at predicting lifting postures. Minimization of maximum and total joint torque objective functions likely performed well for predicting symmetrical lifting tasks and joint angles in the sagittal plane, as these torque based objective functions were initially created with the intention of explaining sagittal plane muscle activations in locomotion (i.e., also a predominantly sagittal plane movement) (Crowninshield & Brand, 1981; Ghista, Toridis, & Srinivasan, 1975; Pedotti, Krishnan, & Stark, 1978). When considering all joint degrees of freedom in the current thesis, the torque based objective functions were not often weighted above zero when predicting the seeded motion. This may imply that transverse and frontal plane degrees of freedom do not optimize for torque based objective functions with lifting tasks and perhaps there is an opportunity for new objective functions to improve non-sagittal joint angle prediction. This also

57

suggests that the joint angles that were adopted by participants during lifting were effectively predicted by the minimization of discomfort.

8.2.3 Discomfort and Torque Objective Function Overlap

Aspects of the minimization of discomfort objective function may overlap with some of the intended goals for the minimization of maximum and total joint torque objective functions. The minimization of discomfort objective function is within itself a kinematics-based MOO problem with three factors that it considers: the tendency to maintain a neutral position, the tendency to move body segments in a sequence (limbs, the spine, and then clavicle), and the tendency to avoid joint limits (Marler et al., 2005). The tendency to avoid joint limits objective may encompass the overarching goals of the minimization of maximum and total joint torque objective functions. Depending on the task being modelled, avoiding joint end ranges of motion may predict postures that reduce the moment arms to joints thereby decreasing the resultant torque. If minimizing the tendency to use joint end ranges of motion indirectly minimizes the torques this may explain why previous research has found minimization of total and maximum joint torques to be good predicters of lifting posture and this thesis did not (Ayoub, 1998; Song et al., 2016; Xiang et al., 2012, 2010). The reason why the torque based objective functions may not have outweighed the discomfort objective function in the opposing way even though they have overlapping objectives, may be due to the added predictive ability that the two additional objectives in the minimization of discomfort considers. In addition, torques for frontal and transverse plane degrees of freedom may not be as high in sagittal plane dominant movements such as a symmetrical box lifting. Since the torques are likely lower, the overarching control mechanism for these degrees of freedom may drift away from a torque consideration whereas the control laws may still try to avoid bringing joints to their end range. Having aspects of torque

58

based objective functions within discomfort may explain why it tended to predict the lowest normalized RMSE between motion seeded and optimization predicted postures.

8.3 Objective Function Weighting Changes with Fatigue

It was hypothesized that objective function weightings would change as participants altered their lifting strategies over the course of the protocol due to fatigue. This objective function change was not observed which may suggest that although participants altered their movement strategy throughout the lifting protocol, they maintained the objective of minimizing discomfort. This does not necessarily suggest, however, that maximum and total joint torque do not play a role in the way human's control movement. Previous research has found these torque based objectives effective at representing lifting tasks (Ayoub, 1998; Song et al., 2016; Xiang et al., 2012, 2010), and as previously discussed the formulation of the discomfort objective function may include aspects of torque based considerations. In addition, discomfort may outperform torque based objective functions when prediction joint angles in the frontal and transverse planes, as the torque based objective functions were originally developed and validating for use in sagittal plane muscles and joint torque optimization (Crowninshield & Brand, 1981; Ghista, Toridis, & Srinivasan, 1975; Pedotti, Krishnan, & Stark, 1978). Thus, sagittal plane joint angles may be controlled by a different set of objectives than the frontal and transverse planes. Future work should investigate this theory by evaluating error prediction performance for specific planes of motion and potentially specific joints individually.

Origin lifting postures of the included participants changed from an un-fatigued to a fatigued state; however, the best objective function weightings to model these postures did not. These findings may suggest that factors other than objective function weightings, such as external constraints, may have compensated for these changes. More specifically, external

constraints were determined based on hand and foot marker locations of the participant's origin

and destination postures. During the collection, participants had the freedom to move their hands

and feet as desired to accomplish the lifting task; thus, the external constraints in the two fatigue

conditions were likely different. If the external constraints between fatigue states were different

for a given participant, the same objective function weighting may predict the different lifting

strategies demonstrated by the postural index differences. If participants hand and foot locations

were constrained to the same locations within the lifting protocol, objective function weighting

changes may have been the primary driver explaining the different lifting postures with fatigue.

8.4 Surface Response Model Fitting

The multivariate polynomial regressions that were used to fit a curved to the normalized

RMSE data had an average R-squared values of 0.50. This means 50% of the normalized RMSE

response data were explained by the model variables (different powers and interaction variables

of the three tested objective functions. For the most accurate predictions a higher R-squared

value is always preferred. It may be the case that competing objectives for different joints or

joint degrees of freedom may have led to a non-uniform response surface that was difficult to

model. For example, at the shoulder height destination of the lift, the elbow and shoulder joint

may have been minimizing the maximum joint torque so when higher weightings of that

objective were applied the total RMSE decreased for those values while the ankle, knee, hip and

trunk may have been minimizing objectives that align more with discomfort which increased the

RMSE response data. These types of competing interests between joints and/or joint degrees of

freedom might support the consideration of joint or joint degree of freedom level optimization

for better predictive capabilities over a whole-body optimization approach. Future research

should investigate objective function weighting performance for different joints and degrees of

freedom for a given task to understand the effects of joint specific optimization for posture prediction.

The normalized RMSE response surface may have been difficult to model using the multivariate regression approach due to special cases where the underlying optimization was forced to find solutions which lies on a constraint plane. Figure 14 below, shows an example of an optimization design space where the possible solutions lies on the beige/textured plane. Constraints (linear and non-linear) are expressed by g and the different minima for the three objective functions (F1, F2, and F3) are represented by the black dots. When examining the F2 minimum and the g1 constraint, the true minimum for F2 is outside of the feasible solution space and the resultant possible solution near the F2 minimum all lie on the line of g1. We believe this type of phenomenon was seen throughout the simulations that were conducted within this thesis. Figure 15 shows a response surface for Participant 4 in the un-fatigued, lift origin condition. At discomfort weightings at and above 80, the normalized RMSE response is consistently the same value. This likely suggests that the true minimum solution for these weighting configurations lie outside of the feasible solution space and a constraint boundary is limiting the posture prediction to that one posture that produces the same RMSE value. This phenomenon was seen on a larger scale in this example; however, it is possible that smaller cases of solutions falling on constraint planes occurred elsewhere within the analysis. This phenomenon creates inconsistencies within the response data which may contribute to the difficulties seen in predicting the error response surfaces.
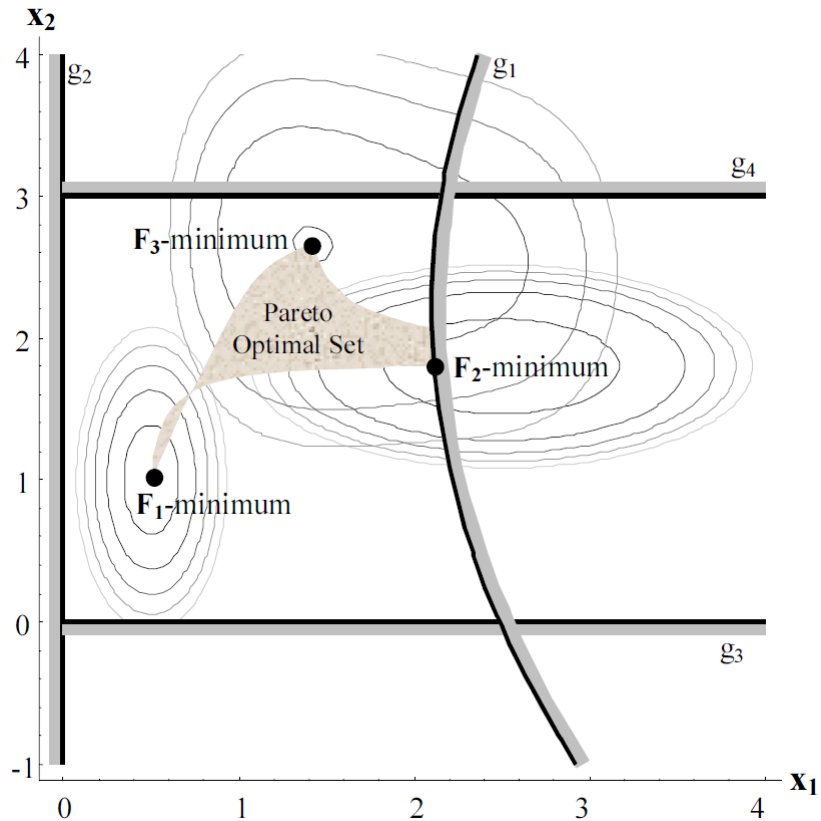
Figure 14. Example design space for an optimization problem obtained from Marler (2005).

Where F1-3 minimum are the different objective function minimum solutions, g1-4 are the linear

and non-linear constraint in the optimization problem, and x1-2 are the design variables which

are being solved for. The beige/textured surface represents the pareto optimal set of potential

solutions between the three objective functions.
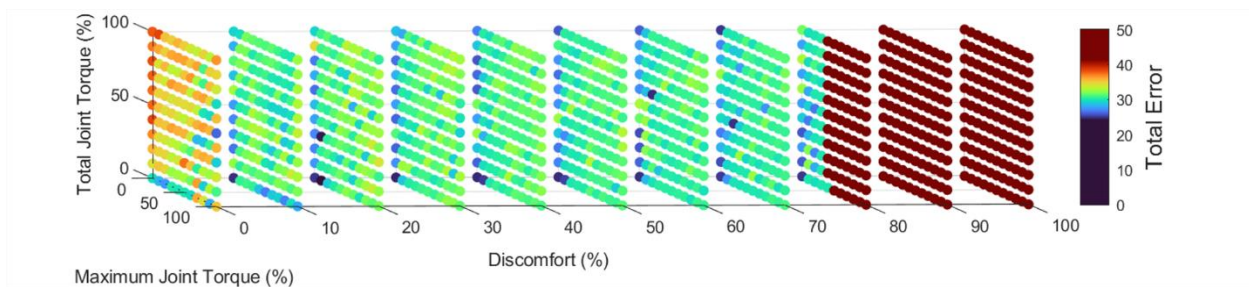
Figure 15. Shows a sample response surface where a constraint plane may have limited the

possible solutions to a single value at or above an 80% weighting for discomfort.

8.5 Impact to Human-In-The-Loop Simulations

The present work is the first of its kind to leverage a response surface methodology to determine the best objective function weightings for modelling human postures. This method can be leveraged when determining objective function weightings for unique tasks while under different physiological states (i.e. fatigue) and environmental conditions (i.e. thermal). Determining the best objective function weightings for unique tasks, states, and environments can lead to a suite of more informed modelling guidelines for optimization-based human-in-the-loop simulation software. Following this, human-in-the-loop software end-users will have the necessary resources to inform objective function weightings which allow for the most accurate predictive kinematic modelling of a variety of relevant tasks, states, and environments of interest. With better predictive models, more weight can be given to the evaluation of human-systems interactions within the virtual environment, leading to decreased reliance on physical prototyping and improved cost effectiveness.

8.6 Limitations

A sample size total of 15 participants were recruited for the experimental protocol within this study and 10 total participants met the fatigue criteria to be included within the simulations and therefore statistical analysis. This may have limited our ability to see potential differences in the least error weighting coefficients for the discomfort objective function from an un-fatigued to a fatigued state. This small sample may have also limited the variability seen within the maximum and total joint torque objective function weightings. In addition to the sample being small, the participants were all recruited within the university and therefore were all university aged. Using various ages may have shown differing results in least error objective function weightings as Song et al., (2016) suggested.

Though experimental participants were excluded if they did not meet the specific fatigue criteria outlined in section 6.1.5, the dependent fatigue factors that were assessed are indirect measures of fatigue. Subject RPE values greater than 14 have been associated with muscle fatigue (Jakobsen et al., 2014; Sundelin & Hagberg, 1992); however, since it is a perception based measure, other factors such as boredom or changes in attention can influence the perceived exertion of a participant other than fatigue. Maximum voluntary efforts of critical muscle groups required in lifting as well as electromyographic signal measurements of those muscle groups would have been more direct ways to quantify and assess participant fatigue states. Additionally, a more directed subjective measure of general fatigue, such as the fatigue visual analog scale, would better compliment maximum voluntary effort and/or electromyography measures.

This study leveraged the postural index as a way to generally quantify lifting strategy change at the origin lift posture (Burgess-Limerick & Abernethy, 1997). Lifting induced fatigue has been shown to produce kinematic lifting strategy changes from an un-fatigued state to a fatigued state (Bonato et al., 2003; Fischer et al., 2015; Fogleman & Smith, 1995; Sparto et al., 1997; Van Dieën et al., 1998). The postural index was used in this study as an effective way to simplify the joint angles into a single measure to be compared across fatigue conditions. All participants that were included within the optimization-based DHM simulations demonstrated a large effect size between the first ten and last ten lift origin postures. Although postural changes were confirmed via postural index changes, postural changes may have been artifacts of factors other than fatigue such as a learning effect over the course of the lifting protocol.

The anthropometry of the digital human model avatar was scaled to the height of the participants based on the ISO-3411 anthropometric survey. Unlike the Visual3D model development, the subject link lengths were only scaled based on participant height rather than

segment lengths as determined by anatomical landmark markers. This difference in segment length estimation may have led to postural differences between the experimentally collected data and the avatar seeded motion data. It is not known the specific segment length errors that were present between the participants and their unique avatars; however, segment length measures or estimates may be useful in the future to scale the avatar segments of interest for improved validity in seeding avatar motion with motion capture.

9.0 Conclusions

A novel surface response methodology approach was leveraged to quantify normalized RMSE between motion-capture seeded postures and multi-objective optimization-based predicted postures with varying objective function weighting coefficients. This approach yielded an individual specific best objective function weighting for the origin and destination postures of a lift under un-fatigued and fatigued states. When identifying the optimal objective function weightings, it was found that the minimization of discomfort alone tended to predict the best postures that match the motion capture data regardless of lift posture or fatigue state and therefore there were no observed systematic changes in objective function weightings with fatigue state. Although torque based objective functions have been reported as effective at predicting sagittal plane joint angles, discomfort may be able to better capture transverse and frontal plane joint angles. The discomfort objective function tendency to avoid joint end ranges of motion may indirectly consider minimizing joint torques which also explains its high prevalence in predicting low errors between motion seeded and optimization predicted postures.

The results from this thesis build on existing literature exploring the optimal control theory and its utility within digital human models. The use of multi-objective optimization-based digital human models is growing as they do not directly rely on pre-recorded motion data to simulate novel tasks. Further research is still needed to build on the existing suite of objective functions to be considered within the models as well as to validate modelling state factors that influence movement such as fatigue. Ultimately, more accurate digital human models which can consider state and environment factor's effects on human kinematics will greatly improve virtual prototype assessments of products and workspaces with humans-in-the-loop.

10.0 References

Abdel-Malek, K., & Arora, J. S. (2013). *Human Motion Simulation: Predictive Dynamics*. Academic Press.

Ahmed, S., Irshad, L., Demirel, H. O., & Tumer, I. Y. (2019). A comparison between virtual reality and digital human modeling for proactive ergonomic design. *Lecture Notes in Computer Science (Including Subseries Lecture Notes in Artificial Intelligence and Lecture Notes in Bioinformatics)*, *11581 LNCS*, 3–21. https://doi.org/10.1007/978-3-030-22216-1_1

Allen, D. G., Lamb, G. D., & Westerblad, H. (2008, January). Skeletal muscle fatigue: Cellular mechanisms. *Physiological Reviews*, Vol. 88, pp. 287–332. https://doi.org/10.1152/physrev.00015.2007

Arendt-Nielsen, L., & Mills, K. R. (1988). Muscle fibre conduction velocity, mean power frequency, mean EMG voltage and force during submaximal fatiguing contractions of human quadriceps. *European Journal of Applied Physiology and Occupational Physiology*, *58*(1–2), 20–25. https://doi.org/10.1007/BF00636598

Arora, J. S. (2017). Additional Topics on Optimum Design. In *Introduction to Optimum Design* (pp. 795–849). https://doi.org/10.1016/b978-0-12-800806-5.00019-6

Ayoub, M. M. (1998). A 2-D simulation model for lifting activities. *Computers and Industrial Engineering*, *35*(3–4), 619–622. https://doi.org/10.1016/s0360-8352(98)00173-9

Bataineh, M. H. (2012). Artificial neural network for studying human performance. *ProQuest Dissertations and Theses*, *1518568*, 179. Retrieved from http://ezproxy.net.ucf.edu/login?url=http://search.proquest.com/docview/1039557097?acco untid=10003%5Cnhttp://sfx.fcla.edu/ucf?url_ver=Z39.88-2004&rft_val_fmt=info:ofi/fmt:kev:mtx:dissertation&genre=dissertations+&+theses&sid=P roQ:ProQuest+Dissertations+&+

Beck, D. J., & Chaffin, D. B. (1992). An evaluation of inverse kinematics models for posture prediction. *Computer Applications in Ergonomics, Occupational Safety and Health*, 329–336.

Bell, A. L., Brand, R. A., & Pedersen, D. R. (1989). Prediction of hip joint centre location from external landmarks. *Human Movement Science*, *8*(1), 3–16. https://doi.org/10.1016/0167-9457(89)90020-1

Berret, B., Delis, I., Gaveau, J., & Jean, F. (2019). Optimality and modularity in human movement: From optimal control to muscle synergies. In *Springer Tracts in Advanced Robotics* (Vol. 124, pp. 105–133). https://doi.org/10.1007/978-3-319-93870-7_6

Bigland-Ritchie, B., & Woods, J. J. (1984). Changes in muscle contractile properties and neural control during human muscular fatigue. *Muscle & Nerve*, *7*(9), 691–699. https://doi.org/10.1002/mus.880070902

Blanchonette, P. (2010). Jack Human Modelling Tool: A Review. *Air Operations Division*, 1–37.

Bonato, P., Ebenbichler, G. R., Roy, S. H., Lehr, S., Posch, M., Kollmitzer, J., & Della Croce, U.

(2003). Muscle Fatigue and Fatigue-Related Biomechanical Changes During a Cyclic Lifting Task. *Spine*, *28*(16), 1810–1820. https://doi.org/10.1097/01.BRS.0000087500.70575.45

Bordegoni, M., & Rizzi, C. (2011). *Innovation in product design: from CAD to virtual prototyping*. https://doi.org/10.1007/978-0-85729-775-4

Borg, G. A. (1982). Psychophysical bases of perceived exertion. *Medicine and Science in Sports and Exercise*, *14*(5), 377–381.

Broman, H., Bilotto, G., & De Luca, C. J. (1985). Myoelectric signal conduction velocity and spectral parameters: Influence of force and time. *Journal of Applied Physiology*, *58*(5), 1428–1437. https://doi.org/10.1152/jappl.1985.58.5.1428

Burgess-Limerick, R., & Abernethy, B. (1997). Toward a quantitative definition of manual lifting postures. *Human Factors*, *39*(1), 141–148. https://doi.org/10.1518/001872097778940632

Cahalan, T. D., Johnson, M. E., Liu, S., & Chao, E. Y. S. (1989). Quantitative measurements of hip strength in different age groups. *Clinical Orthopaedics and Related Research*, (246), 136–145. https://doi.org/10.1097/00003086-198909000-00022

Cashaback, J. G. A., & Cluff, T. (2015). Increase in joint stability at the expense of energy efficiency correlates with force variability during a fatiguing task. *Journal of Biomechanics*, *48*(4), 621–626. https://doi.org/10.1016/j.jbiomech.2014.12.053

Center for Ergnomics. (n.d.). *3DSSPP*. Retrieved from https://c4e.engin.umich.edu/tools-services/3dsspp-software/

Chaffin, D. (2005). Improving digital human modelling for proactive ergonomics in design. *Ergonomics*, *48*(5), 478–491. https://doi.org/10.1080/00140130400029191

Chaffin, D. B. (2009). Some Requirements and Fundamental Issues in Digital Human Modeling. In V. G. Duffy (Ed.), *Handbook of Digital Human Modeling* (pp. 1–10). CRC Press.

Chen, Y. L. (2000). Changes in lifting dynamics after localized arm fatigue. *International Journal of Industrial Ergonomics*, *25*(6), 611–619. https://doi.org/10.1016/S0169-8141(99)00048-7

Cheng, H., Obergefell, L., & Rizer, A. (1994). Generator of body (GEBOD) manual. *Air Force Material Command*.

Cohen, J. (1992). A power primer. *Psychological Bulletin*, *112*(1), 155–159. https://doi.org/10.1037/0033-2909.112.1.155

Crowninshield, R. D., & Brand, R. A. (1981). A physiologically based criterion of muscle force prediction in locomotion. *Journal of Biomechanics*, *14*(11), 793–801. https://doi.org/10.1016/0021-9290(81)90035-X

Damsgaard, M., Rasmussen, J., Christensen, S. T., Surma, E., & de Zee, M. (2006). Analysis of musculoskeletal systems in the AnyBody Modeling System. *Simulation Modelling Practice and Theory*, *14*(8), 1100–1111. https://doi.org/10.1016/j.simpat.2006.09.001

Davidson, J. B., Graham, R. B., Beck, S., Marler, R. T., & Fischer, S. L. (2021). Improving human-in-the-loop simulation to optimize soldier-systems integration. *Applied Ergonomics*, *90*(August 2020), 103267. https://doi.org/10.1016/j.apergo.2020.103267

De Luca, C. J., Roy, A. M., & Erim, Z. (1993). Synchronization of motor-unit firings in several human muscles. *Journal of Neurophysiology*, *70*(5), 2010–2023. https://doi.org/10.1152/jn.1993.70.5.2010

Demirel, H. O., & Duffy, V. G. (2007). Applications of digital human modeling in industry. *Lecture Notes in Computer Science (Including Subseries Lecture Notes in Artificial Intelligence and Lecture Notes in Bioinformatics)*, *4561 LNCS*, 824–832. https://doi.org/10.1007/978-3-540-73321-8_93

Duffy, V. G. (2012). Human Digital Modeling In Design. In G. Salvendy (Ed.), *Handbook of Human Factors and Ergonomics* (Fourth Edi, pp. 1016–1028). Wiley.

Fischer, S. L., Greene, H. P., Hampton, R. H., Cochran, M. G., & Albert, W. J. (2015). Gender-Based Differences in Trunk and Shoulder Biomechanical Changes Caused by Prolonged Repetitive Symmetrical Lifting. *IIE Transactions on Occupational Ergonomics and Human Factors*, *3*(3–4), 165–176. https://doi.org/10.1080/21577323.2015.1034382

Fogleman, M., & Smith, J. L. (1995). The use of biomechanical measures in the investigation of changes in lifting strategies over extended periods. *International Journal of Industrial Ergonomics*, *16*(1), 57–71. https://doi.org/10.1016/0169-8141(94)00087-J

Frost, D. M., Beach, T. A. C., McGill, S. M., & Callaghan, J. P. (2015). A proposed method to detect kinematic differences between and within individuals. *Journal of Electromyography and Kinesiology*, *25*(3), 479–487. https://doi.org/10.1016/j.jelekin.2015.02.012

Gandevia, S. C. (2001). Spinal and supraspinal factors in human muscle fatigue. *Physiological Reviews*, Vol. 81, pp. 1725–1789. https://doi.org/10.1152/physrev.2001.81.4.1725

Gates, D. H., & Dingwell, J. B. (2008). The effects of neuromuscular fatigue on task performance during repetitive goal-directed movements. *Experimental Brain Research*, *187*(4), 573–585. https://doi.org/10.1007/s00221-008-1326-8

Ghista, D. N., Toridis, T. G., & Srinivasan, T. M. (1976). Human gait analysis: determination of instantaneous joint reactive forces, muscle forces and the stress distribution in bone segments. *Biomedical Tech*, *21*(2), 66–74.

Ghista, Dhanjoo N., Toridis, T. G., & Srinivasan, T. M. (1975). Human Gait Analysis: Determination of instantaneous joint reactive forces, muscle forces and the stress distribution in bone Segments Part l. *Biomedical Engineering/Biomedizinische Technik*, *20*(6), 204–213. https://doi.org/10.1515/bmte.1975.20.6.204

Gill, P. E., Murray, W., & Saunders, M. A. (2002). SNOPT: an SQP algorithm for large-scale constrained optimization. *SIAM Journal on Optimization*, *4*(12), 979–1006.

International Organization for Standardization. (2007). *ISO 3411*. ISO.

Jakobsen, M. D., Sundstrup, E., Persson, R., Andersen, C. H., & Andersen, L. L. (2014). Is Borg's perceived exertion scale a useful indicator of muscular and cardiovascular load in

blue-collar workers with lifting tasks? A cross-sectional workplace study. *European Journal of Applied Physiology*, *114*(2), 425–434. https://doi.org/10.1007/s00421-013-2782-9

Jin, W., Kulic, D., Lin, J. F.-S., Mou, S., & Hirche, S. (2019). Inverse Optimal Control for Multiphase Cost Functions. *IEEE Transactions on Robotics*, *PP*, 1–1. https://doi.org/10.1109/tro.2019.2926388

Jun, C., Lee, J. Y., Kim, B. H., & Noh, S. Do. (2019). Automatized modeling of a human engineering simulation using Kinect. *Robotics and Computer-Integrated Manufacturing*, *55*, 259–264. https://doi.org/10.1016/j.rcim.2018.03.014

Kaminski, T. W., Perrin, D. H., & Gansneder, B. M. (1999). Eversion Strength Analysis of Uninjured and Functionally Unstable Ankles. *Journal of Athletic Training*, *34*(3), 239–245.

Kingma, I., De Looze, M. P., Van Dieën, J. H., Toussaint, H. M., Adams, M. A., & Baten, C. T. M. (1998). When is a lifting movement too asymmetric to identify lowback loading by 2-D analysis? *Ergonomics*, *41*(10), 1453–1461. https://doi.org/10.1080/001401398186207

Kumar, S. (1996). Isolated planar trunk strengths measurement in normals: Part III - Results and database. *International Journal of Industrial Ergonomics*, *17*(2), 103–111. https://doi.org/10.1016/0169-8141(95)00042-9

Kuorinka, I., Jonsson, B., Kilbom, A., Vinterberg, H., Biering-Sørensen, F., Andersson, G., & Jørgensen, K. (1987). Standardised Nordic questionnaires for the analysis of musculoskeletal symptoms. *Applied Ergonomics*, *18*(3), 233–237. https://doi.org/10.1016/0003-6870(87)90010-X

Li, W., Todorov, E., & Pan, X. (2004). Hierarchical optimal control of redundant biomechanical systems. *Annual International Conference of the IEEE Engineering in Medicine and Biology - Proceedings*, *26 VI*, 4618–4621. https://doi.org/10.1109/iembs.2004.1404280

Li, Y., Delfs, N., Mårdberg, P., Bohlin, R., & Carlson, J. S. (2018). On motion planning for narrow-clearance assemblies using virtual manikins. *Procedia CIRP*, *72*, 790–795. https://doi.org/10.1016/j.procir.2018.03.181

Ma, L., Zhang, W., Chablat, D., Bennis, F., & Guillaume, F. (2009). Multi-objective optimisation method for posture prediction and analysis with consideration of fatigue effect and its application case. *Computers and Industrial Engineering*, *57*(4), 1235–1246. https://doi.org/10.1016/j.cie.2009.06.003

Marler, R. T., & Arora, J. S. (2010). The weighted sum method for multi-objective optimization: New insights. *Structural and Multidisciplinary Optimization*, *41*(6), 853–862. https://doi.org/10.1007/s00158-009-0460-7

Marler, R. T., Arora, J. S., Yang, J., Kim, H. J., & Abdel-Malek, K. (2009). Use of multi-objective optimization for digital human posture prediction. *Engineering Optimization*, *41*(10), 925–943. https://doi.org/10.1080/03052150902853013

Marler, Tim, Knake, L., & Johnson, R. (2011). Optimization-based posture prediction for analysis of box lifting tasks. *Lecture Notes in Computer Science (Including Subseries Lecture Notes in Artificial Intelligence and Lecture Notes in Bioinformatics)*, *6777 LNCS*,

151–160. https://doi.org/10.1007/978-3-642-21799-9_17

Marler, Timothy. (2005). *A STUDY OF MULTI-OBJECTIVE OPTIMIZATION METHODS FOR ENGINEERING APPLICATIONS*. Retrieved from http://dx.doi.org/10.1016/j.cirp.2016.06.001%0Ahttp://dx.doi.org/10.1016/j.powtec.2016.12 .055%0Ahttps://doi.org/10.1016/j.ijfatigue.2019.02.006%0Ahttps://doi.org/10.1016/j.matlet .2019.04.024%0Ahttps://doi.org/10.1016/j.matlet.2019.127252%0Ahttp://dx.doi.o

Marler, Timothy, Rahmatalla, S., Shanahan, M., & Abdel-Malek, K. (2005). A new discomfort function for optimization-based posture prediction. *SAE Technical Papers*, (724). https://doi.org/10.4271/2005-01-2680

Marler, Timothy, Yang, J., Arora, J. S., & Abdel-Malek, K. (2005). Study of bi-criterion upper body posture prediction using pareto optimal sets. *Proceedings of the IASTED International Conference on Modelling, Simulation, and Optimization*, *2005*, 229–234.

Matheson, L. N., Mooney, V., Grant, J. E., Affleck, M., Hall, H., Melles, T., … McIntosh, G. (1995). A Test to Measure Lift Capacity of Physically Impaired Adults Part 1— Development and Reliability Testing. *Spine*, *20*(19), 2119–2129. https://doi.org/10.1097/00007632-199510000-00010

Matsunaga, N., Okimura, Y., & Kawaji, S. (2004). Kinematic analysis of human lifting movement for biped robot control. *International Workshop on Advanced Motion Control, AMC*, 421–426. https://doi.org/10.1109/amc.2004.1297906

Matthews, G., & Hancock, P. A. (2017). *The Handbook of Operator Fatigue*. CRC Press.

Mi, Z., Yang, J., & Abdel-Malek, K. (2009). Optimization-based posture prediction for human upper body. *Robotica*, *27*(4), 607–620. https://doi.org/10.1017/S0263574708004992

Miller, R. H., Umberger, B. R., Hamill, J., & Caldwell, G. E. (2012). Evaluation of the minimum energy hypothesis and other potential optimality criteria for human running. *Proceedings of the Royal Society B: Biological Sciences*, *279*(1733), 1498–1505. https://doi.org/10.1098/rspb.2011.2015

NATO RTO Technical Task Group 019. (2009). *Optimizing Operational Physical Fitness*. https://doi.org/10.14339/RTO-TR-HFM-080

NexGen Ergonomics Inc. (1997). *HumanCAD*. Retrieved from http://www.nexgenergo.com/ergonomics/humancad_prods.html

Nguyen, V. Q., Johnson, R. T., Sup, F. C., & Umberger, B. R. (2019). Bilevel Optimization for Cost Function Determination in Dynamic Simulation of Human Gait. *IEEE Transactions on Neural Systems and Rehabilitation Engineering*, *27*(7), 1426–1435. https://doi.org/10.1109/TNSRE.2019.2922942

Nibbeling, N., Oudejans, R. R. D., Ubink, E. M., & Daanen, H. A. M. (2014). The effects of anxiety and exercise-induced fatigue on shooting accuracy and cognitive performance in infantry soldiers. *Ergonomics*, Vol. 57, pp. 1366–1379. https://doi.org/10.1080/00140139.2014.924572

Noakes, T. D., & Gibson, A. S. C. (2004, October). Logical limitation to the "catastrophe"

models of fatigue during exercise in humans. *British Journal of Sports Medicine*, Vol. 38, pp. 648–649. https://doi.org/10.1136/bjsm.2003.009761

Nussbaum, M. A., & Zhang, X. (2000). Heuristics for locating upper extremity joint centres from a reduced set of surface markers. *Human Movement Science*, *19*(5), 797–816. https://doi.org/10.1016/S0167-9457(00)00020-8

O'Brien, P. R., & Potvin, J. R. (1997). Fatigue-related EMG responses of trunk musctes to a prolonged, isometric twist exertion. *Clinical Biomechanics*, *12*(5), 306–313. https://doi.org/10.1016/s0268-0033(97)00013-2

Pandy, M. G., & Zajac, F. E. (1991). Optimal muscular coordination strategies for jumping. *Journal of Biomechanics*, *24*(1), 1–10. https://doi.org/10.1016/0021-9290(91)90321-D

Pedotti, A., Krishnan, V. V., & Stark, L. (1978). Optimization of Muscle-Force Sequencing in Human locomotion. *Mathematical Biosciences*, 57–76.

Petrofsky, J. S. (1979). Frequency and amplitude analysis of the EMG during exercise on the bicycle ergometer. *European Journal of Applied Physiology and Occupational Physiology*, *41*(1), 1–15. https://doi.org/10.1007/BF00424464

Psek, J. A., & Cafarelli, E. (1993). Behavior of coactive muscles during fatigue. *Journal of Applied Physiology*, *74*(1), 170–175. https://doi.org/10.1152/jappl.1993.74.1.170

Reeves, N. P., Cholewicki, J., Milner, T., & Lee, A. S. (2008). Trunk antagonist co-activation is associated with impaired neuromuscular performance. *Experimental Brain Research*, *188*(3), 457–463. https://doi.org/10.1007/s00221-008-1378-9

SantosHuman Inc. (n.d.). *SANTOS^{TM} ENGINE - SOFTWARE USER GUIDE* (pp. 1–390). pp. 1–390. Mount Vernon, Iowa: SantosHuman Inc.

Scott, S. H. (2004, July). Optimal feedback control and the neural basis of volitional motor control. *Nature Reviews Neuroscience*, Vol. 5, pp. 532–544. https://doi.org/10.1038/nrn1427

Singh, N. B., Arampatzis, A., Duda, G., Heller, M. O., & Taylor, W. R. (2010). Effect of fatigue on force fluctuations in knee extensors in young adults. *Philosophical Transactions of the Royal Society A: Mathematical, Physical and Engineering Sciences*, *368*(1920), 2783–2798. https://doi.org/10.1098/rsta.2010.0091

Soldier Systems Technology Roadmap: Capstone Report and Action Plan. (2011). Ottawa.

Song, J., Qu, X., & Chen, C. H. (2016). Simulation of lifting motions using a novel multi-objective optimization approach. *International Journal of Industrial Ergonomics*, *53*, 37–47. https://doi.org/10.1016/j.ergon.2015.10.002

Sparrow, W. A., & Newell, K. M. (1998). Metabolic energy expenditure and the regulation of movement economy. *Psychonomic Bulletin and Review*, *5*(2), 173–196. https://doi.org/10.3758/BF03212943

Sparto, P. J., Parnianpour, M., Reinsel, T. E., & Simon, S. (1997). The effect of fatigue on multijoint kinematics and load sharing during a repetitive lifting test. *Spine*, *22*(22), 2647–

2654. https://doi.org/10.1097/00007632-199711150-00013

Sundelin, G., & Hagberg, M. (1992). Electromyographic signs of shoulder muscle fatigue in repetitive arm work paced by the Methods-Time Measurement system. Retrieved January 28, 2021, from Scandinavian Journal of Work, Environment and Health website: https://www.jstor.org/stable/40966004?seq=1#metadata_info_tab_contents

Todorov, E. (2004, September). Optimality principles in sensorimotor control. *Nature Neuroscience*, Vol. 7, pp. 907–915. https://doi.org/10.1038/nn1309

Todorov, E., & Jordan, M. I. (2002). Optimal feedback control as a theory of motor coordination. *Nature Neuroscience*, *5*(11), 1226–1235. https://doi.org/10.1038/nn963

Van Dieën, J. H., Van Der Burg, P., Raaijmakers, T. A. J., & Toussaint, H. M. (1998). Effects of repetitive lifting on kinematics: Inadequate anticipatory control or adaptive changes? *Journal of Motor Behavior*, *30*(1), 20–32. https://doi.org/10.1080/00222899809601319

Vøllestad, N. K. (1997). Measurement of human muscle fatigue. *Journal of Neuroscience Methods*, *74*(2), 219–227.

Westerblad, H., Bruton, J. D., Allen, D. G., & Lannergren, J. (2000). Functional significance of Ca2+ in long-lasting fatigue of skeletal muscle. *European Journal of Applied Physiology*, *83*(2–3), 166–174. https://doi.org/10.1007/s004210000275

Westerblad, Håkan, Allen, D. G., & Lännergren, J. (2002). Muscle Fatigue: Lactic Acid or Inorganic Phosphate the Major Cause? *Physiology*, *17*(1), 17–21. https://doi.org/10.1152/physiologyonline.2002.17.1.17

Winter, D. A. (2009). *Biomechanics and motor control of human movement*. John Wiley & Sons.

Winter, David A. (1976). Biomechanical Model Relating EMG to Changing Isometric Tension. *Digest of the 11th International Conference on Medical and Biological Engineering*, 362–363. Ottawa.

Wu, G., Siegler, S., Allard, P., Kirtley, C., Leardini, A., Rosenbaum, D., … Stokes, I. (2002, April 1). ISB recommendation on definitions of joint coordinate system of various joints for the reporting of human joint motion - Part I: Ankle, hip, and spine. *Journal of Biomechanics*, Vol. 35, pp. 543–548. https://doi.org/10.1016/S0021-9290(01)00222-6

Wu, G., Van Der Helm, F. C. T., Veeger, H. E. J., Makhsous, M., Van Roy, P., Anglin, C., … Buchholz, B. (2005). ISB recommendation on definitions of joint coordinate systems of various joints for the reporting of human joint motion - Part II: Shoulder, elbow, wrist and hand. *Journal of Biomechanics*, *38*(5), 981–992. https://doi.org/10.1016/j.jbiomech.2004.05.042

Xia, T., & Frey Law, L. A. (2008). A theoretical approach for modeling peripheral muscle fatigue and recovery. *Journal of Biomechanics*, *41*(14), 3046–3052. https://doi.org/10.1016/j.jbiomech.2008.07.013

Xiang, Y., Chung, H. J., Mathai, A., Rahmatalla, S., Kim, J., Marler, T., … Obusek, J. (2007). Optimization-based dynamic human walking prediction. *SAE Technical Papers*, (724). https://doi.org/10.4271/2007-01-2489

Xiang, Yujiang, Arora, J. S., & Abdel-Malek, K. (2012). 3D human lifting motion prediction with different performance measures. *International Journal of Humanoid Robotics*, *9*(2). https://doi.org/10.1142/S0219843612500120

Xiang, Yujiang, Arora, J. S., Rahmatalla, S., Marler, T., Bhatt, R., & Abdel-Malek, K. (2010). Human lifting simulation using a multi-objective optimization approach. *Multibody System Dynamics*, *23*(4), 431–451. https://doi.org/10.1007/s11044-009-9186-y

Xiang, Yujiang, Rahmatalla, S., Chung, H. J., Kim, J., Bhatt, R., Mathai, A., … Obusek, J. P. (2008). Optimization-based dynamic human lifting prediction. *SAE Technical Papers*. https://doi.org/10.4271/2008-01-1930

Yang, J. (2009). Human Modeling and Simulation. In V. G. Duffy (Ed.), *Handbook of Digital Human Modeling* (pp. 1–23). Taylor & Francis.

Yang, J., Marler, R. T., Kim, H., Arora, J. S., & Abdel-Malek, K. (2004). Multi-objective optimization for upper body posture prediction. *Collection of Technical Papers - 10th AIAA/ISSMO Multidisciplinary Analysis and Optimization Conference*, *4*, 2288–2305. https://doi.org/10.2514/6.2004-4506

Yang, J., Marler, T., & Rahmatalla, S. (2011). Multi-objective optimization-based method for kinematic posture prediction: Development and validation. *Robotica*, *29*(2), 245–253. https://doi.org/10.1017/S026357471000010X

Yettram, A. L., & Jackman, M. J. (1982). Structural analysis for the forces in the human spinal column and its musculature. *Journal of Biomedical Engineering*, *4*(2), 118–124. https://doi.org/10.1016/0141-5425(82)90072-3

Zhu, W., Fan, X., & Zhang, Y. (2019). Applications and research trends of digital human models in the manufacturing industry. *Virtual Reality & Intelligent Hardware*, *1*(6), 558–579. https://doi.org/10.1016/j.vrih.2019.09.005

11.0 Appendices
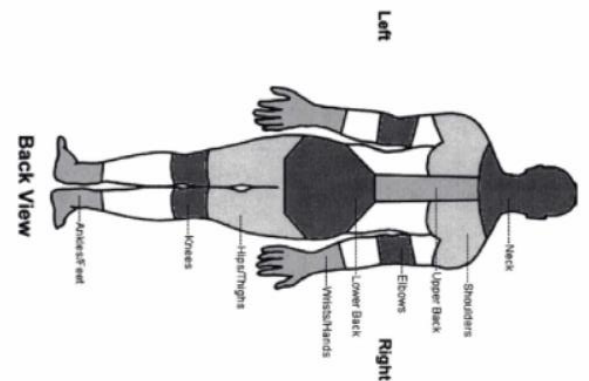
11.1 Appendix A

Mine: _____

Initial of first name: _____   Initial of last name: _____   Last 4 digits of social security number: _____   Immediate Supervisor: _____   Date: ___/___/___

Job Title: _____   Section: _____   Gender: M   F   Age: _____   Height: _____ ft. _____ in.   Weight: _____

How long have you been doing this job? _____ years _____ months   On average, how many hours do you work each week? _____

Left

Back View

Right

Neck — Shoulders — Upper Back — Elbows — Lower Back — Wrists/Hands — Hips/Thighs — Knees — Ankles/Feet

To be answered by everyone		To be answered by those who have had trouble	
Have you at any time during **the last 12 months** had trouble (ache, pain, discomfort, numbness) in:		Have you at any time during the **last 12 months** been **prevented from doing your normal work** (at home or away from home) because of the trouble?	Have you had trouble at any time during **the last 7 days?**
Neck			
☐ No	☐ Yes	☐ No ☐ Yes	☐ No ☐ Yes
Shoulders			
☐ No	☐ Yes, right shoulder ☐ Yes, left shoulder ☐ Yes, both shoulders	☐ No ☐ Yes	☐ No ☐ Yes
Elbows			
☐ No	☐ Yes, right elbow ☐ Yes, left elbow ☐ Yes, both elbows	☐ No ☐ Yes	☐ No ☐ Yes
Wrists/Hands			
☐ No	☐ Yes, right wrist/hand ☐ Yes, left wrist/hand ☐ Yes, both wrists/hands	☐ No ☐ Yes	☐ No ☐ Yes
Upper Back			
☐ No	☐ Yes	☐ No ☐ Yes	☐ No ☐ Yes
Lower Back (small of back)			
☐ No	☐ Yes	☐ No ☐ Yes	☐ No ☐ Yes
One or Both Hips/Thighs			
☐ No	☐ Yes	☐ No ☐ Yes	☐ No ☐ Yes
One or Both Knees			
☐ No	☐ Yes	☐ No ☐ Yes	☐ No ☐ Yes
One or Both Ankles/Feet			
☐ No	☐ Yes	☐ No ☐ Yes	☐ No ☐ Yes

*Based on the Nordic Questionnaire

75

11.2 Appendix B
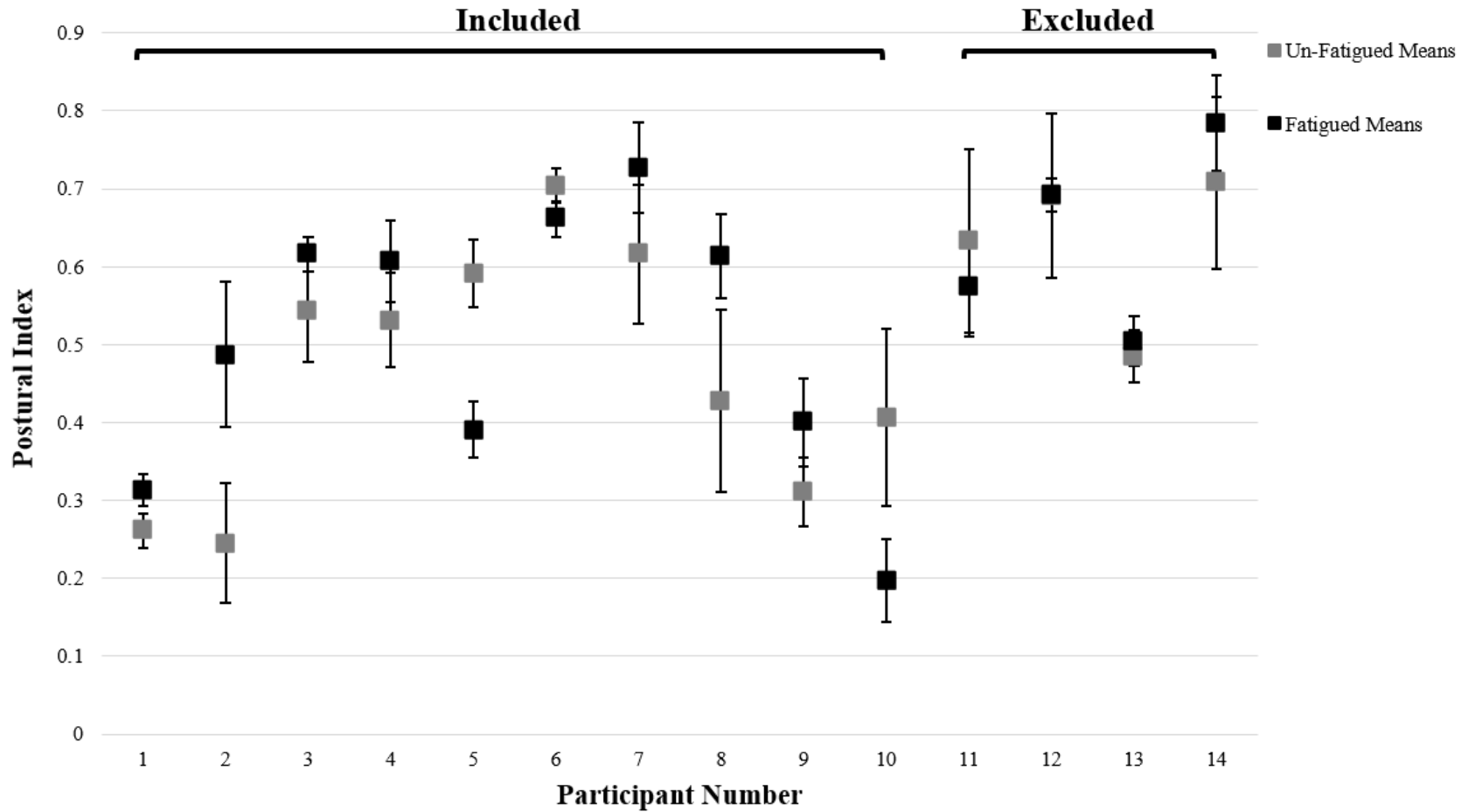
Figure 16. Origin lift postural index scores and standard deviations for each participant under each fatigue condition. Participants 1-10 were included within the simulation study and participants 11-15 did not meet the criteria for inclusion. Data from Participant 15 was excluded prior to analysis due to their protocol completion time being less than 10 minutes.

11.3 Appendix C

Un-Fatigued Origin
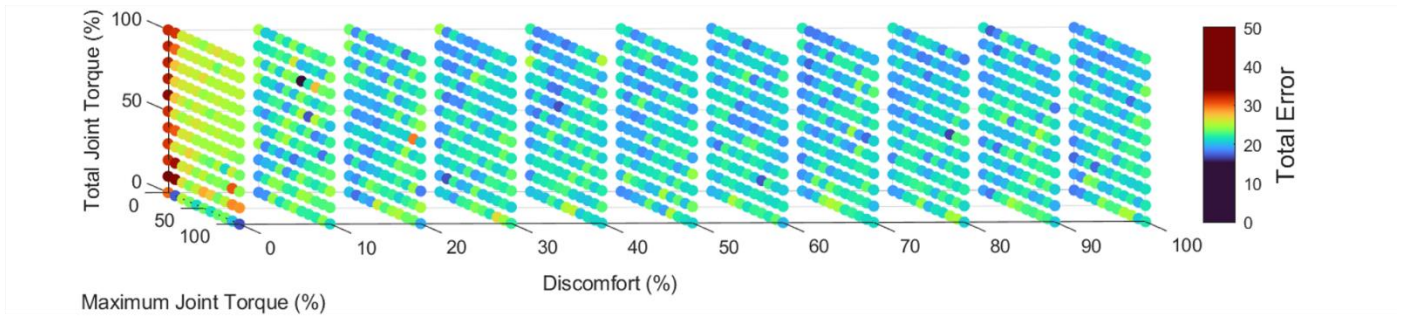
Un-Fatigued Destination
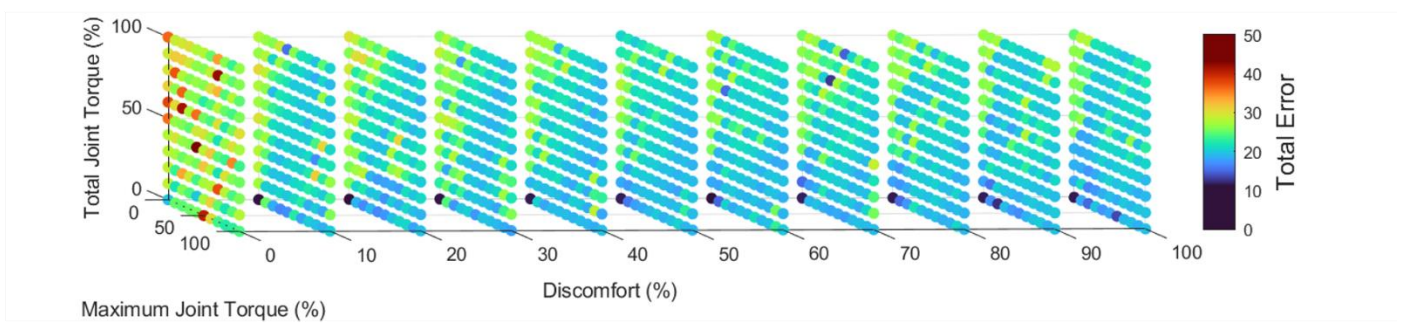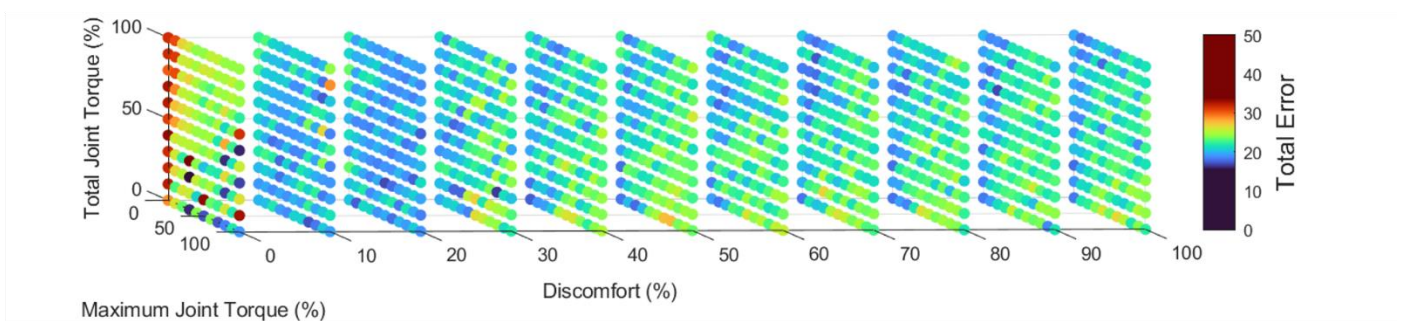
Fatigued Origin

Fatigued Destination
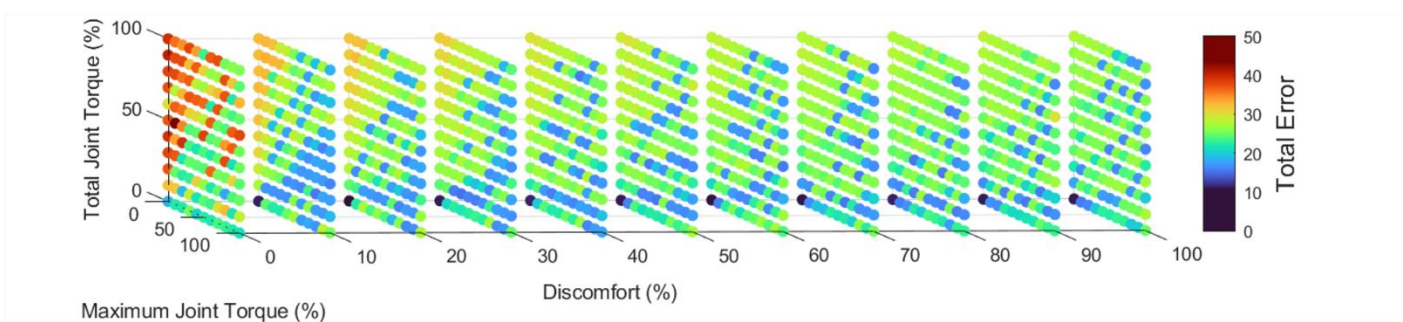
Figure 17. Normalized root mean squared error surfaces for Participant 1.

Un-Fatigued Origin
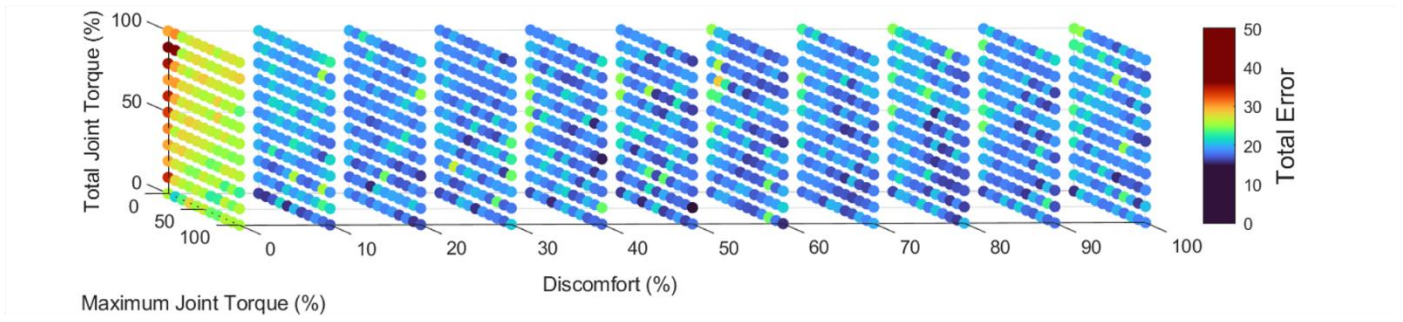
Un-Fatigued Destination
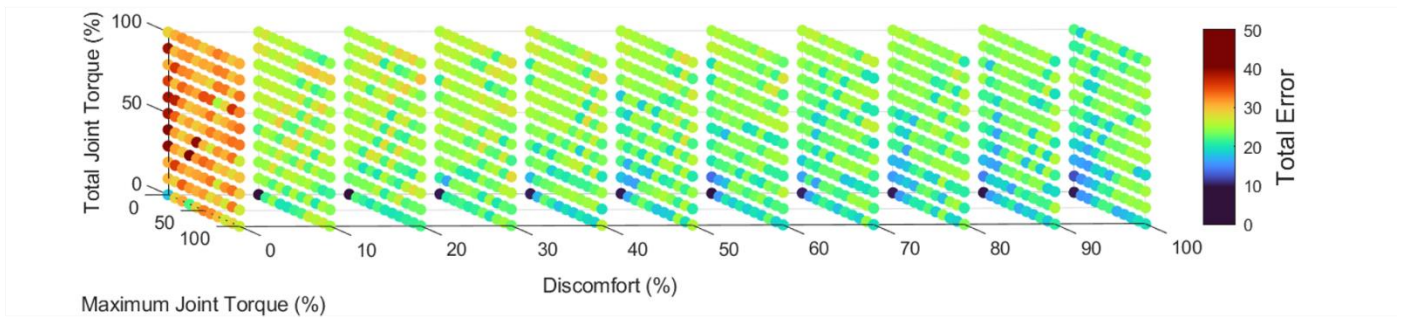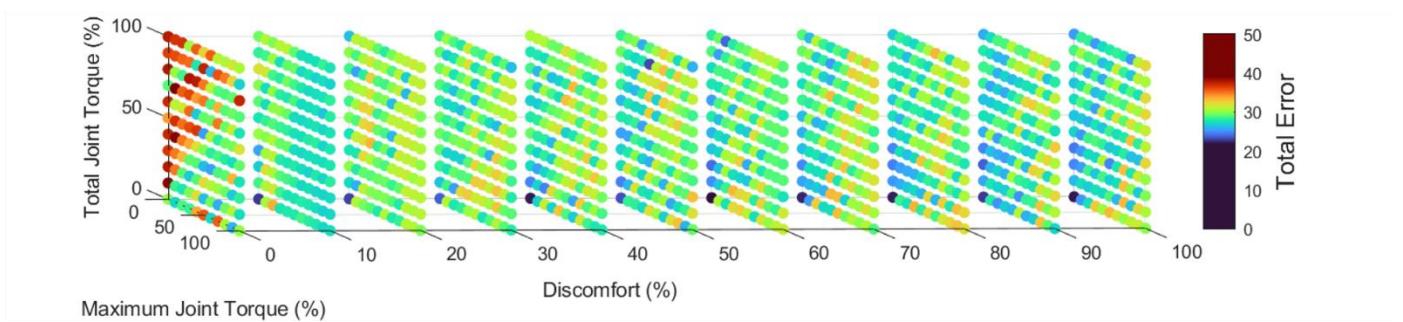
Fatigued Origin

Fatigued Destination
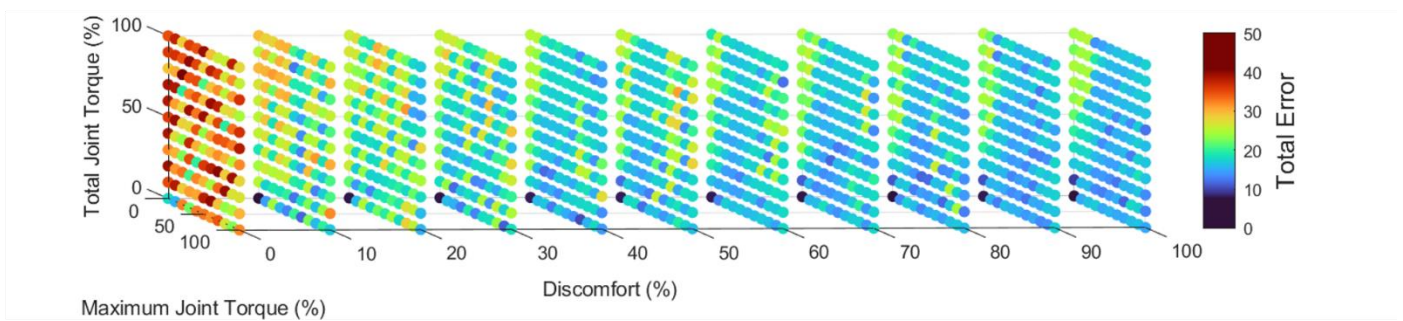
Figure 18. Normalized root mean squared error surfaces for Participant 2.

Un-Fatigued Origin
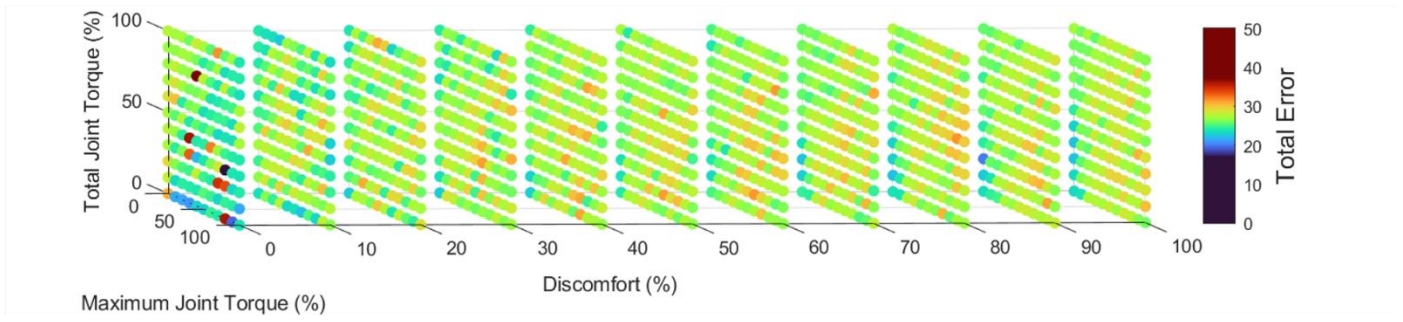
Un-Fatigued Destination
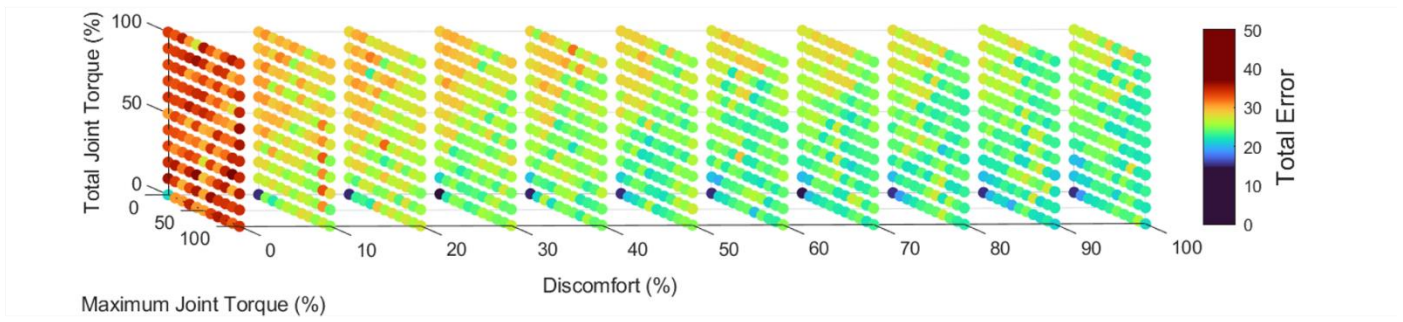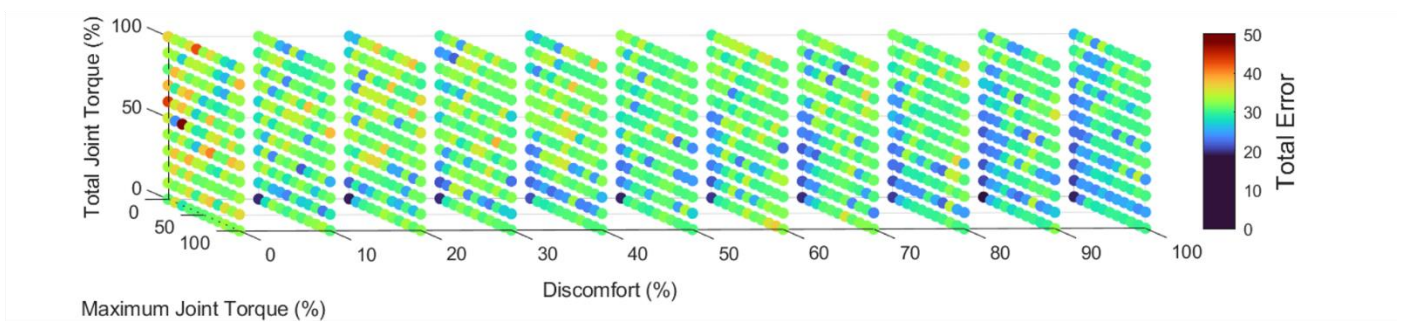
Fatigued Origin

Fatigued Destination
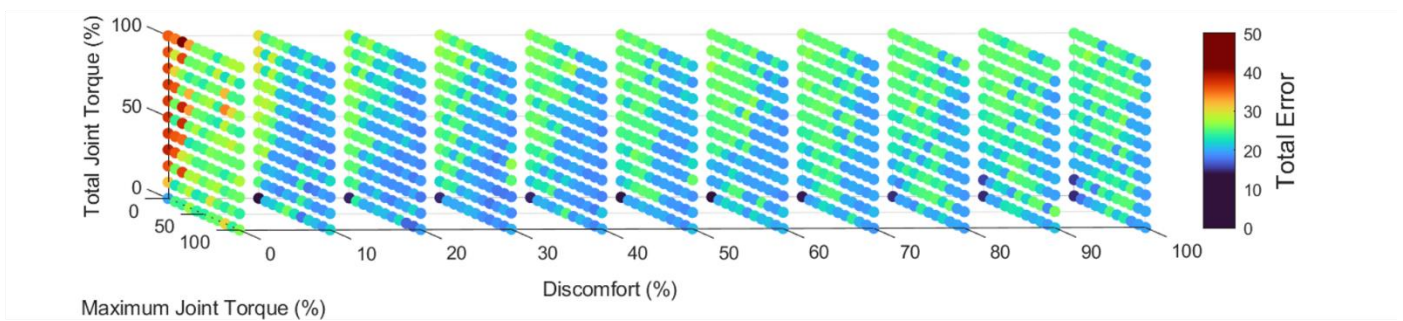
Figure 19. Normalized root mean squared error surfaces for Participant 3.

Un-Fatigued Origin
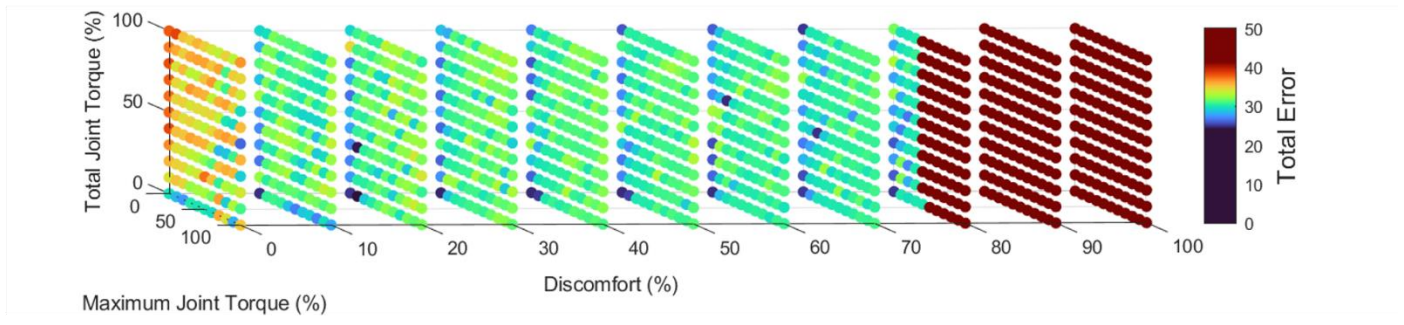
Un-Fatigued Destination
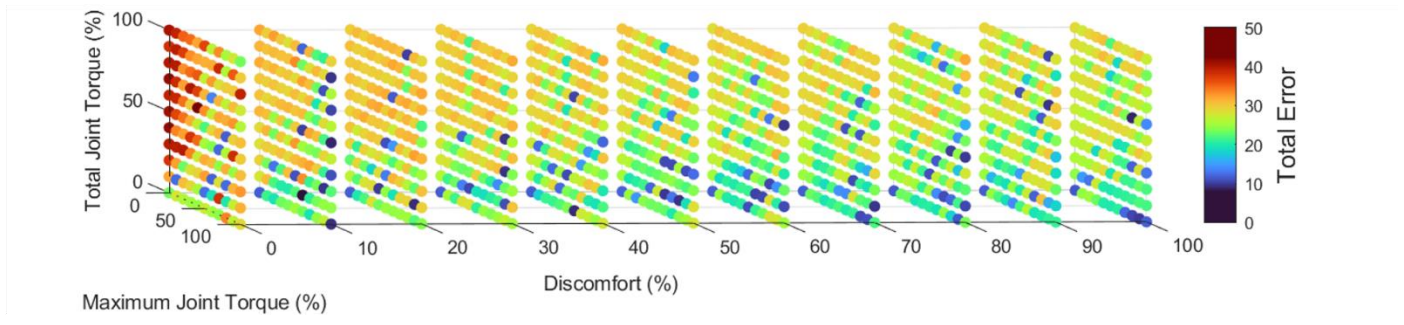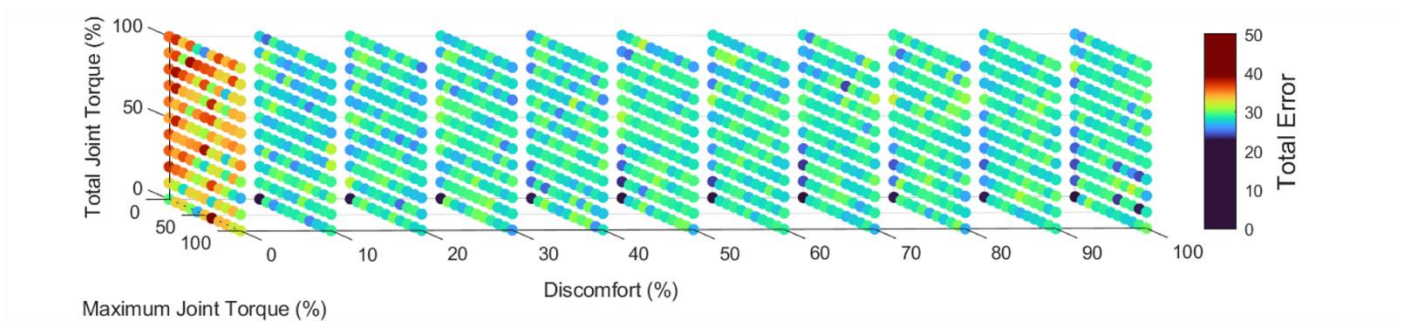
Fatigued Origin

Fatigued Destination
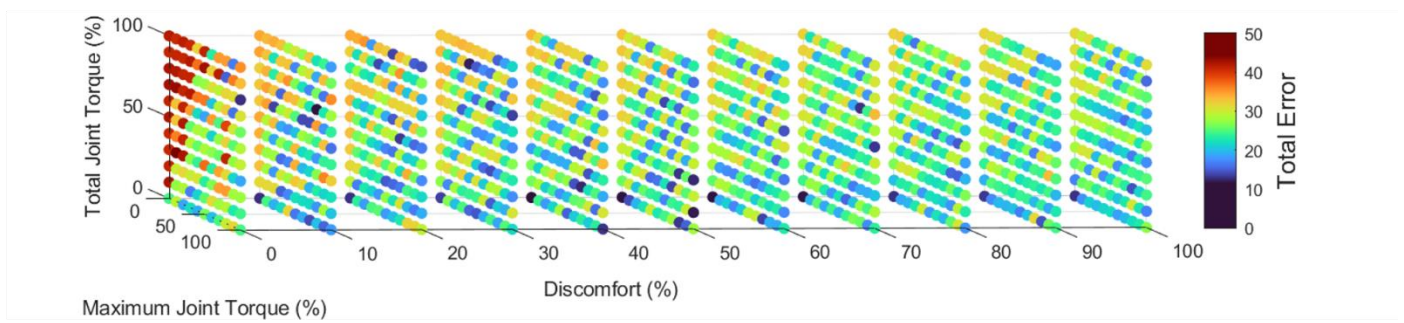
Figure 20. Normalized root mean squared error surfaces for Participant 4.

Un-Fatigued Origin
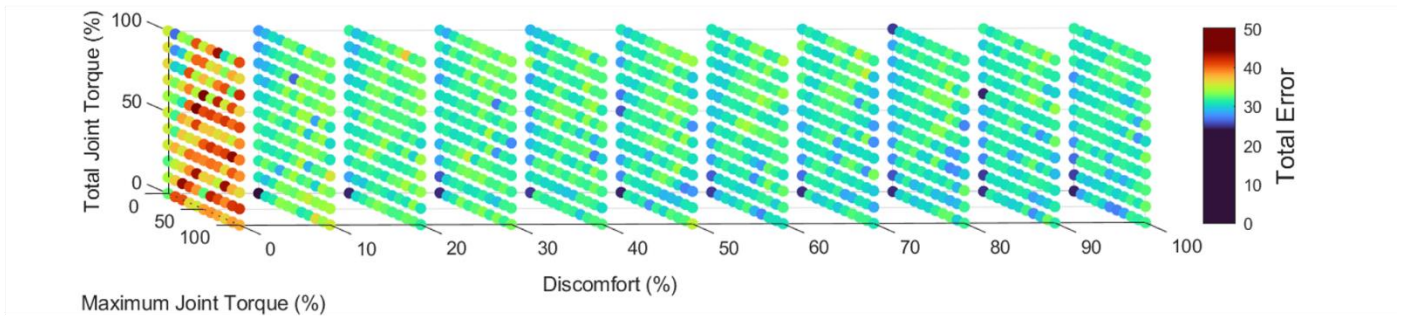
Un-Fatigued Destination
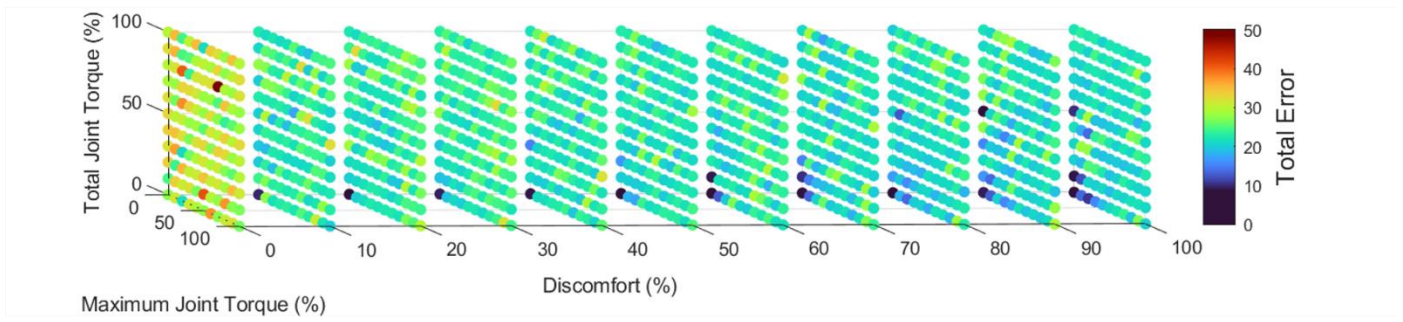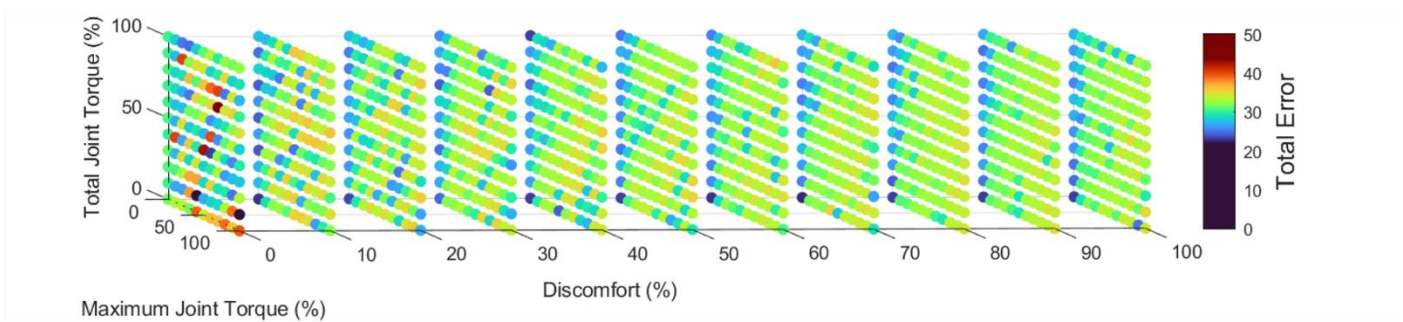
Fatigued Origin

Fatigued Destination
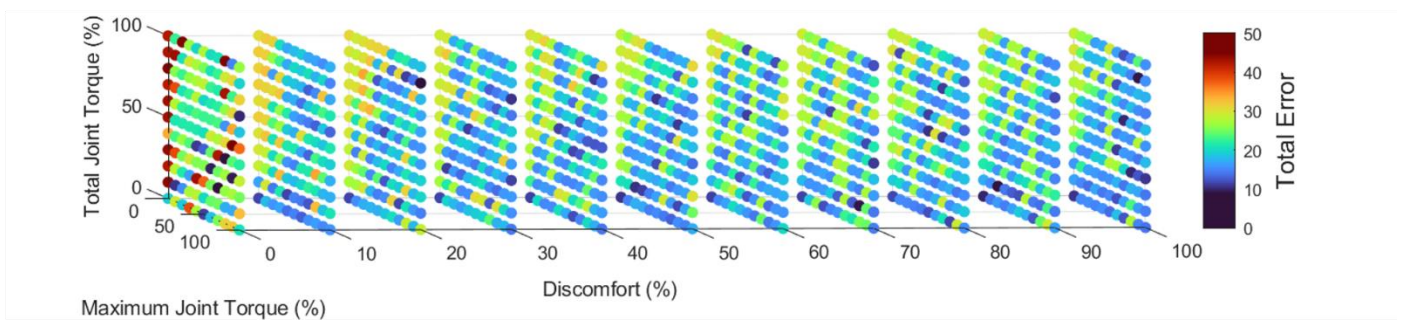
Figure 21. Normalized root mean squared error surfaces for Participant 5.

Un-Fatigued Origin
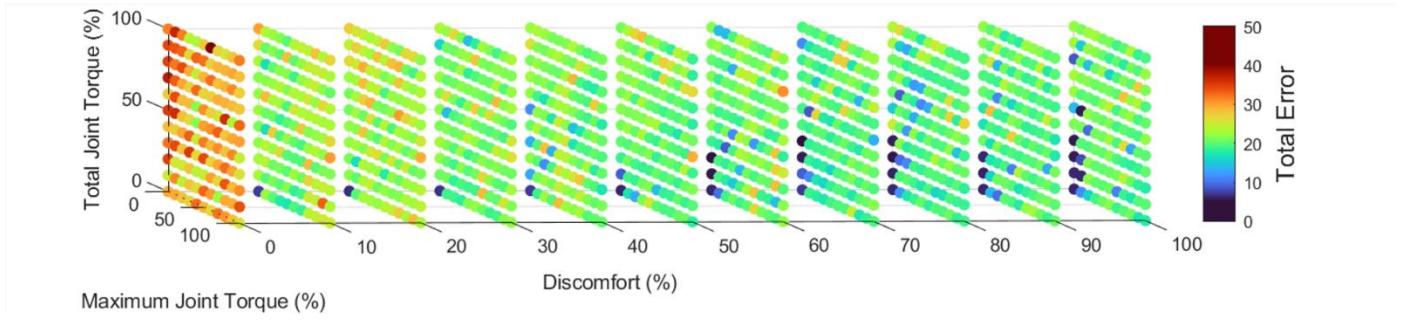
Un-Fatigued Destination
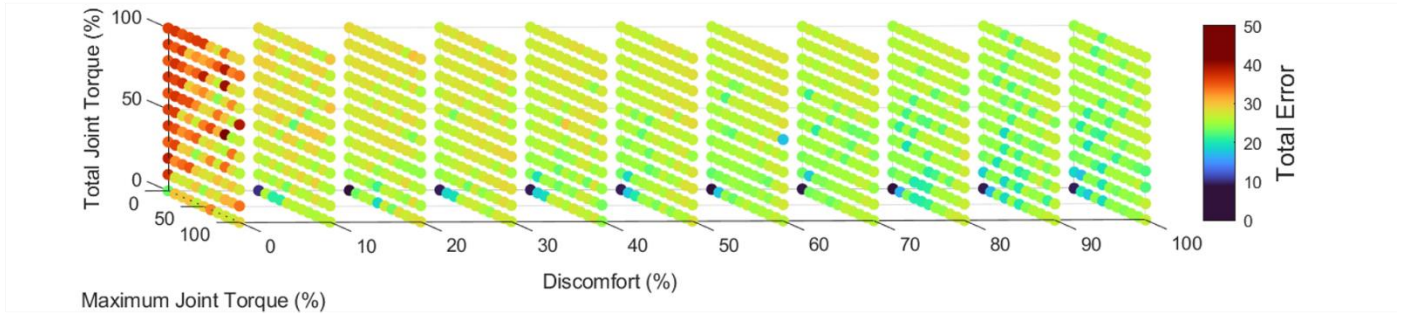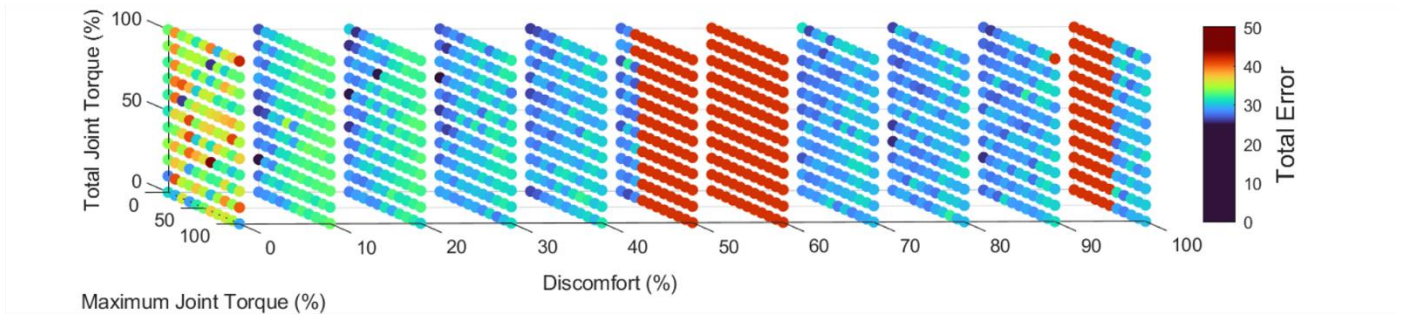
Fatigued Origin

Fatigued Destination
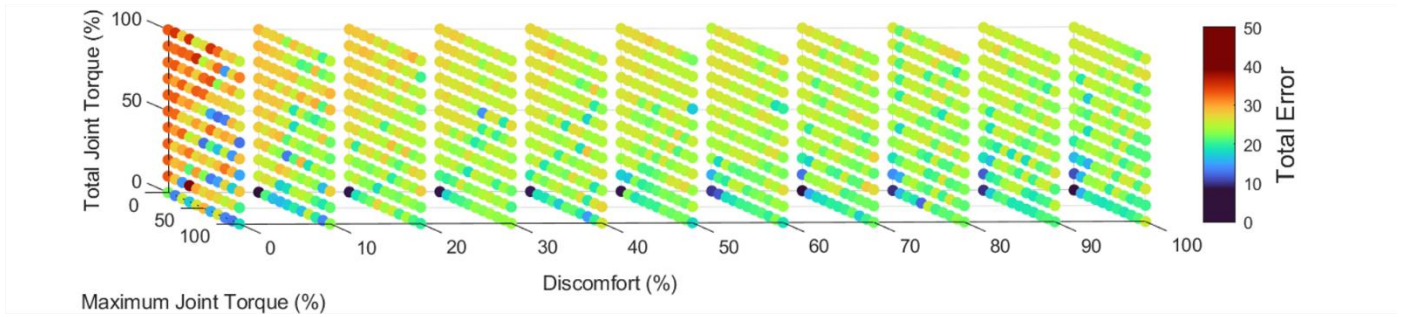
Figure 22. Normalized root mean squared error surfaces for Participant 6.

Un-Fatigued Origin
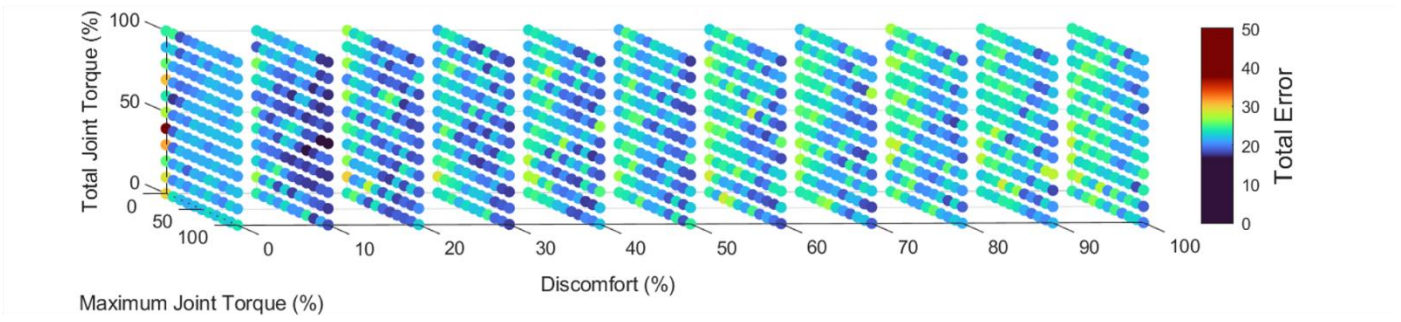
Un-Fatigued Destination
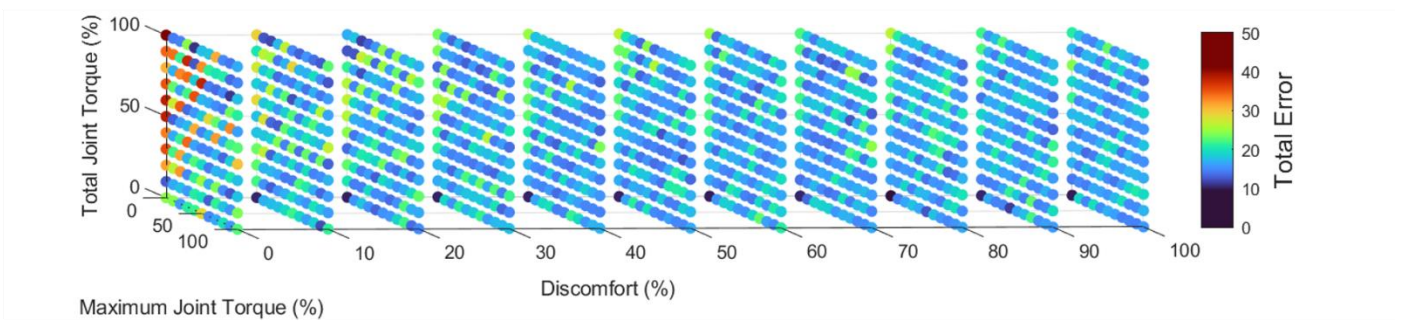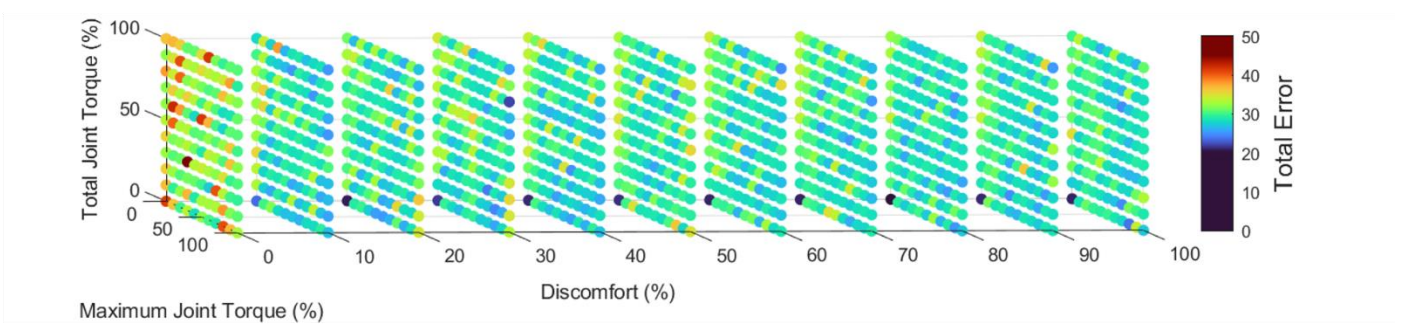
Fatigued Origin

Fatigued Destination
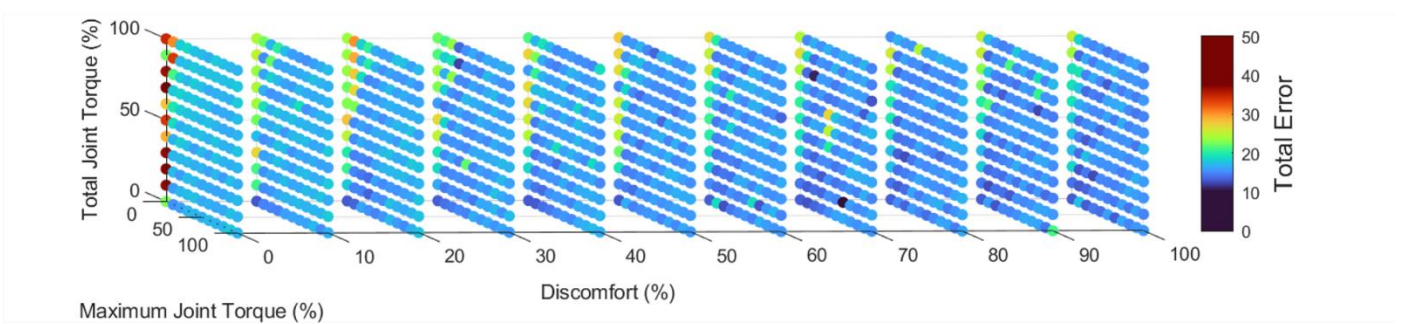
Figure 23. Normalized root mean squared error surfaces for Participant 7.

83
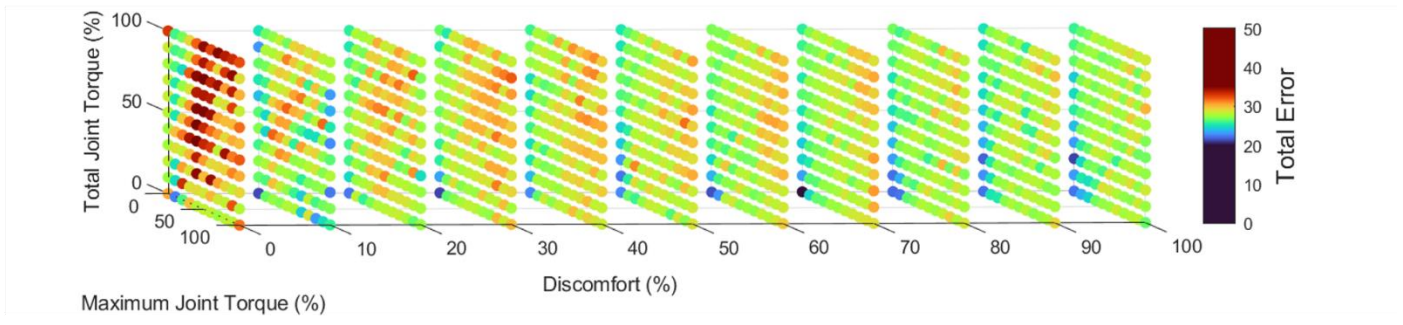
Un-Fatigued Origin

Un-Fatigued Destination
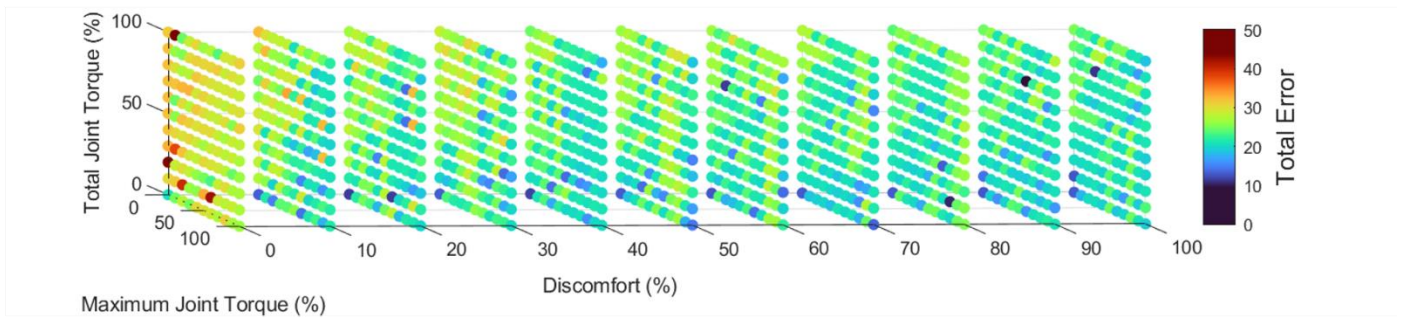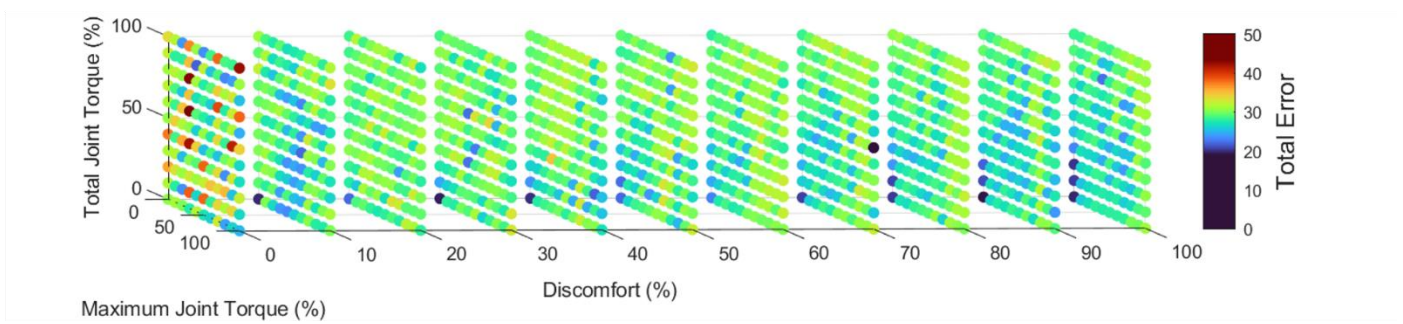
Fatigued Origin

Fatigued Destination
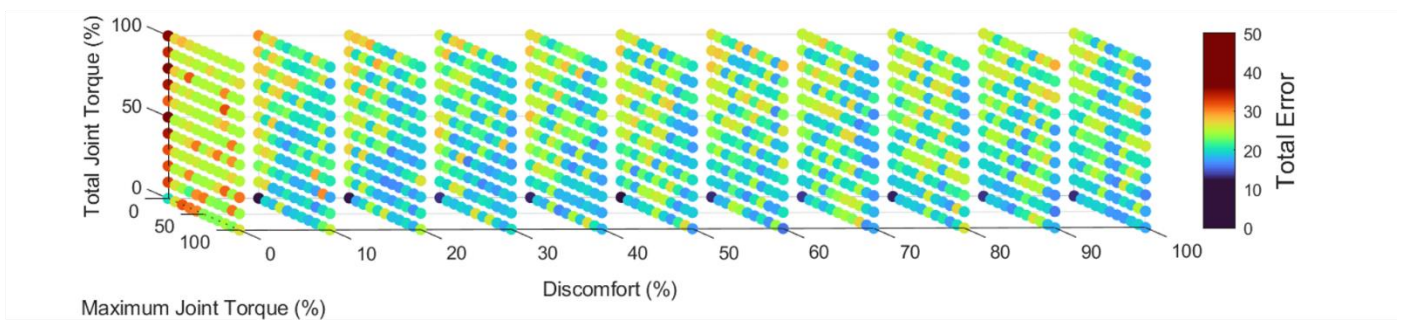
Figure 24. Normalized root mean squared error surfaces for Participant 9.

Un-Fatigued Origin
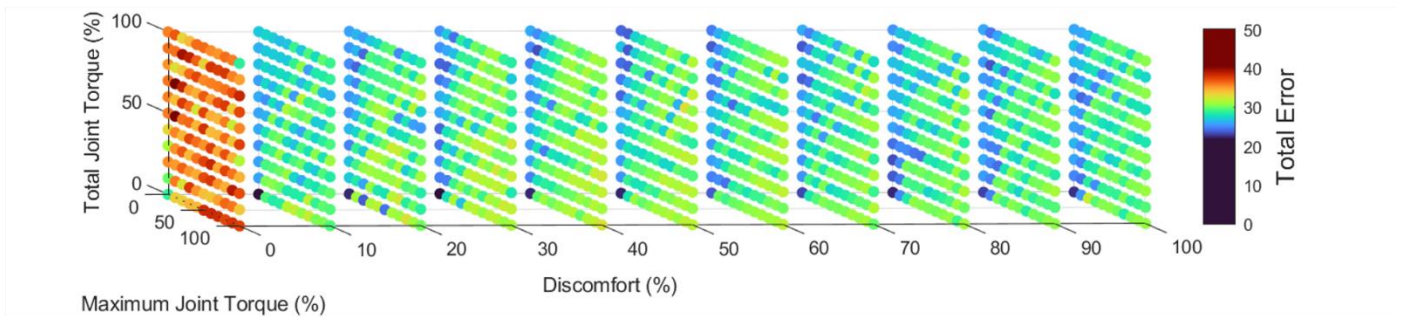
Un-Fatigued Destination
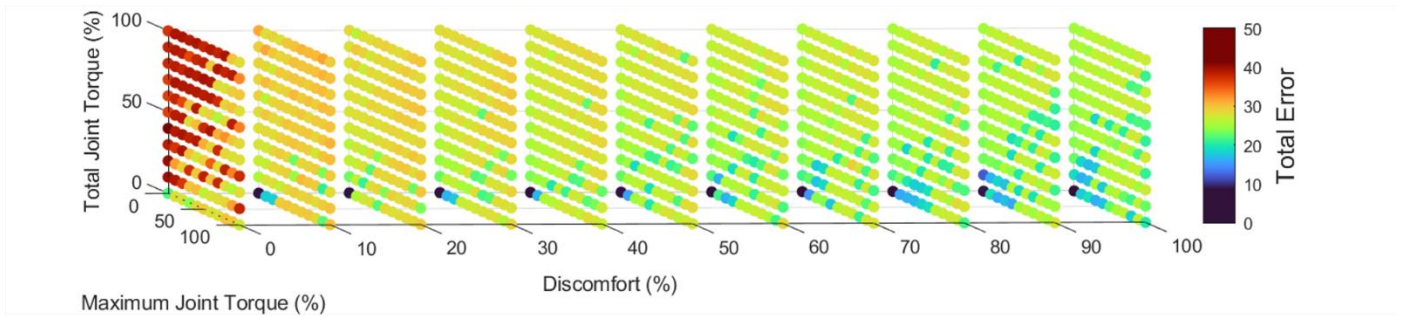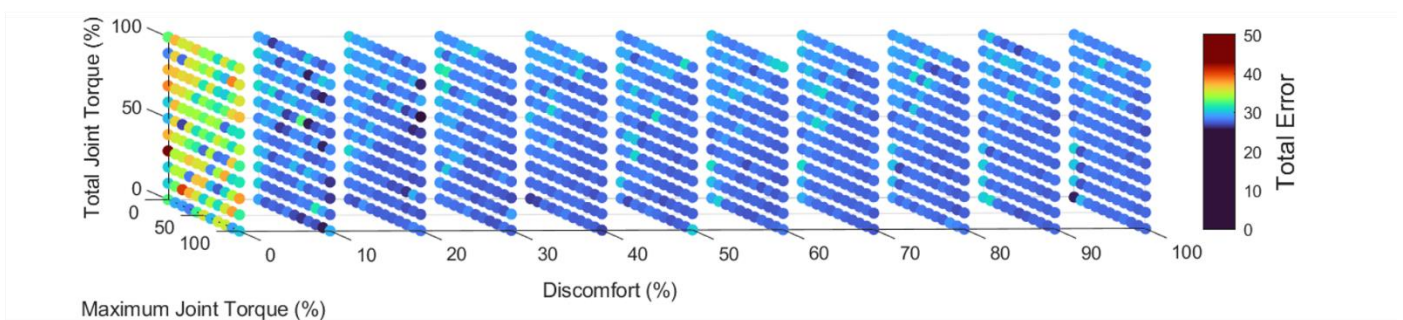
Fatigued Origin

Fatigued Destination
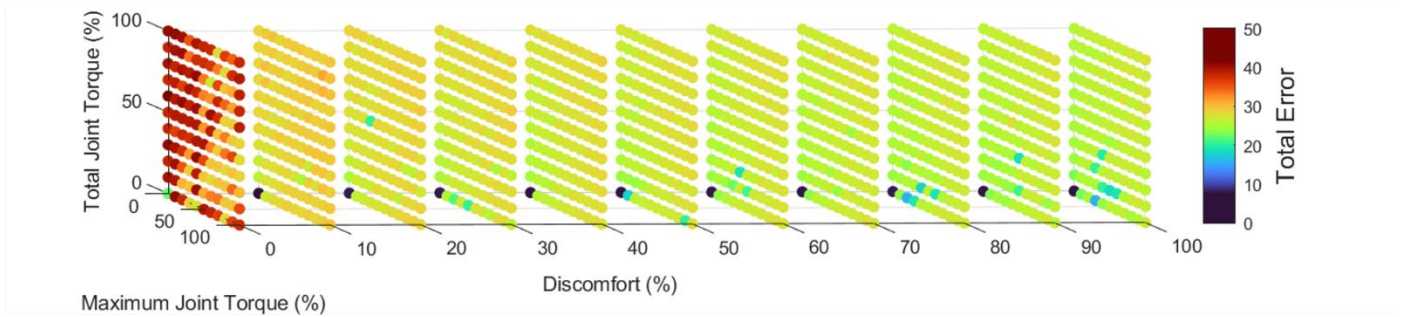
Figure 25. Normalized root mean squared error surfaces for Participant 10.

11.4 Appendix D
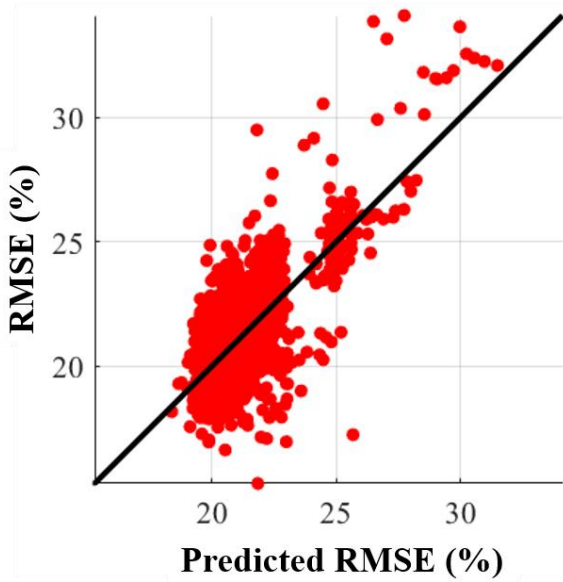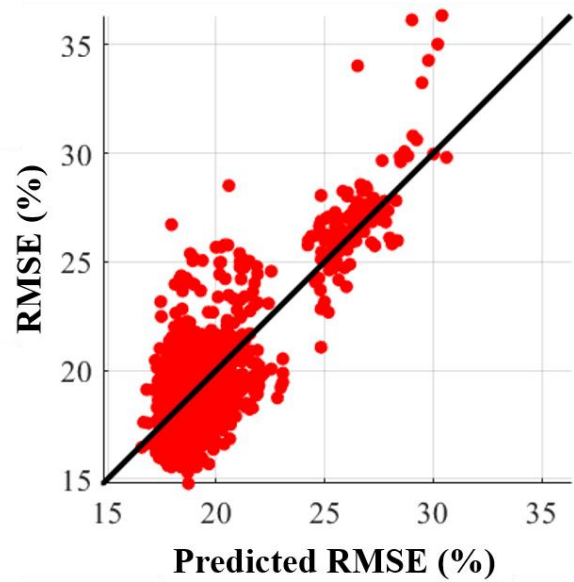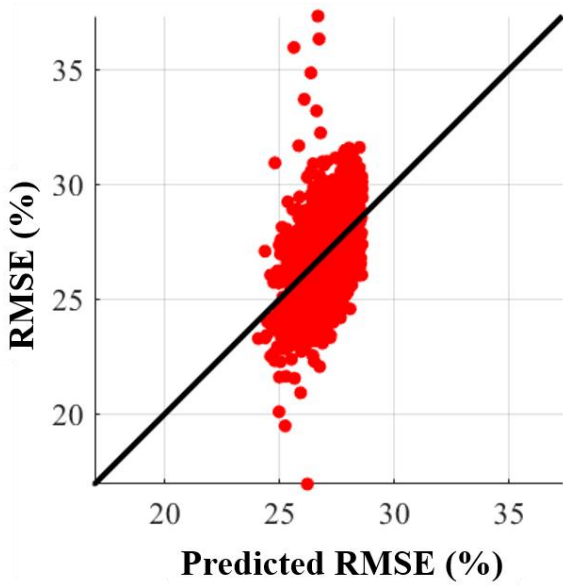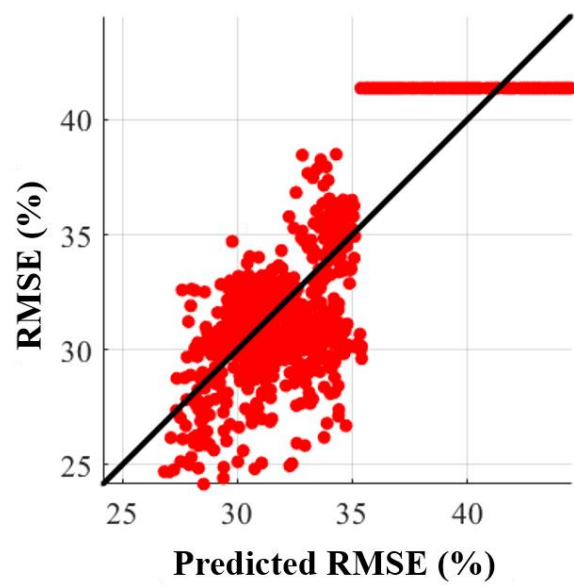
Figure 26. Model fit graph of the predicted (x) vs actual (y) plots plots Participant 1 under each condition.
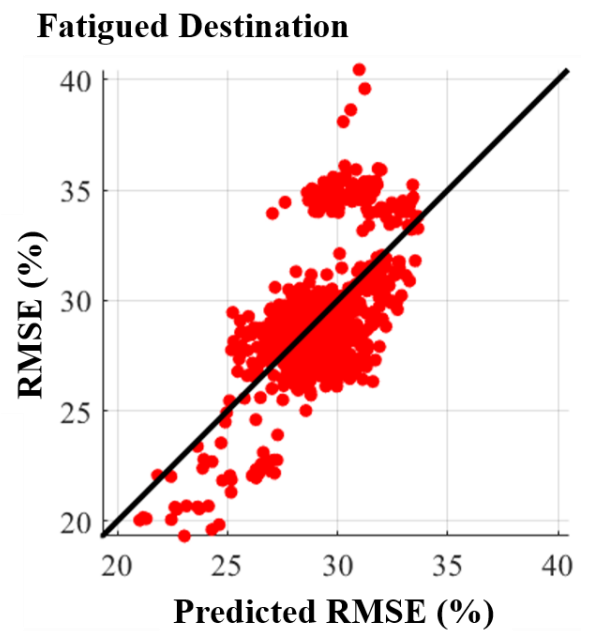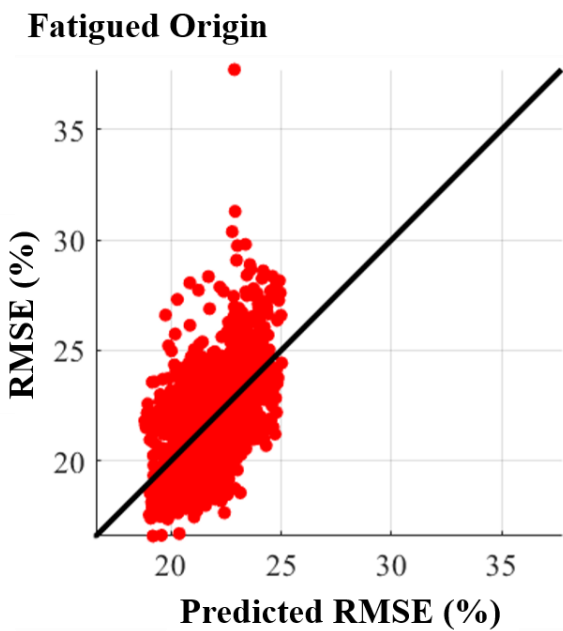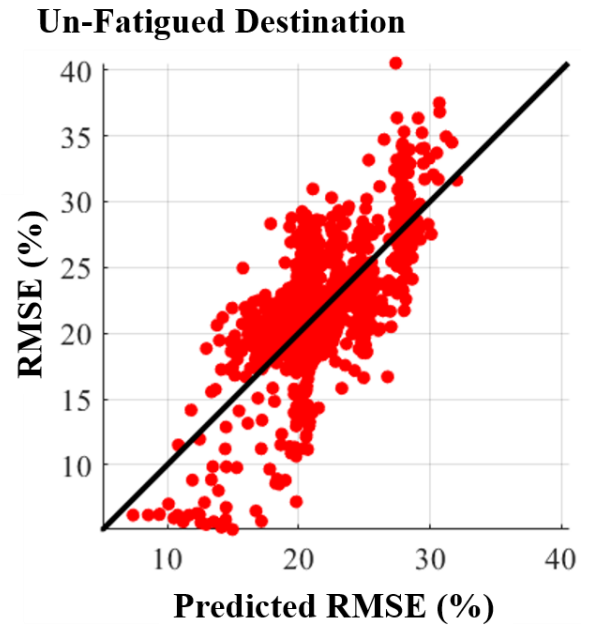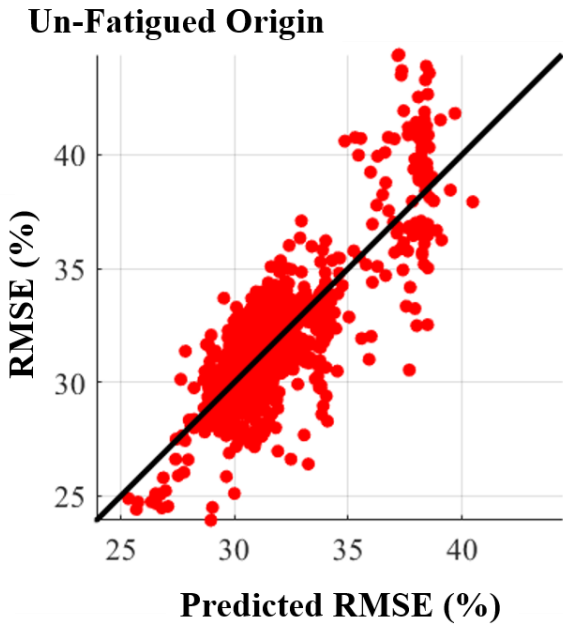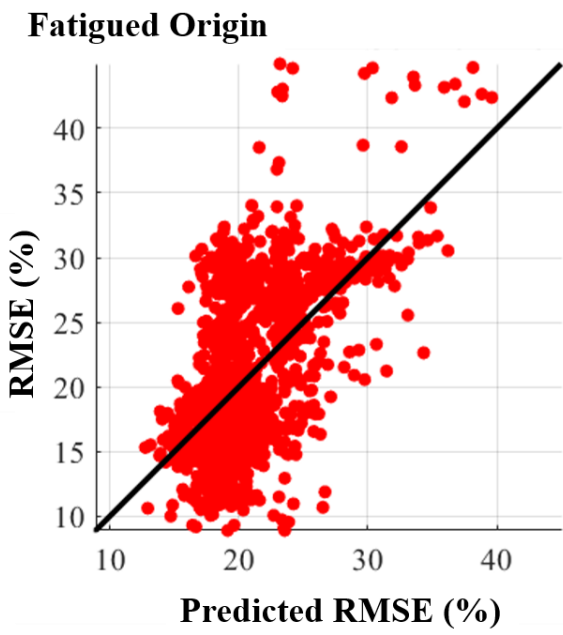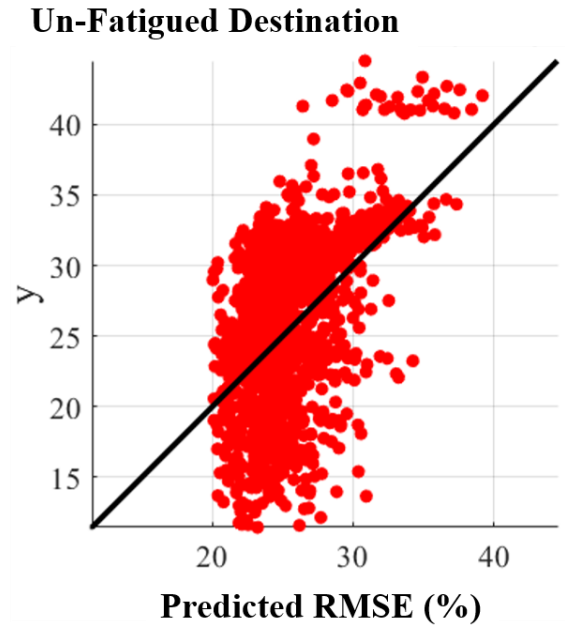
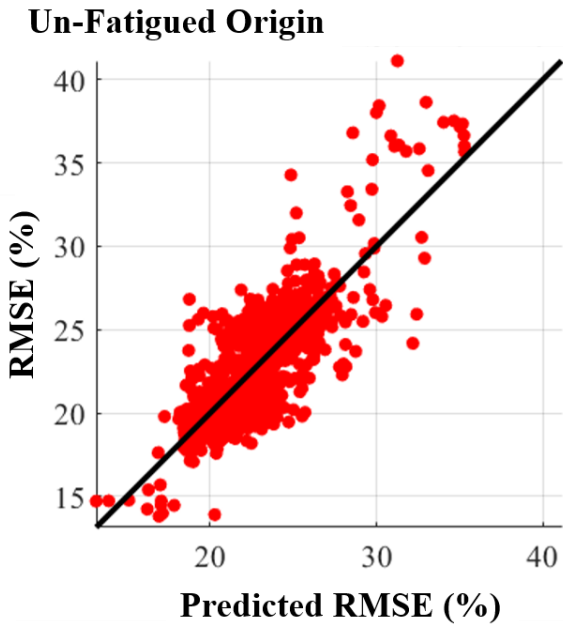Figure 27. Model fit graph of the predicted (x) vs actual (y) plots Participant 2 under each condition.
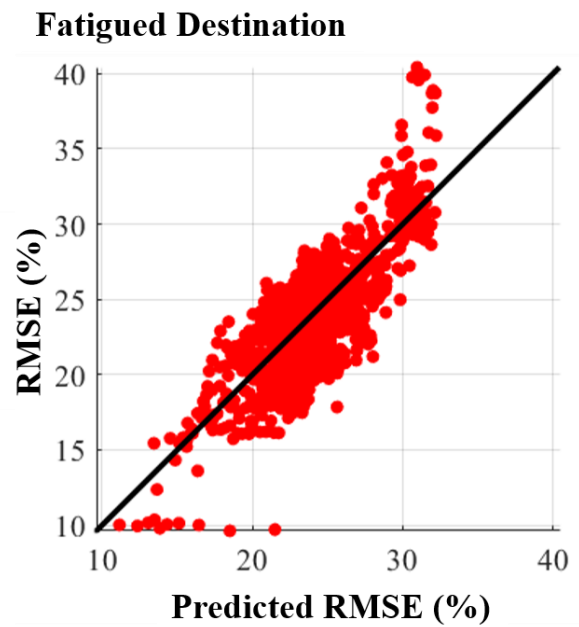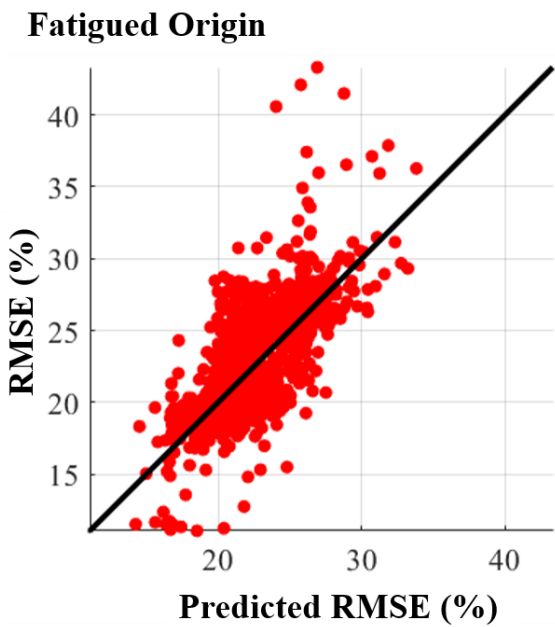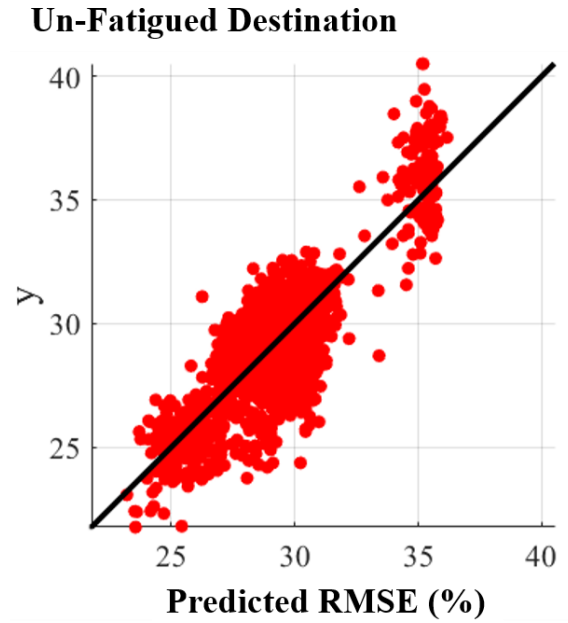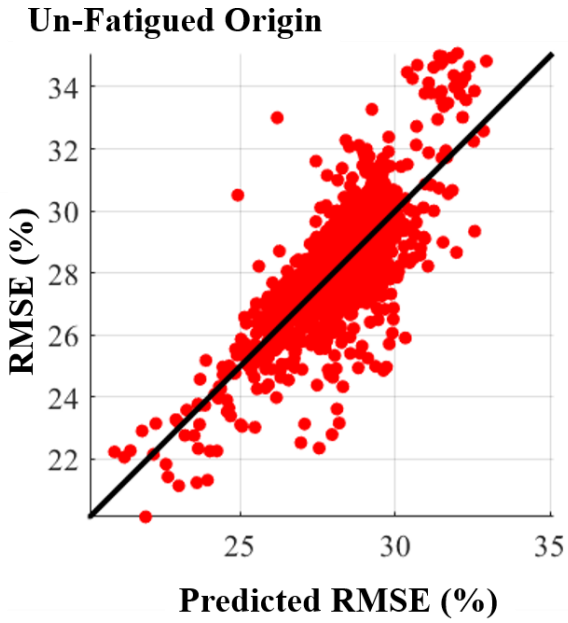
Figure 28. Model fit graph of the predicted (x) vs actual (y) plots Participant 3 under each condition.
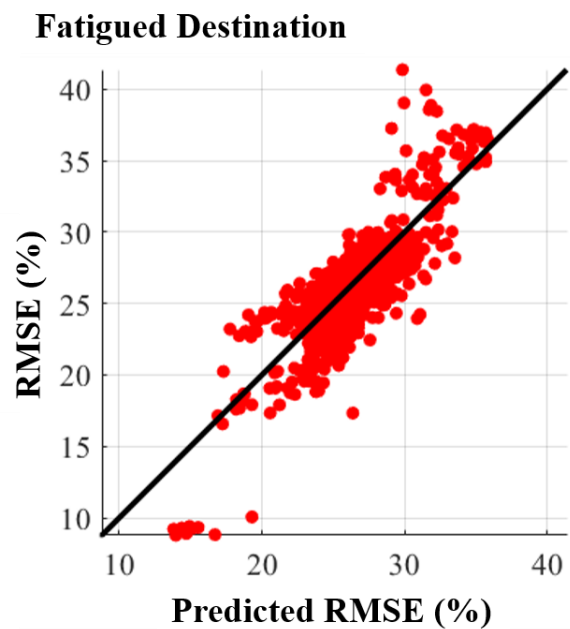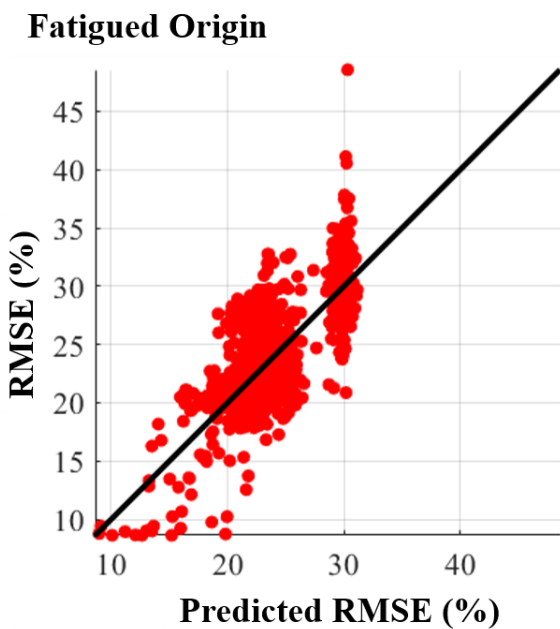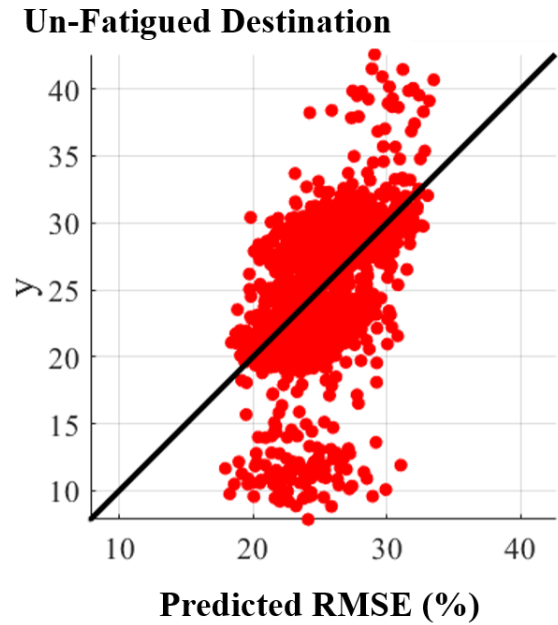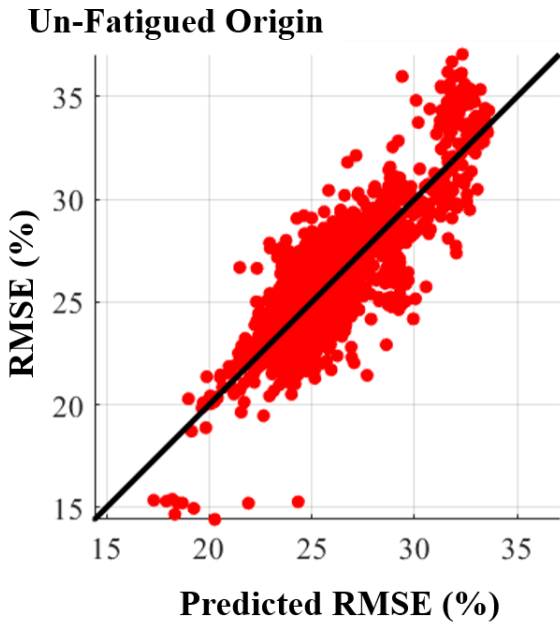
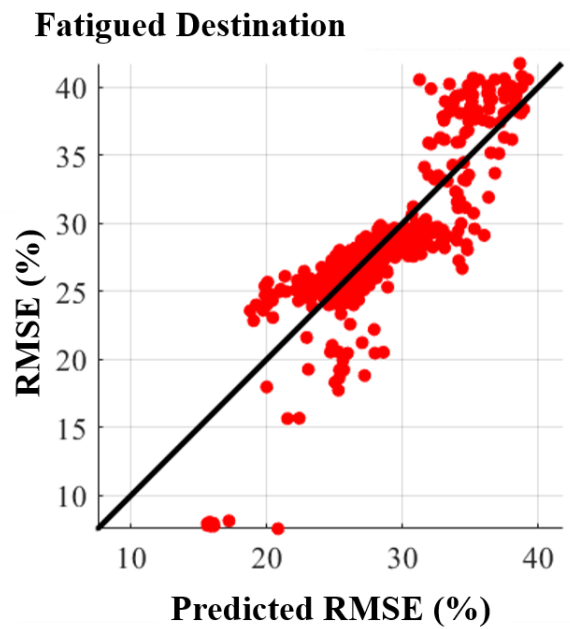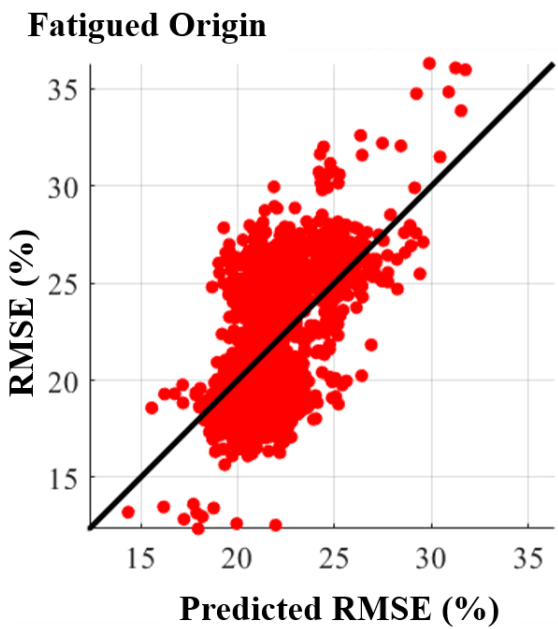Figure 29. Model fit graph of the predicted (x) vs actual (y) plots Participant 4 under each condition.
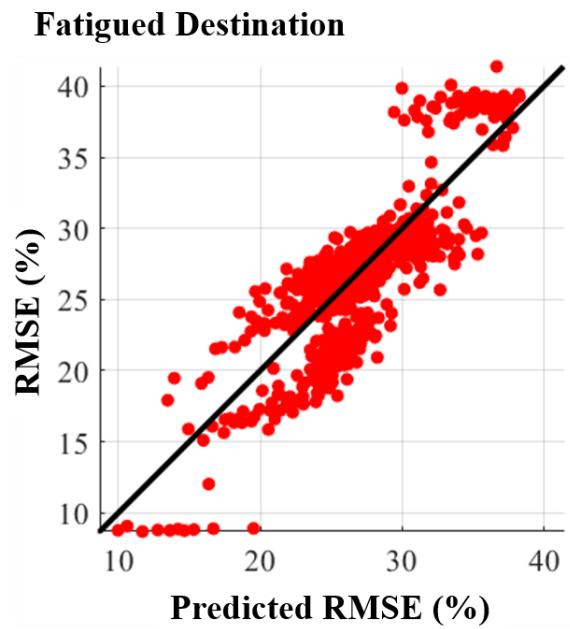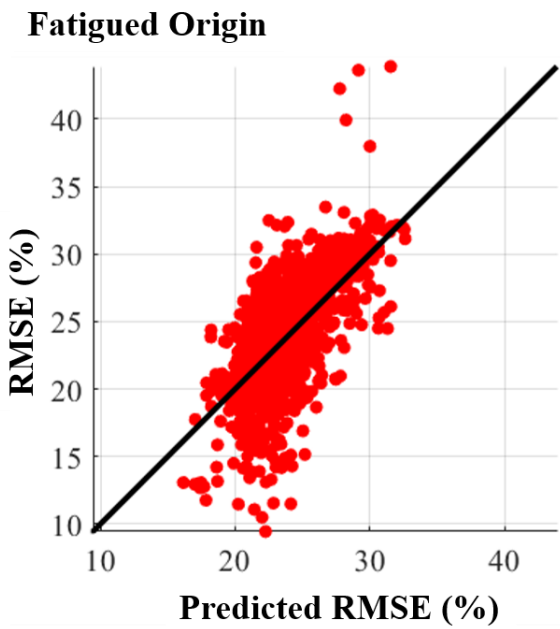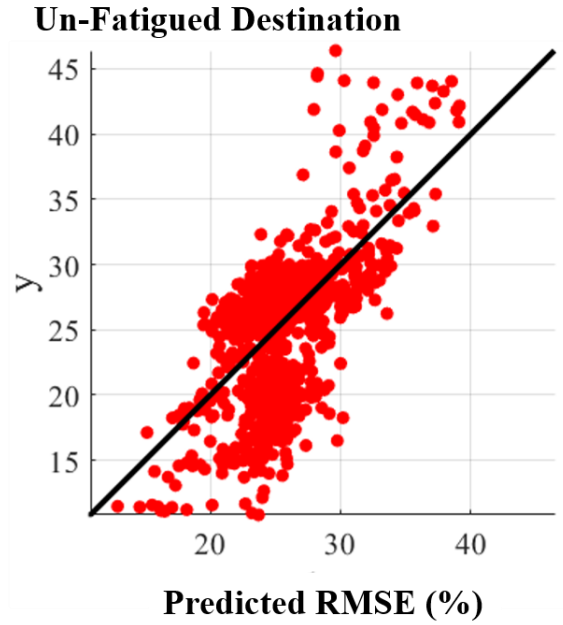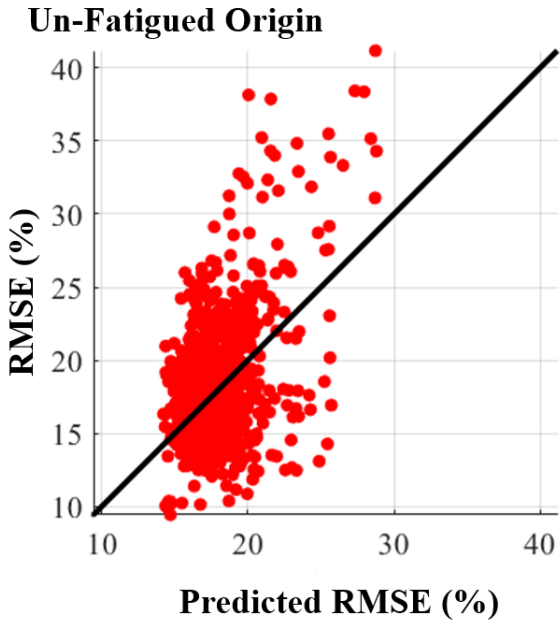
Figure 30. Model fit graph of the predicted (x) vs actual (y) plots Participant 5 under each condition.
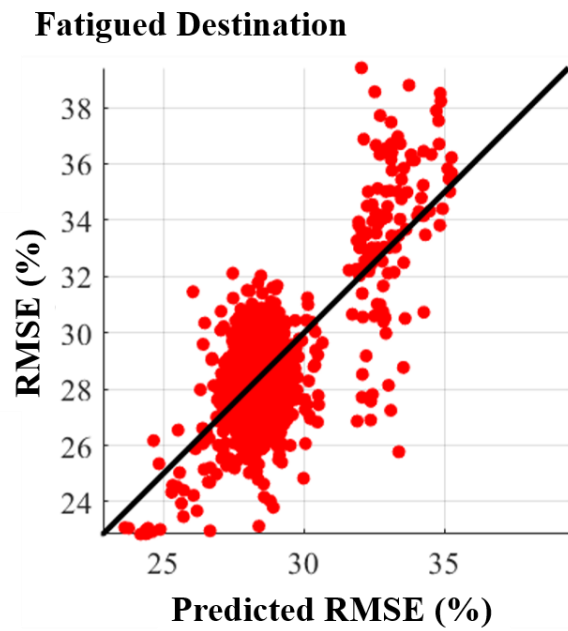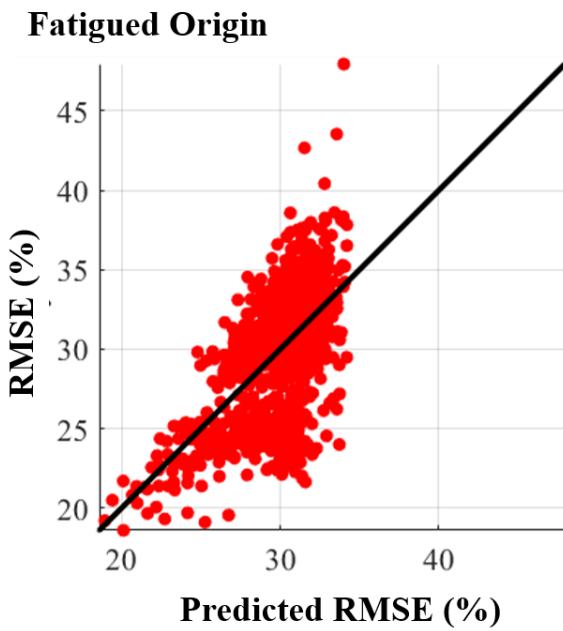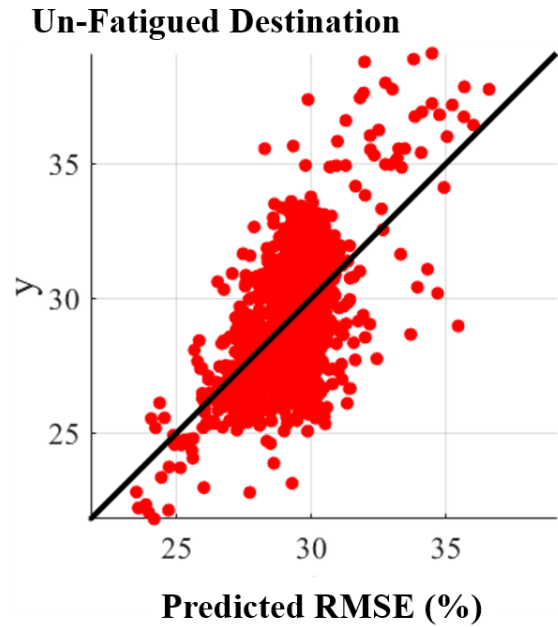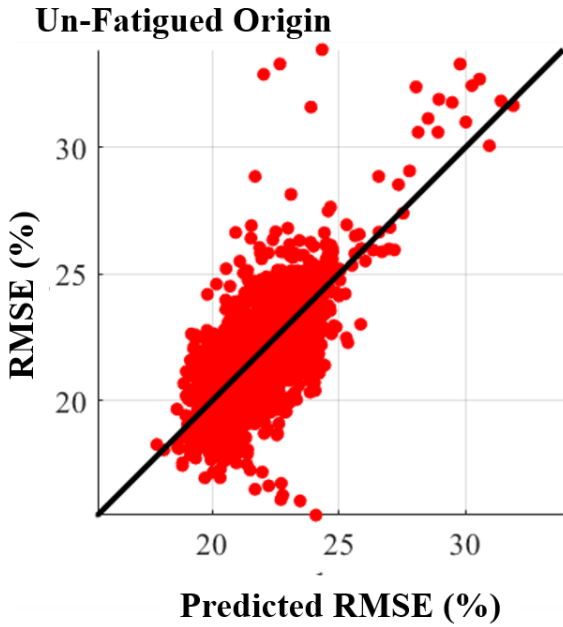
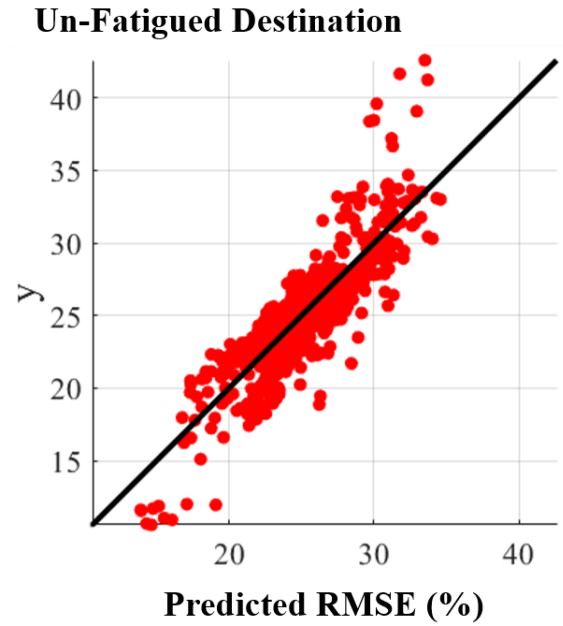Figure 31. Model fit graph of the predicted (x) vs actual (y) plots Participant 6 under each

condition.
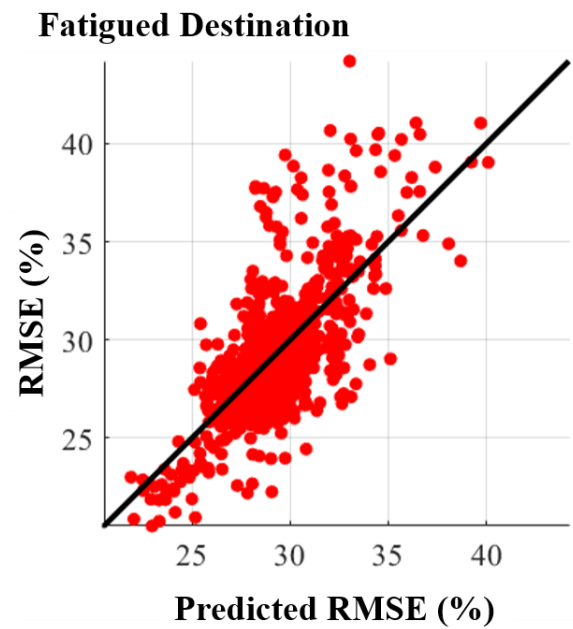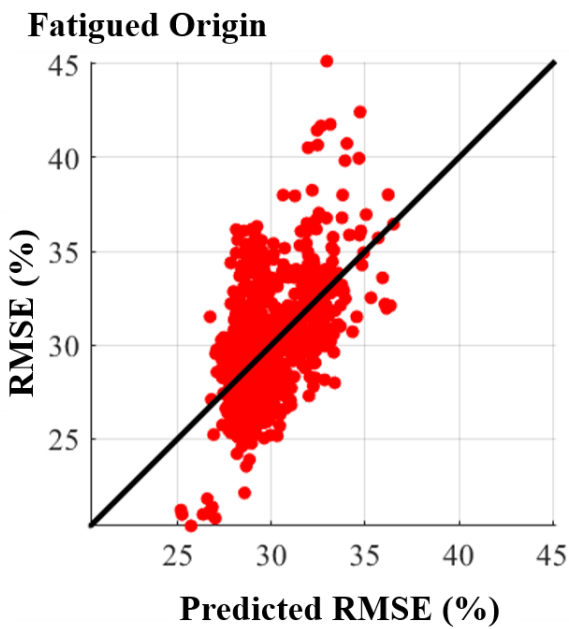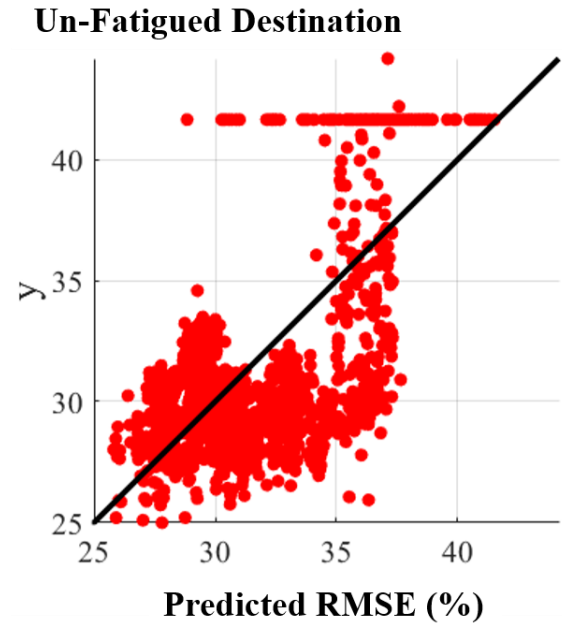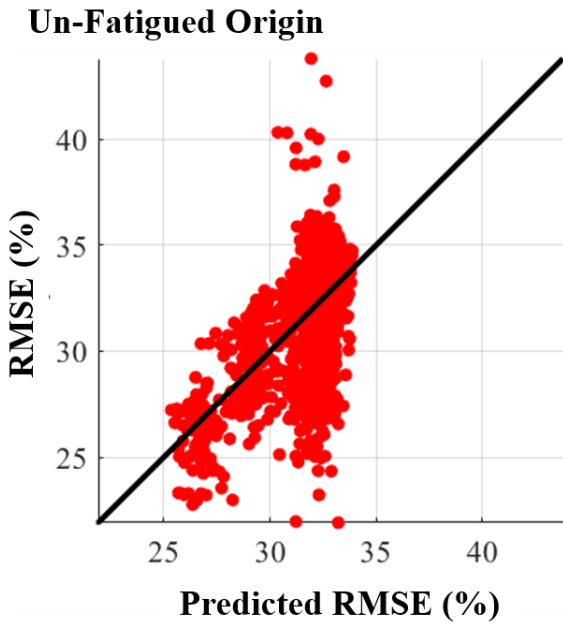
Figure 32. Model fit graph of the predicted (x) vs actual (y) plots Participant 7 under each condition.
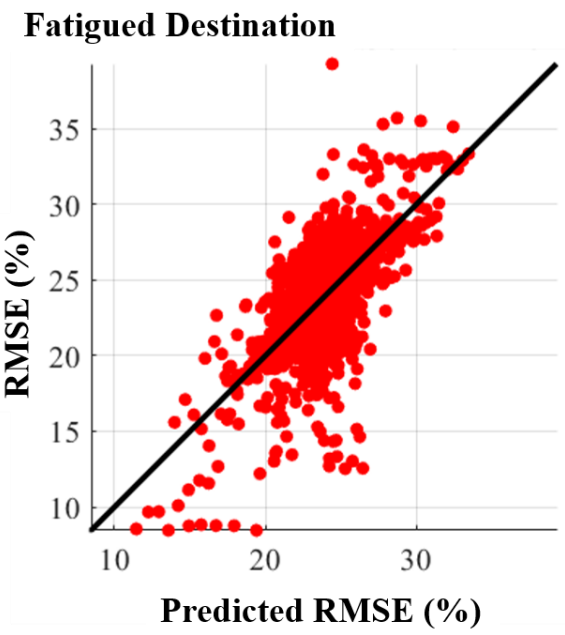
Figure 33. Model fit graph of the predicted (x) vs actual (y) plots Participant 9 under each condition.
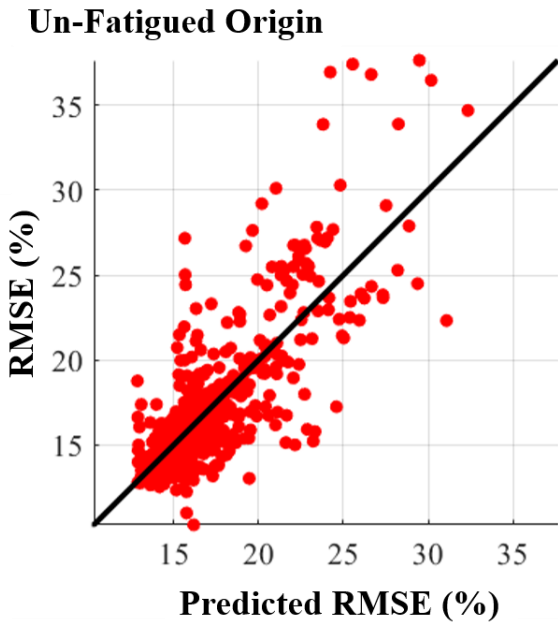
Figure 34. Model fit graph of the predicted (x) vs actual (y) plots Participant 10 under each condition.